Instabilities in the envelope of stars

Dissertation
zur
Erlangung des Doktorgrades (Dr. rer. nat.)
der
Mathematisch-Naturwissenschaftlichen Fakultät
der
Rheinischen Friedrich-Wilhelms-Universität Bonn

vorgelegt von
Luca Grassitelli
aus
Terlizzi (Italien)

Bonn 2016

Angefertigt mit Genehmigung der Mathematisch-Naturwissenschaftlichen Fakultät der Rheinischen Friedrich-Wilhelms-Universität Bonn

1. Gutachter: Prof. Dr. Norbert Langer
2. Gutachterin: Prof. Dr. Peter Schneider

Tag der Promotion:
Erscheinungsjahr:

Contents

1 A more modern view of stars **5**
1.1 The beginning of stellar evolution . . . 5
1.2 Energy source and thermodynamic equilibrium . . . 6
1.3 Energy transport in stars . . . 7
1.3.1 Radiative transport . . . 7
1.3.2 Convection . . . 8
1.4 Outer layers . . . 9
1.5 Stellar evolution . . . 11
1.5.1 Low & Intermediate Mass Stars . . . 14
1.5.2 Massive Stars . . . 14
1.6 Stellar pulsations . . . 18
1.7 This thesis . . . 19

2 Observational consequences of turbulent pressure in the envelopes of massive stars **21**
2.1 Introduction . . . 22
2.2 Method . . . 22
2.3 Results . . . 23
2.3.1 Evolutionary Tracks . . . 23
2.3.2 The structure of the outer layers . . . 25
2.4 Comparison with observations . . . 25
2.5 The connection to high-order pulsations . . . 28
2.6 Conclusions . . . 30

3 Relating turbulent pressure and macroturbulence across the HR diagram with a possible link to γ Dor stars **33**
3.1 Introduction . . . 34
3.2 Method . . . 34
3.3 Results . . . 35
3.4 Observational consequences of turbulence pressure . . . 36
3.4.1 Macroturbulence broadening . . . 36
3.4.2 The γ Dor instability strip . . . 38
3.5 Conclusions . . . 38

4 On the metallicity dependence of turbulent pressure and macroturbulence in stellar envelopes **45**
4.1 Introduction . . . 45
4.2 Method . . . 47

4.3 Results . . . 47
4.3.1 OB stellar models . . . 47
4.3.2 Late-type main sequence stars and red giant models . . . 50
4.3.3 Evolution at 40 $M_\odot$ . . . 51
4.4 Observational diagnostic . . . 54
4.4.1 Comparison to macroturbulence measurements . . . 56
4.5 Conclusions . . . 57

5 Diagnostics of the unstable envelopes of Wolf-Rayet stars 61
5.1 Introduction . . . 62
5.2 Method . . . 63
5.3 Sub-surface convection . . . 66
5.4 Pulsations . . . 69
5.5 Comparison with observations . . . 72
5.5.1 Spectral variability . . . 73
5.5.2 Characteristic timescale and number of clumps . . . 75
5.5.3 Magnetic fields . . . 76
5.5.4 Pulsations . . . 77
5.6 Conclusions . . . 78

A Other Publications 89

Acknowledgements 103

ABSTRACT

Stars shine, i.e. they release energy from the surface in the form of radiation. This energy is mostly provided by thermonuclear fusion in their cores. However, as the enormous amount of energy produced in their cores needs to be transported outwards, in certain conditions stars might struggle transporting such fluxes. This can happen especially in the low density outer regions of a star where the recombination of some elements takes place, breeding ground for the establishment of instabilities such as convection and pulsations.

Here the conditions in the outer layers of stars with different mass, metallicity, and evolutionary stage are discussed via the use of hydrodynamic stellar structure calculations and a direct or indirect comparison between theoretical predictions and observational phenomena. While investigating the structure of Galactic and Magellanic Clouds stars, we include and consider the pressure arising from the turbulent motion within the convective zones, finding a striking correlation between the strength of the sub-surface turbulent motion and the appearance of a non-local broadening of the absorption lines in stellar spectra, of importance especially, but not only, in the context of massive stars. The correlation with this extra broadening of still unknown origin, called macroturbulence, suggests that inefficient convective energy transport might lead to the excitation of waves which propagate to the surface, generating the velocity field observed as macroturbulent broadening.

Moreover, convection seems to play a key role also as triggering mechanism for the appearance of density inhomogeneities in the winds of massive stars in the late stages of their lives. In fact, due to their proximity to the Eddington limit, massive stars in an advanced stage of their evolution show very high mass-loss by stellar wind which shrouds their hydrostatic layers. These are the Wolf-Rayet stars, and a phenomenological investigation of their stellar winds shows the presence of a high number of randomly distributed clumps within their outflows. We suggest that the origin of this phenomenon could be found considering the convective zone at the base of the wind, which may effectively act as trigger for the formations of clumping in the wind. We also find that the extreme mass-loss by stellar winds distinctive of this class of stars have a damping effect on otherwise present pulsations. Low order pulsations are, in fact, theoretically expected but at the moment without observational counterpart in Wolf-Rayet stars, and our finding that the strong stellar wind might be the reason for such a discrepancy helps reconciling this disagreement.

Mass-loss by stellar wind and rotation are two of the most important agents influencing the evolution, the structure, and thus the final fate of stars, second only to the initial mass. The results of this work point to the importance of the effects of turbulent motion and instabilities while investigating the physics taking place in the outer layers of especially stars close to their Eddington limit. As our understanding of these phenomena increase, we can better constrain stellar parameters such as the projected rotational velocities, stellar wind mass-loss, or in general the physics in the low density radiation pressure dominated layers close to the Eddington limit, a step forward in the human challenge for a better understanding of the physics of stars.

Introduction

dixitque Deus fiat lux et facta est lux
YHWH

The epic tale of the stars filling up the sky is the story of how we are here, the universal song of life and death. The Sun, born out of the ashes of a monumental explosion, is made of the same ashes we are made of, and it was always portrayed as the *deity* which gave us life. Indeed, life on the planet would not be possible without the energy from our nearest star. Our planet itself would not be here. And, sadly, it will not be here forever. One day, in quite some time, fireworks will dress the red sky of a desert Earth, a rain of fire will transport this planet into its final oblivion. Wonder and mystery, life and death, light and darkness, this is the story portrayed here, vulgarly known as stellar astrophysics.

The Sun (Fig.0.1) is one of the countless daughters of this Galaxy, a young star according to its chemical composition. Though it took millennia for humankind to place the Sun in the center of the Solar system, since the rise of men the Sun plays a central role in human life. Days and nights, springs and falls, eclipses and auroras, these are all phenomena due to the interaction between our home planet and our nearby star. Consequently astronomy is the oldest of the natural sciences, vestige of mythology until the Scientific Revolution when, thanks to an *Astronomia nova* (Keplero, J., 1609), the doors for our modern scientific dialogue were opened. This is the time when a dialogue about the two chief world systems of *Dialogo sopra i due massimi sistemi del mondo* (Galilei,G. 1632), the ptolemaic-aristotelic and the copernican systems, led to the understanding that the Earth and the *Heavens* were not separated, but rather united and governed by the same natural laws. Since the Renaissance and thanks to pioneer works such as *Philosophiae Naturalis Principia Mathematica* (Newton,I.,1687), physics and math step by step built the framework for the current understanding of the mathematical principia of the natural philosophy. Science was born.

From classical to quantum mechanics, from general relativity to the most exotic new physical theories, nowhere else Nature offers a greater laboratory than in the physics of stars. And there are plenty of them out there, rich in phenomena which have been only partially understood. Only our Galaxy, the Milky Way, counts approximately 10^{11} stars, some (most) of them are slightly smaller than the Sun, some others are as big as the orbit of Saturn, many of them also have a companion star. The stars do not last forever: they arise from majestic cosmic clouds, they undergo different phases depending on their mutable chemical composition, and once their time comes, as alchemists they enrich the galaxies with the material for other stars to come, as well as other bizarre things like the humans.

It is our gift and duty as sentient and self-conscious living beings to fulfil the eager for knowledge and understanding, as we still carry the fascination for the shiny starry sky of our elder ancestors. The hope left to the future must lead us to keep pursuing the dream of a more familiar Universe. We can not unburden humans of this heavy task for *wisdom* as far as, up to now, we only are blessed with life in a Cosmo where we just started to find other planets.

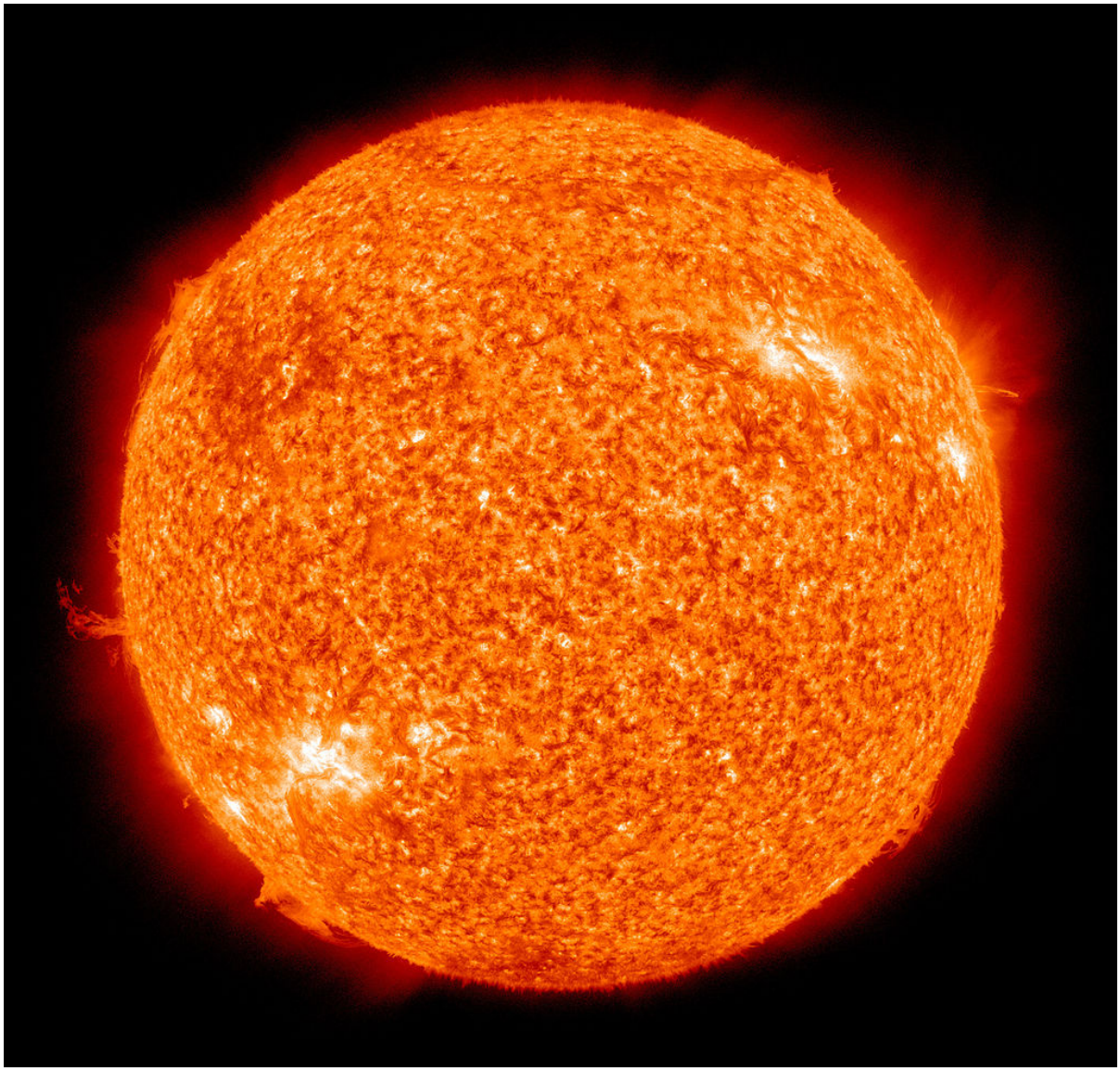

Figure 0.1: The Sun photographed in false-color at 304 angstroms by NASA's Solar Dynamics Observatory (SDO). Credit NASA

As the stars are known to the Night;
As the stars that shall be bright when we are dust,
Moving in marches upon the heavenly plain;
As the stars that are starry in the time of our darkness,
To the end, to the end, they remain
(Binyon,L.,1914).

CHAPTER 1

A more modern view of stars

Poets say science takes away from the beauty of the stars - mere globs of gas atoms.
I too can see the stars on a desert night, and feel them. But do I see less or more?
The vastness of the heavens stretches my imagination -
stuck on this carousel my little eye can catch one - million - year - old light.
A vast pattern - of which I am a part...
What is the pattern, or the meaning, or the why?
It does not do harm to the mystery to know a little about it.

R.P. Feynman

1.1 The beginning of stellar evolution

A star is a luminous celestial body held together by its own gravity, a sphere of plasma that shines thanks to the energy provided by thermonuclear fusion in its core to balance the energy loss at the surface. A couple of thousands years ago the first astronomers across the world tended to group the apparently immutable stars of the *heavens* into constellations. In spite of long time evidences of the non-immutability of the sky as the Chinese astronomers observed a short-lived new star in 185 AD (Fig.1.1), and of the *novae* from *De nova stella* by Tycho Brahe, still nowadays we can easily recognize the constellations named by ancient astronomers. Astronomers still group the multitude of stars, but now instead of classifying them according to their position in the firmament, scientists commonly group them according to their spectral class and magnitude in the so called Hertzsprung-Russel diagram (HR diagram). The HR diagram relates the luminosity (or magnitude) of a star to its surface temperature[1] (or color/spectral class), physical quantities strictly related to the characteristic of a star (age, mass, chemical composition, etc.). From the breakthrough of the discovery that most of the stars tend to be clustered in two distinct locations of the HR diagram (Russell 1914; Hertzsprung 1915), the main-sequence band and the red giants branch, scientist of the last century set the bases for "stellar evolution" as we know it now.

[1] the surface temperature is commonly called effective temperature, as the Stefan-Boltzmann law $L = 4\pi R^2 \sigma T^4$ applies at the surface of a star.

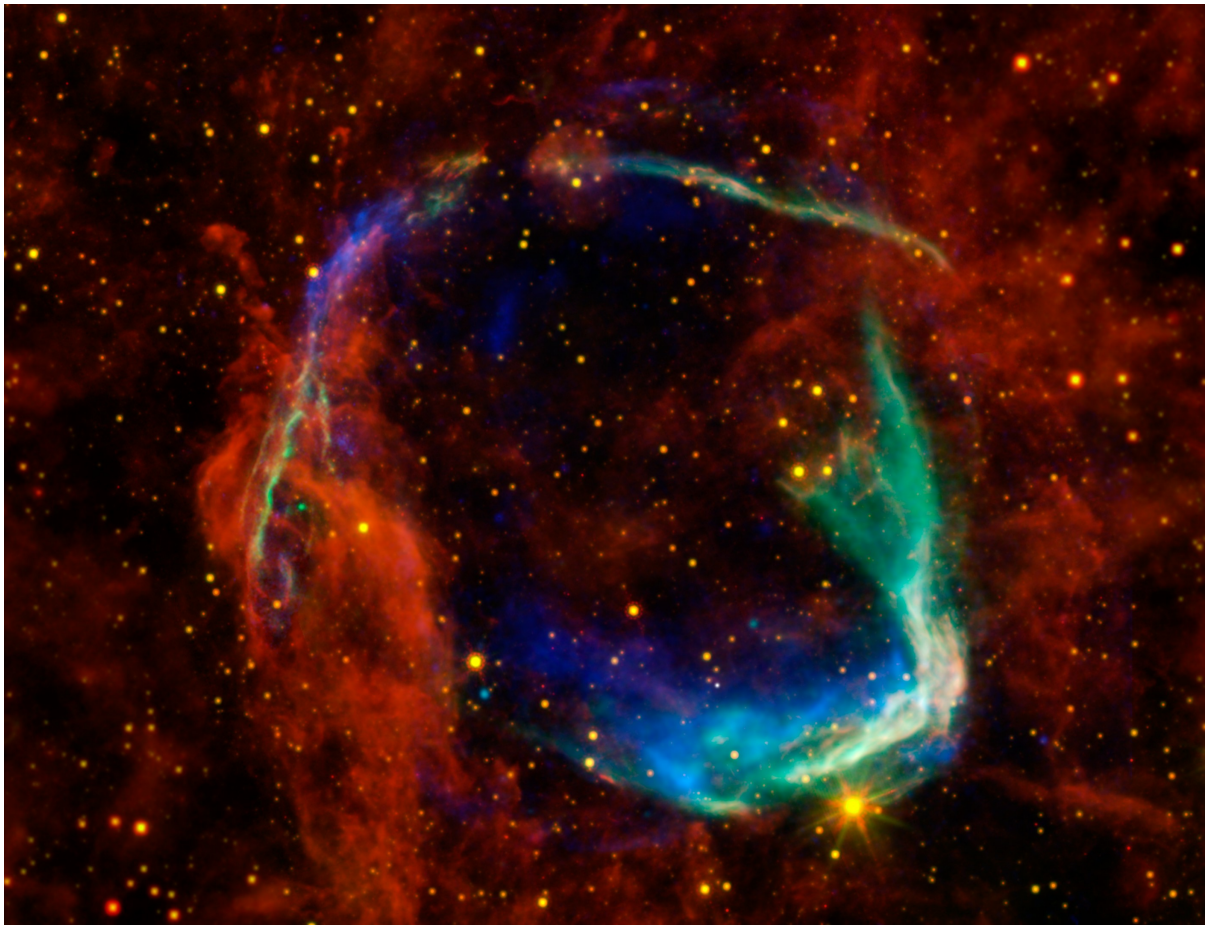

Figure 1.1: Infrared images from NASA's Spitzer Space Telescope and WISE are combined with X-ray data from the Chandra X-ray Observatory and ESA's XMM-Newton Observatory of the supernova remnants of RCW 86 (aka SN185).

1.2 Energy source and thermodynamic equilibrium

Stars are formed from clouds of material in the interstellar medium, mostly consistent of hydrogen and helium from the Big Bang nucleosynthesis, which contract under their own gravity. As the density of the contracting cloud drastically increases, temperature and pressure become high enough for quantum effects to lead to the ignition of thermonuclear fusion in the dense center of the cloud, i.e. a star is born. At first, thermonuclear fusion involves the lightest atoms by fusing 4 hydrogen atoms into a helium atom. As the rest mass of a helium atom is slightly smaller than the sum of its constituent nucleons, the theory of Relativity (Einstein 1916) tells us[2] that the fusion process is exothermic, i.e. the process releases energy. The nuclear reactions provide energy to a star during most of its life. The energy production in the hot, dense core counteracts the self-gravity of the plasma spheroid by setting a negative pressure gradient in its interior. When an equilibrium is reached between the force of gravity and the pressure gradient, the star is said to be in hydrostatic equilibrium. This is however not enough to guarantee the long lasting stability that we observe in stars, as one needs to introduce the concept of thermodynamic equilibrium. The classical macroscopic definition of thermodynamic equilibrium refers to a isolated

[2] As from $\Delta E = \Delta m\, c^2$ (Einstein 1916)

system where hydrostatic, chemical/nuclear, and thermal equilibrium are achieved, a condition closely related to the microscopic physics involved. With thermal equilibrium we refer to the situation in which the temperature within a system is spatially and temporally uniform. As the star needs to transport the energy which makes it shine from its core, a thermal gradient coupled to the pressure gradient has to be present. This implies that, globally, a star is not in strict thermal equilibrium, as it is not an isothermal system. However, the thermal gradient in the interior of a star is so small[3] that, locally, this approximation applies very well. As for the changes in chemical composition, these usually take place on a very long time-scale given the enormous mass involved and the high efficiency of the fusion process in supplying energy. Therefore one can conclude that each portion of a star is in a good approximation in local thermodynamic equilibrium, although globally stars can undergo phases of non-equilibrium with different time-scales[4](Kippenhahn & Weigert 1990).

1.3 Energy transport in stars

The fusion reactions in the core of the Sun release energy in the form of high energy photons. The energy released in the core of the Sun then takes of the order of 10^7 years to emerge at the solar surface, following the spectral energy distribution of a black body[5] (Mitalas & Sills 1992; Stix 2003). The energy transport processes taking place in the interior are of crucial importance in defining the structure of a star by defining the local temperature gradient. As already stated, a star needs to build a temperature gradient in order to have a net energy flux throughout its interior while preserving hydrostatic equilibrium. The transport processes effective in stars are mostly two (Rybicki & Lightman 1979): radiative transport and convection.

1.3.1 Radiative transport

The transport of energy via electromagnetic radiation is called radiative transport. This transport mechanism relies on the emission of photons in hotter regions and their absorption or scattering in slightly cooler regions. The radiative transport of energy is a diffusive process, i.e. the net movement of a quantity under a concentration gradient via random walk (opposite to bulk motion, Einstein 1906). The diffusive approximation for the radiative transfer holds when the mean free path of a photon is small compared to the scale at which the thermodynamical quantities change, as e.g. in the interior of a star. This process is governed by the opacity of the stellar matter, which is the coefficient defining the amount of intensity of radiation diminished when radiation travels through a medium of a certain density (Rybicki & Lightman 1979). The high number of scattering events thermalize the photons produced by the nuclear reactions, redistributing their energies in the form of the black body spectrum we observe at the surface. This allows to describe the power radiated from a star simply in terms of its temperature via the Stefan-Boltzmann law (Rybicki & Lightman 1979; Kippenhahn & Weigert 1990). However, given a temperature gradient, there is a limit to the amount of energy that can be transported by radiation in a star, and that is the so called Eddington limit (Eddington 1925; Langer 2012). This limit corresponds to a configuration in which the outward directed radiative acceleration equals the inward directed gravity:

$$\frac{\nabla P}{\rho} = -\frac{\kappa}{c} F_{rad} \tag{1.1}$$

[3] Small compared to the mean free path of a photon.
[4] Strictly speaking, a star is in *quasi*-thermodynamic equilibrium due to the continuous energy loss and chemical evolution.
[5] A black body is a ideal body which absorbs all the radiation, independently from the frequency, and re-emits it according to the Planck law.

where ρ is the density, κ is the opacity, c is the speed of light, ∇P the pressure gradient, and F_{rad} the radiative flux. In other words, this is the maximum luminosity that can be carried by radiation preserving hydrostatic equilibrium. The Eddington limit plays a key role in the physics of massive stars and relates to phenomena like e.g. turbulence or the upper limit for the initial mass of stars (de Jager 1984; Blomme et al. 1991; Langer 2012; Schneider et al. 2014; Jiang et al. 2015; Sanyal et al. 2015; Owocki 2015). This is because especially massive stars need to transport a great amount of energy from their interior (a flux up to 6 orders of magnitude higher than the energy flux within the Sun or more), and especially when the local temperature is not high enough to sustain a fully ionized plasma, stars can have troubles preserving hydrostatic equilibrium. The physics taking place in these extreme, radiation pressure dominated conditions is not yet fully understood.

1.3.2 Convection

In certain conditions, the temperature gradient defined by radiative transport may lead to a dynamically unstable configuration in which another energy transport mechanism is involved: convection (Fig.1.2). Convection is a generally efficient heat transfer process involving macroscopic bulk motion. It consists of upward and downward turbulent motion of material which stores heat and rapidly/dynamically transports it to another location as a consequence of the buoyancy force acting onto the convective eddies. The action of the buoyancy force on the convective eddies is important especially in presence of a steep temperature gradient. Buoyancy leads, strictly speaking, to local deviation from hydrostatic equilibrium, as large scale blobs of material are displaced in the zones unstable to convection (Schwarzschild 1992). Convective motion in stars is very turbulent, as the flow regime in convective zones is characterized by drastic property changes and stresses in pressure and flow velocity (Lighthill 1952; Landau & Lifshitz 1959). Hence the dynamic and kinematic of the convective regions is very complex and chaotic, as it is governed by the full set of multi-scale time-dependent Navier-Stokes equations (Landau & Lifshitz 1959; Maeder 2009). However, convection plays a fundamental role influencing the structure and the evolution of a star, as it can efficiently mix elements affecting the chemical profile of a star, it can rapidly transport energy and angular momentum, and it can perturb the layers of a star inducing oscillations (Kippenhahn & Weigert 1990; Goldreich & Kumar 1990; Canuto & Mazzitelli 1991; Stein & Nordlund 2001). The criteria for the establishment of convection can be written as:

$$L(r) > \frac{16\pi r^2 ac}{3\kappa\rho} T^3 \nabla T \tag{1.2}$$

with $L(r)$ being the local luminosity, r the radius, T the temperature, a the radiation constant, and ∇T the temperature gradient.

The inequality 1.2 shows that convection can usually take place within stars in two different conditions:

- in presence of a high local energy production as in a fully ionized plasma in the core of stars more massive than the Sun,
- in locations where the local temperature decreases to the point that partial recombination of some ionized atoms takes place (i.e. the outer cooler layers), increasing the opacity of matter which in turn reduces significantly the amount of energy that can be transported by the electromagnetic field.

The two configurations for the establishment of convection lead also to different regimes for convection: while in the core the high densities and the low opacities (given mostly by the electron scattering) lead to adiabatic - and therefore very efficient - transport of energy via convection, in the outer layers where the

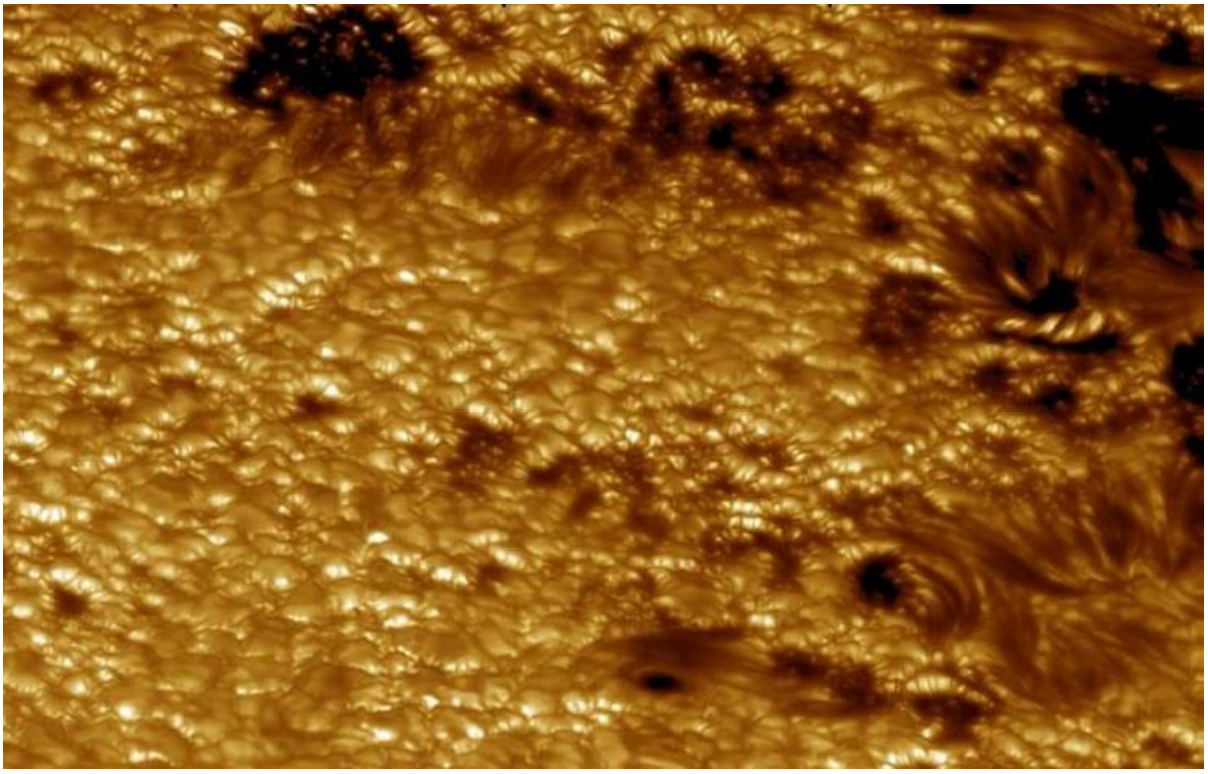

Figure 1.2: Close-up of granulation and sunspots on the limb of the Sun. Credit: G.Scharmer (ISP, RSAS) et al., Lockheed-Martin Solar & Astrophysics Lab

opposite is true, convection is often not easily able to transport the internal energy flux, especially if the flux is very high. In the latter regime in fact, the convective eddies - where the heat is stored - tend to lose part of their heat content on their path via radiative loss, leading to a more turbulent and vigorous convective motion (Böhm-Vitense 1958; Kippenhahn & Weigert 1990). The treatment of convection especially in non-adiabatic conditions is the Achilles' Heel of stellar evolution calculations, due mostly to the complexity of the phenomenon (Feynman 1963; Canuto & Mazzitelli 1991).

1.4 Outer layers

While the conditions in the core set the evolutionary stage of a star and its final fate (more about it in the next section), the conditions in the outer layers define how a star appears to an observer. This is also where numerous hydrodynamic instabilities can occur (e.g. convection, pulsations, etc.). The atmosphere is by far the major source of information we have an access to, since it is the location where the radiation we can observe is emitted. From the local physical conditions in the atmosphere one can derive effective temperature, gravity, chemical composition, etc.. of a star. It is therefore useful to introduce the basic concepts of envelope, atmosphere, and wind.

Envelope

The envelope can be qualitatively defined as the low density low temperature outer region of a star where the recombination of some elements takes place. Recombination/ionization of the different elements

happens at fixed temperature ranges, leading to a local increase of opacity compared to the pure electron scattering conditions (in jargon: a "bump" in opacity). For the interior of stars there are 3 major sources of opacities associated with the recombination of certain atoms, happening at well defined temperatures; these are (Iglesias & Rogers 1996):

- the hydrogen opacity bump associated with the recombination of hydrogen (and helium I), at T≈ 8000 K;
- the helium opacity bump associated with the recombination of helium II, at T≈ 40000 K;
- the iron opacity bump associated with the high number of atomic transitions of iron and iron-group elements at T≈ 160000 K.

The complex physics taking place in the envelope of the stars and associated with these drastic increase in opacity can trigger instabilities and considerably affect the structure of the outer layers. This is especially true if the layers are already dominated by radiation pressure, and if the radiative energy flux is close to the maximum amount that can be transported in a hydrostatic configuration, i.e. if the layers are close to the local Eddington limit.

The most important instability that can arise is the establishment of convective zones in the regions where the ionization of these elements takes place. As previously mentioned, in certain regions radiation might not be able to transport the whole energy flux from the interior of a star due to a high opacity. Thus convection can provide an extra contribution to the energy transport. However, in the low density environment of the outer layers of a star, radiative energy loss from the convective eddies during their path might make convection an inefficient mean to transport energy. In these conditions, common especially in the very massive and very extended stars, the star needs to readjust the structure of their outer layers in order to be able to transport its luminosity. It does it by reducing the slope of the temperature gradient and the local density, thus reducing and "spreading" the local opacity, which in turn leads to a very extended low density envelope. This phenomenon is called inflation, it is characteristic of stars having envelopes very close to the Eddington limit, and can significantly affect the position of these stars in the HR diagram (Langer 2012; Köhler et al. 2015).

Another important instability which can originate in the envelope is the pulsational instability, i.e. the periodic contraction and expansion of the star. The appearance of pulsations is strictly related to the opacity profile in the outer layers or to the presence of convection (Cox 1980). Pulsations have become a hot topic in the latest years, giving birth to a new branch of astrophysics: asteroseismology. The reason is that oscillations can travel from the interior of a star to its surface, carrying with them indirect informations on the otherwise veiled internal structure of a star (Miglio et al. 2008, see Sect.1.6.).

Atmosphere

In the earliest concept the HR diagram was relating the magnitude of a star to its spectral class, i.e. based on star's spectral characteristics. In fact the spectrum of a star exhibits plenty of absorption lines on top of the black body continuum, each of them fingerprint of a certain ion. The absorption lines are originated in the atmosphere of a star, i.e. in the outer region where radiation becomes free to escape in the surrounding space and consequently can be observed. Shape and strength of the absorption lines are great diagnostic tools to determine the stellar parameters (Gray 2005). In fact the compared strength of the lines indicates the relative abundances and the ionization states of the different ions. This, together with the knowledge of atomic physics, gives precise estimates of the surface temperature of a star. Moreover, as in the last century the tools to investigate the atmosphere of stars have significantly improved, scientists have been able to use the line profile shape as an indicator also of the surface gravity, the surface pressure, the mass

loss rate, and the projected surface rotational velocity of a star. This is done mostly by investigating the shift and broadening of the absorption lines (Gray 2005). Some of the main sources of broadening of spectral lines of stars are local broadening mechanisms as the natural broadening (due to the Uncertainty Principle), the pressure broadening (due to particle collisions), the Stark broadening (due to the presence of electric fields), and the thermal broadening (due to the velocity distribution of the particles). On top of this there can be non-local broadening mechanisms due to macroscopic phenomena at the surface, such as the rotational broadening (due to the Doppler effect as the star rotates) and pulsational broadening (due to a velocity field appearing at the surface).

Stellar wind mass-loss

A star does not only lose energy from its surface in the form of radiation, but also mass and kinetic energy in the form of a stream of particles, the stellar wind (Parker 1958). Stellar winds are an outflow of material from a star which plays a major role especially in massive star evolution (Lamers & Cassinelli 1999). In fact, a massive star can lose up to half of its initial mass via stellar winds, thus enriching the interstellar medium and influencing the structure of the outer layers (Chiosi & Maeder 1986), not mentioning the interaction between the solar wind and the magnetic field of our planet. The key concept behind mass loss by stellar wind is that material from the surface can gain enough kinetic energy to overcome the gravitational potential of a star. This can happen in numerous ways, from magnetic reconnection to stellar pulsations, from sound or Alfven waves to pressure gradients and momentum transfer from the radiation field of the star. The latter winds are called radiation driven winds, and are the stellar winds with the most important effects. They are found in massive stars driving very high mass loss rates which do not only influence their evolution, but strongly affect their observational appearance. In the very outer layers of extended and massive stars, in fact, the high radiation pressure implies that those layers are poorly bounded to the star. Therefore material can easily gain enough kinetic energy to overcome the gravitational potential, in turn leading to strong stellar outflows. The outflow can also show the appearance of instabilities as, e.g., localized density inhomogeneities or violent eruptive mass loss events (Fig.1.3).

1.5 Stellar evolution

A star spends most of its life in a phase of equilibrium, converting hydrogen into helium and irradiating into the outer space almost the same amount of energy that is produced in the core per unit time. This is the main-sequence phase, a relatively long and quiet phase which defines the most populated region in the HR diagram (Fig.1.4), and it is the phase the Sun currently is in. Once the hydrogen fuel in the core is exhausted, the core of the star is composed mostly by the ashes of the previous burning process, i.e. helium, and lacking energy production, it contracts while the outer layers of the star expand. During the contraction gravitational energy is released, heating up the inert core until another fusion process starts to take place at higher temperature. The star has reached the red giant phase, where its main source of energy becomes the fusion of helium into carbon and oxygen atoms[6]. This new phase of equilibrium has a shorter life compared to the main sequence (approximately a tenth of it), but defines the second most populated region in the HR diagram. The following evolution instead is very rapid.

We now need to define the most important parameter for the life of a star: its mass. Depending mostly on its initial mass, the final stages of the life of a single star can be divided in to three categories:

[6] however also the hydrogen burning is present in a shell surrounding the core and contributes significantly to the energy production.

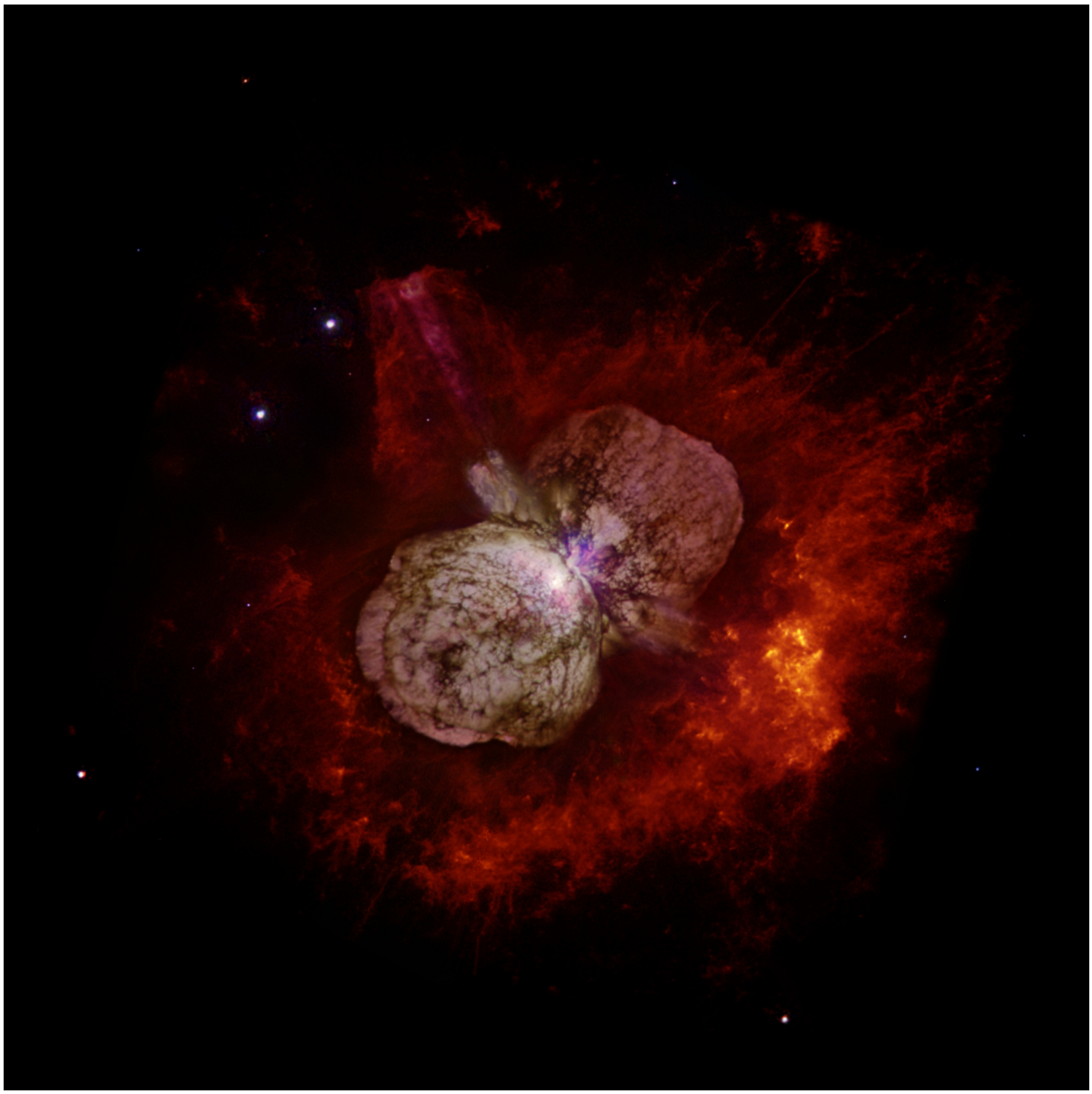

Figure 1.3: Hubble Space Telescope image showing the bipolar Homunculus Nebula which surrounds the very massive binary system Eta Carinae

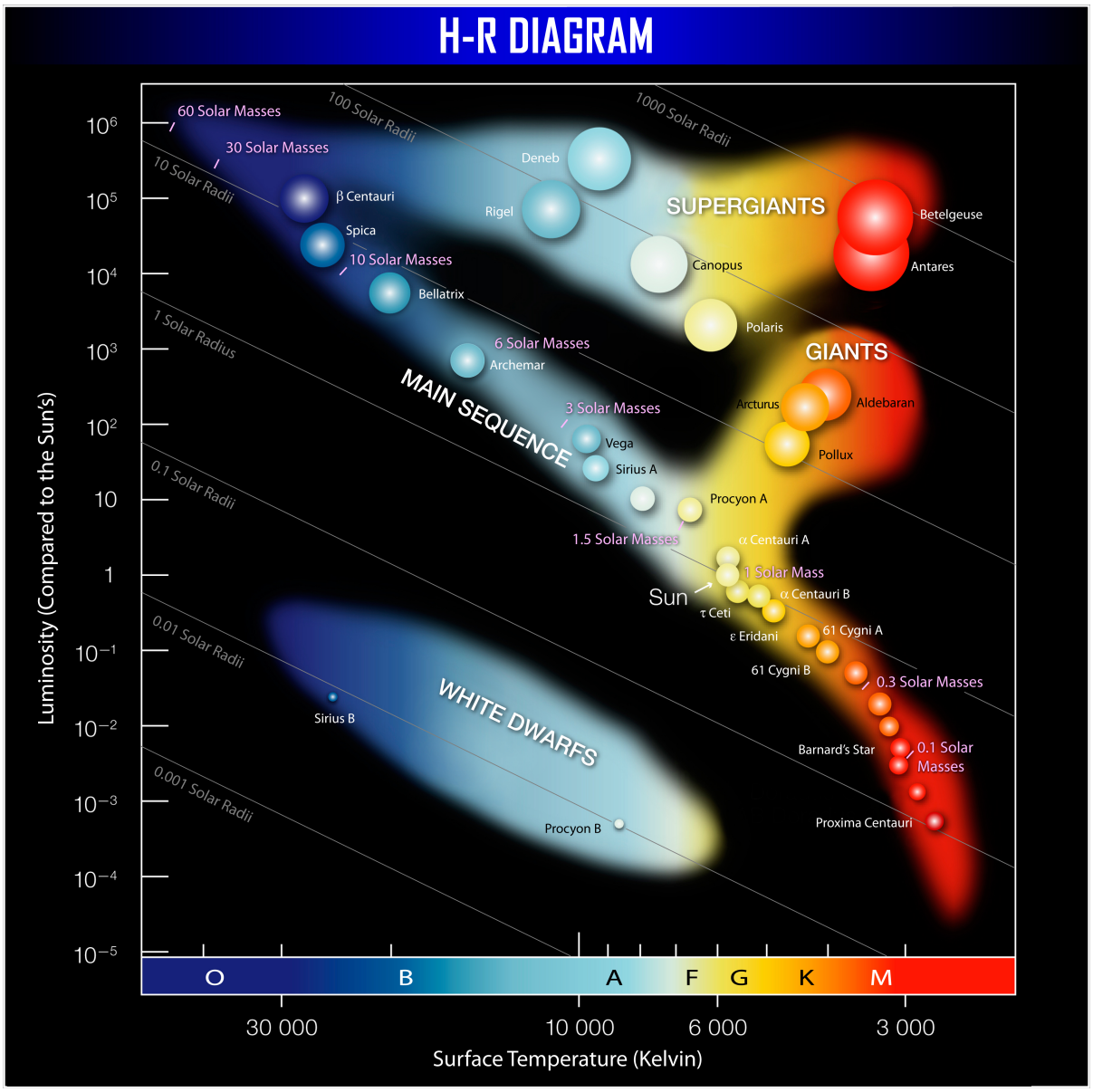

Figure 1.4: HR Diagram showing additionally names of stars in the Galactic neighbourhood. Credit: ESO

1.5.1 Low & Intermediate Mass Stars

Low mass stars are defined as stars with initial mass between 0.08–2 $M_\odot$. These stars spend a long ($\approx 10^{10}$ years or more) part of their life in the main-sequence phase, burning H into He. As they deplete the H content in their central core, the burning moves into a shell surrounding the inert H-exhausted He ashes of the core. In this phase the isothermal core contracts while the outer layers expand and cool significantly. The star moves to the red giants part of the HR diagram at low ($\approx 3 - 7$kK) surface temperatures. Owing to the contracting core, the densities increase so much that quantum mechanical effects become important at a macroscopic level and an extra pressure arises, the electron degeneracy pressure (Landau 1938; Fermi 1956), slowing the further contraction. If the initial mass of the star is higher than 0.8 $M_\odot$ [7], the release of gravitational energy is able to increase the temperature of the core until the He burning process ignites abruptly. This ignition is called core He-flash, and with it, helium starts to be converted via thermonuclear fusion into carbon and oxygen. Once also this nuclear fuel is exhausted, there is not enough gravitational energy for the temperature to increase to the point where carbon and oxygen burn too. When nuclear fusion turns off the outer layers are expelled into the outer space[8], leaving behind the naked, hot C-O core to form a very compact cosmic "diamond" sustained by the electron degeneracy pressure, i.e. a white dwarf.

Intermediate mass stars (2–8 $M_\odot$) have higher central temperatures and consequently higher energy production rates in their central regions. They experience a shorter main-sequence phase compared to the lower mass stars, with the hydrogen-exhausted helium core which does not contract enough for the quantum mechanical degeneracy pressure to arise before helium burning ignites. Therefore the helium core does not experience a flash, but rather a smooth and stable helium ignition. However the electron degeneracy pressure becomes important as these stars are left with a carbon-oxygen core. The end product of stars in this initial mass range are also white dwarfs.

1.5.2 Massive Stars

Massive stars are rare objects, given that most of the stars seem to be born with mass approximately 0.8 $M_\odot$ (Salpeter 1955). However, they are key agents in the evolution of galaxies, as they trigger star formation with their intense outflows (Prialnik 2000; Deharveng et al. 2010; Elmegreen 2012), they emit great amounts of ionizing photons which probably played an important role in re-ionizing the early Universe (Lu et al. 1998; Gnedin 2000), and they are the main source of heavy elements polluting the interstellar medium (Burbidge et al. 1957), not to mention that their death coincides with the most powerful events in the Universe (Yoon & Langer 2005).

Qualitatively, the early phases of the evolution are similar to those of intermediate mass. During the main-sequence phase, these stars appear as the most luminous and hot stars, although the duration of this phase is considerably shorter compared to that of the lower mass stars (i.e. approximately 10^7 years), as their higher self-gravity requires much higher energy production rates. The radiation pressure dominates the equation of state in their interior, and they can undergo all the burning stages until iron with a non-degenerate core. This means that, for relatively short time in the very late stages of the evolution of these stars also carbon and oxygen can experience thermonuclear fusion, synthesizing elements as heavy as iron. The subsequent nuclear transmutation of iron is a endothermic process (Maeder 2009), because the iron atom has the highest binding energy per nucleon. Therefore nuclear fusion can not provide the energy necessary to prevent the collapse of the star. Moreover, the temperature of the degenerate iron

[7] Stars less massive than 0.8 $M_\odot$ are not expected to undergo a helium burning phase, however their main-sequence evolution is longer than the actual age of the universe, therefore there are few possibilities to observe and constrain them.

[8] forming the so called Planetary Nebula, which anyhow has no connection to planets.

core becomes sufficiently high (i.e. $\approx 10^9$ K), that the photons of the radiation field can be so energetic that scattering with the iron atoms induces photodissociation[9] before the iron burning process could take place, triggering the rapid collapse of the star. As the battle between gravity and nuclear energy production is won by the first, if the initial mass of the star is between 8 and 25 $M_\odot$, the star's destiny is to collapse to form a very high density core in which protons and electrons are forced to be so close together that they can merge, similarly to what happened in the early stages of the Universe. This process forms a compact object known as neutron star. Once the neutron star is born, an enormous number of neutrinos are produced and released, interacting with the still infalling/imploding star. This very high neutrino flux triggers the ejection of the remnants of the star in a colossal explosion, the supernova. As much as the energy produced during the whole life of a star is released in few seconds during the formation of a neutron star, leading to luminosities associated with the supernova event that can outshine an entire galaxy for few months.

Although the evolution of massive stars can be very sensitive to metallicity, rotation, magnetic fields, and binarity, a key feature of massive stars is certainly their high mass loss rate by stellar wind. Stellar winds can lead the star to lose an important fraction of their mass already starting from the main sequence phase, affecting significantly their evolution in the HR diagram (Chiosi & Maeder 1986). In fact the most massive stars tend to be depleted of part of their outer layers due to the intense winds, exposing the hotter internal material previously processed by the core (and brought up to the surface by convection). Consequently, the mass loss favours an evolution that does not reach low surface temperatures, but rather they move toward higher surface temperatures already during their main sequence evolution, populating the region in the HR diagram of the Wolf-Rayet class of stars. This is the case for stars bigger than $\approx 25\,M_\odot$. However the inner core is almost insensitive to the high mass loss rate.

All the massive stars experience all the burning stages of elements heavier than the hydrogen, until a dense iron core is formed. However if the mass of the star is bigger than $\approx 25\,M_\odot$, the neutrons which form in the core can not provide enough degeneracy pressure to counterbalance the gravitational force, and matter reaches an exotic state due to the immense density, forming what is known as a black hole. The formation of a black hole releases as well an enormous amount of energy which can power the most energetic phenomena in the universe, e.g. a Gamma-Ray Burst.

Wolf-Rayet Stars

Wolf-Rayet (WR) stars are hot, highly luminous stars experiencing a strong mass loss by stellar wind (Fig.1.5). This phenomenon is characteristic of the late stages of the evolution of very massive stars, where the spectra of these stars show broad emission lines of highly ionised gas (see Fig.1.6). The emission lines arise thanks to the extended partially optically thick outflow from these stars, while the broadening of the lines is due to Doppler shift as these outflow can reach speed as high as 3000 km/s (Lamers & Cassinelli 1999). The high wind densities veil the hydrostatic subsonic part of the WR stars from direct observation, leading to uncertain stellar parameters.

The very high mass loss rates take place due to the absorption of the UV photons (and their momenta) from the radiation field by the high number of absorption lines of the elements in the atmosphere. This process is enhanced by the fact that the expanding atmosphere has a velocity gradient which allows the atoms to "see" the radiation from the photosphere as redshifted. As a result the expanding outflow can absorb unattenuated radiation, making the radiative acceleration from the lines a very efficient driving mechanism.

Moreover, the strong and fast winds from this class of stars very close to the Eddington limit also show

[9] photodissociation is a reaction in which a photon is sufficiently energetic to sciss a nucleus or a chemical compound.

Figure 1.5: Hubble Space Telescope image showing the nebula M1-67 surrounding the Wolf-Rayet star WR124.

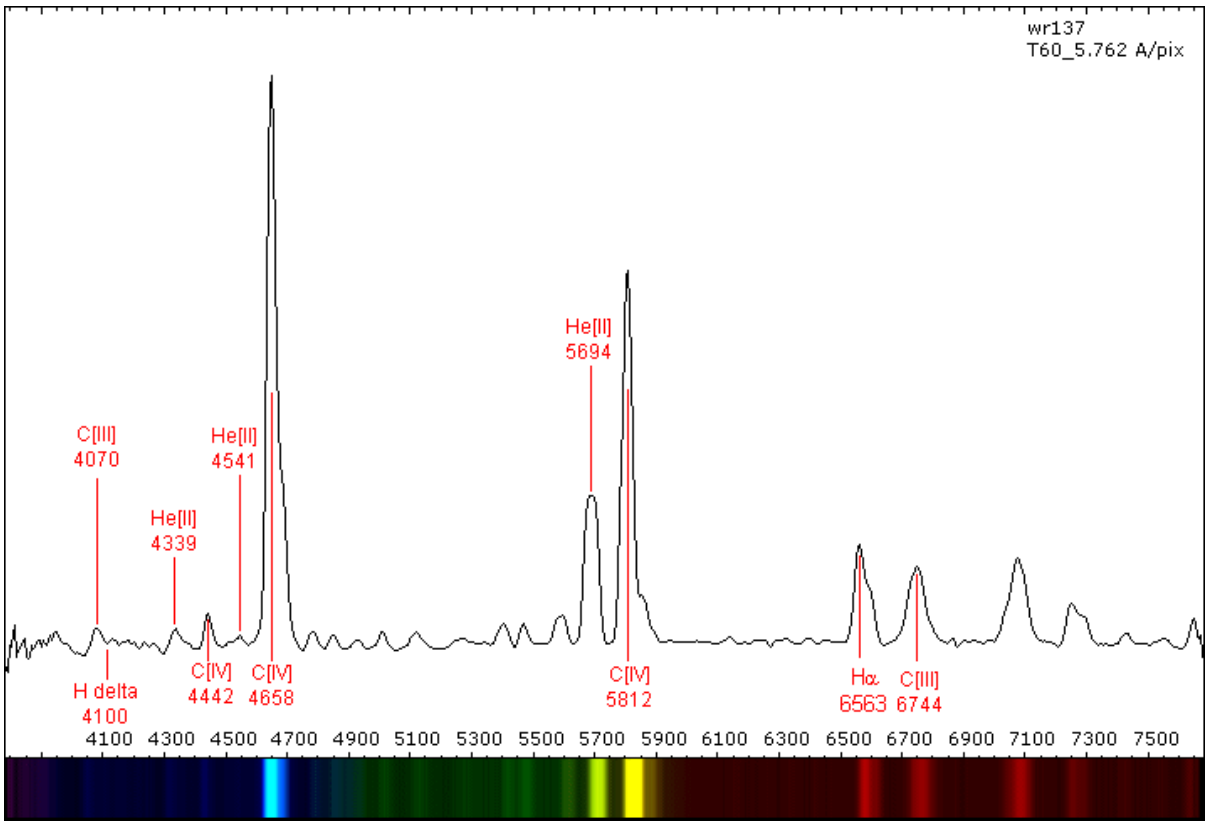

Figure 1.6: Optical spectrum of Wolf-Rayet star WR137, of WC7 spectral type. Spectrum taken at T60, Pic du Midi.

different kind of instabilities. The two most prominent kind of instabilities are:

- the corotating interaction regions, i.e. large scale spiral-like streams of matter corotating with the WR star (Cranmer & Owocki 1996; Dessart & Chesneau 2002) and inducing periodic variability,
- the clumping, i.e. a high number of randomly distributed density inhomogeneities in the outflow of WR stars, phenomenologically associated to the presence of sub-peaks in the emission lines (Moffat et al. 1988; Lépine & Moffat 1999).

Based on the dominance of certain broad emission lines in their spectra, WR stars can be classified as (Conti 1979; Groh et al. 2013):

- WN stars, i.e. WR stars with spectra dominated by the emission lines of nitrogen. This class can be further subdivided into WNE and WNL (or WNh), with the first referring to WR stars thought to correspond to stars in the core helium burning stage, while the latter are WR stars expected to be still in the main-sequence phase. The high nitrogen abundances are a result of the exposure of the nuclear products of the hydrogen burning[10].
- WC stars, i.e. WR stars with spectra dominated by carbon lines. The carbon exposed at the surface is thought to be the ashes of the helium burning process.

[10] via CNO cycle, the nuclear burning process taking place in the core of stars starting from those slightly bigger than the Sun.

- WO stars, i.e. WR stars with spectra dominated by oxygen lines. The oxygen is expected to be produced in the late stages of the helium burning processes.

1.6 Stellar pulsations

Variability in the light from a star is a phenomena known since ancient times. However the fact that these variations are associated with intrinsic changes in the properties of a star and not always due to, for example, an eclipsing companion, is a recent result. In fact we now know that stars can pulsate, i.e. the luminosity fluctuations correspond to changes in radius caused by the expansion and contraction of the star (Cox 1980). These oscillation may arise due to different sources of instabilities, and they are the result of the attempt of the star to restore equilibrium. The most well known class of pulsating stars are the Cepheids and the RR Lyrae, as these classes of stars pulsate radially with well-defined amplitudes, making them great distance indicators (Cox 1968, 1980). However, stars show also non-radial oscillations at many different angular degrees, although in general non-radial oscillations tend to have smaller amplitudes. These oscillations are due to waves, i.e. disturbances that travel through a medium from one location to another, in some cases transporting energy as they move. At first we can define two different kinds of waves (Landau & Lifshitz 1969; Balona 2010):

- Running or travelling waves: a perturbation in a medium that changes position as a function of time and with consequent transport of energy.
- Standing or stationary waves: a wave in a medium in which at each point the wave has constant amplitude as result of interference (thus occuring only at certain frequencies).

As oscillations are due to perturbations of thermodynamical quantities of a system, the system will attempt to restore equilibrium. Depending on which force is acting to restore equilibrium, for stellar purposes waves can be categorized as:

- pressure waves: acoustic waves in which the restoring force is due to the pressure;
- gravity waves: waves in a stratified medium for which the restoring force is due to the buoyancy or gravity;
- surface waves: waves at the interface between two mediums, the restoring force is gravity.

Having defined the main properties of oscillations, we may ask which are the main driving mechanisms exciting stellar oscillations. They can be subdivided into three main categories (Cox 1980; Saio 1993):

- κ mechanism: oscillations excited by a thermal mechanism similar to the Carnot cycle, acting when the opacity of stellar matter increases with increasing temperature and density, causing the local heat flow to be partially blocked, with the layers gaining thermal energy and consequently forcing the star to expand.
- ϵ mechanism: oscillations excited by the modulation of the nuclear reaction rates in the core, acting when the compression of a layer undergoing energy production induces an increase in the reaction rates, in turn forcing the star to expand back and oscillate around the equilibrium condition;
- Stochasic excitation: excitation of oscillations as consequence of the turbulent motion in the convective zones which, thanks to stresses and rapid fluctuation in the thermodynamic quantities, can excite perturbations.

It has been theorized that another driving mechanism of non-thermal origin should give rise to pulsations in the low density envelopes of very massive stars. These pulsations are called *strange* mode pulsations (Glatzel et al. 1993), and as suggested by their name, their origin is unclear. However, up to now there is no clear evidence for their existence (Chené & Moffat 2011).

1.7 This thesis

In order to advance our understanding of stars, in this thesis we focus on the instabilities which can arise in the outer layers of stars. Of particular importance is the appearance of instabilities in the extended envelopes for which radiation is not easily able to transport the whole luminosity of the star and convection tends to be inefficient in transporting energy. Some observational phenomena such as extra broadening of the spectral lines, emission sub-peaks in the spectra of massive stars, and non-radial pulsations, are related to a velocity field at the stellar surface, i.e. to macroscopic surface motion. Here we investigate whether a connection could exist between the conditions in the deep convective envelopes and surface motion.

The main tool adopted to model the internal structure of stars at different stages of their evolution is a 1D Lagrangian hydrodynamic stellar evolution code[11] (Heger et al. 2000; Petrovic et al. 2006; Yoon et al. 2006; Brott et al. 2011; Köhler et al. 2015). The stellar structure is computed based on a set of differential equations, namely the conservation laws for mass, momentum, and energy, coupled to the energy transport equation. The radiative transport equation under the assumption of local thermodynamic equilibrium defines the temperature gradient in radiative zones, while the mixing length theory (Böhm-Vitense 1958) is adopted to account for non-adiabatic convection. On top of this, in order to describe the chemical evolution of the star, another set of differential equations define the nuclear reaction rates and the changes for the most abundant elements (Kippenhahn & Weigert 1990).

In Chapter 2, 3, and 4, we try to answer the questions: when and where in a star can convection be an inefficient mechanism to transport energy? When can the turbulent motion of the convective eddies lead to an important contribution to the total pressure? Can this extra contribution to the total pressure lead to significant structural differences? Is the vigorous convective motion in the sub-surface convective zones related to surface motion? We investigate these aspects of the physics of stars by modifying the hydrodynamic stellar evolution code to account for the extra turbulent terms, and we investigate the consequences by comparing the newly computed calculations to previous ones (Brott et al. 2011; Grassitelli et al. 2015b,a). This is done in the case of hot and massive Galactic stars, as well as low and intermediate mass late type stars, and also as a function of metallicity while considering stellar models for the stars in the Magellanic Clouds.

Numerical calculations per se are a great tool, but they accomplish their main purpose when compared to (and are able to reproduce) observations. Therefore, we then compare the fractional contribution of the turbulent pressure to the equation of state to the appearance of surface motion in the atmosphere of a vast sample of stars spread across the HR diagram, some of which from the Galaxy, some others instead from the Magellanic clouds (Dufton et al. 2006; Carney et al. 2008; Fossati et al. 2011; Doyle et al. 2014; Simón-Díaz 2015). We also compare the strength of the turbulent motion to a class of poorly understood pulsating stars, the γ-Doradus class of pulsators, through comparison of the turbulent pressure fraction with their observational instability strip in the HR diagram (Bruntt et al. 2008; Catanzaro et al. 2011; Fossati et al. 2011; Tkachenko et al. 2012; Bradley et al. 2015; Van Reeth et al. 2015).

[11] *Stellar evolution codes are a lot like religions: there are many of them to choose from, they possess many similarities, and it is not obvious which of them (if any) is correct. (Stancliffe et al. 2016)*

In Chapter 5 we instead focus on the late stages of the evolution of massive stars, investigating the envelopes of the hydrogen-poor WNE Wolf-Rayet stars. Thanks to our numerical calculations we determine the conditions in the outer hydrostatic layers of these stars while posing attention to the effects of convection at the base of the wind. We investigate whether convection can induce a velocity field able to trigger the formation of small scale structures in the dense stellar winds (Moffat et al. 1988). Moreover, given that theoretical studies (Glatzel et al. 1993; Saio 2009) predict the appearance of pulsations in the radiation dominated envelopes close to the Eddington limit of Wolf-Rayet stars, we examine the interplay between these pulsations and the high mass loss by stellar wind characteristic of these stars. We then compare our predictions for the behaviour of the induced velocity field, as well as for the number of density inhomogeneities arising, to a set of observationally derived parameters indicating the variability of the spectral lines originated in the wind as expected from small scale structures, in order to find observational support.

CHAPTER 2

Observational consequences of turbulent pressure in the envelopes of massive stars

L. Grassitelli[1], L. Fossati[1], S.Simón-Díaz [2,3], N. Langer[1], N.Castro [1], D. Sanyal[1]

[1]Argelander-Institut für Astronomie, Universität Bonn, auf dem Hügel 71, 53121 Bonn, Germany
[2]Instituto de Astrofísica de Canarias, 38200 La Laguna, Tenerife, Spain
[3]Departamento de Astrofisica, Universidad de La Laguna, 38205 La Laguna, Tenerife, Spain

The Astrophysics Journal Letters 2015, 808L, 31G

Abstract: The major mass fraction of the envelope of hot luminous stars is radiatively stable. However, the partial ionisation of hydrogen, helium and iron gives rise to extended sub-surface convection zones in all of them. In this work, we investigate the effect of the pressure induced by the turbulent motion in these zones based on the mixing length theory, and search for observable consequences. We find that the turbulent pressure fraction can amount up to $\sim 5\%$ in OB supergiants, and to $\sim 30\%$ in cooler supergiants. The resulting structural changes are, however, not significantly affecting the evolutionary tracks compared to previous calculations. Instead, a comparison of macroturbulent velocities derived from high quality spectra of OB stars with the turbulent pressure fraction obtained in corresponding stellar models reveals a strong correlation of these two quantities. We discuss a possible physical connection, and conclude that turbulent pressure fluctuations may drive high-order oscillations, which — as conjectured earlier — manifest themselves as macroturbulence in the photospheres of hot luminous stars.

2.1 Introduction

Massive stars are of key importance for the enrichment of the interstellar medium (Kobayashi et al. 2006), for regulating star formation (Mac Low & Klessen 2004), and as progenitors of supernovae and gamma ray bursts (Langer 2012). However, various physical processes acting in massive stars are as yet not well understood, therefore preventing the current stellar models to self-consistently explain several general observational properties, such as the mass-discrepancy (Herrero et al. 1992; Markova & Puls 2015), the presence of the Humphreys-Davidson (HD) limit (Humphreys & Davidson 1979), and the position of the terminal-age-main-sequence in the HR diagram (e.g., Vink et al. 2010; Castro et al. 2014). Radiation pressure dominated layers, envelope inflation, clumpy stellar winds, and dynamical instabilities are features which commonly occur in these objects, but which are not yet thoroughly investigated. Some of these phenomena have been connected to the presence of turbulent motions in the outer layers (e.g., de Jager 1984; Cantiello et al. 2009). Despite its simplicity, the mixing-length theory (MLT, Böhm-Vitense 1958) for convection has been very successful in describing the main features of non-adiabatic turbulent stellar envelopes (e.g., Trampedach et al. 2014). However, the MLT is expected to have shortcomings when the convective velocities approach the speed of sound, as it is expected in the envelopes of very luminous stars (Sanyal et al. 2015). In particular, it has been argued by de Jager (1984) and Maeder (2009) that turbulent pressure may become important in this situation. It is the aim of the present paper to discuss the role of turbulent pressure in the envelopes of massive stars, investigate its effects on the stellar structure, and focus on its potential observational signatures.

2.2 Method

We use the Lagrangian one-dimensional hydrodynamic stellar evolution code BEC (Heger et al. 2000; Petrovic et al. 2005; Brott et al. 2011) for computing massive star models. It treats convection following the MLT with a mixing-length parameter of $\alpha = 1.5$ (Brott et al. 2011). The opacity of stellar matter is interpolated from the OPAL opacity tables (Iglesias & Rogers 1996), and mass-loss by stellar wind is adopted following the prescription of Vink et al. (2001).

We modified the BEC code in order to include the turbulent pressure term in the stellar envelopes, in particular in the convective zones associated with the iron opacity peak (FeCZ), and with the partial ionisation of helium (HeCZ), and hydrogen (HCZ). We neglect the turbulent pressure in the convective core, where it is typically more than 7 orders of magnitude smaller than the ideal gas pressure. We included the turbulent pressure $P_{\rm turb}$ and the turbulent energy density $e_{\rm turb}$ in the momentum, energy transport and energy conservation equations, respectively, following (Canuto & Mazzitelli 1991; Jiang & Huang 1997; Stothers 2003; Maeder 2009; Trampedach et al. 2014):

$$P_{turb} = \zeta \rho v_c^2 \quad , \quad e_{turb} = \frac{3}{2}\frac{P_{turb}}{\rho}, \tag{2.1}$$

where ρ is the local mass density, ζ is a parameter chosen to be $\zeta = 1/3$ for isotropic turbulence (Stothers 2003; Maeder 2009), and v_c is the local convective velocity. As the convective velocities approach the local sound speed, we limit the convective velocities to this value, i.e.

$$v_c \leq c_s \quad , \quad c_s^2 = \frac{k_B T}{\mu m_H} = \frac{P_{gas}}{\rho}, \tag{2.2}$$

where T is the local temperature, k_b is the Boltzmann constant, μ is the mean molecular weight, and m_H is the proton mass. Here, we use the isothermal sound speed, as the layers under consideration

are characterised by a small ratio of the local thermal-to-dynamical time scale ($\tau_{th}/\tau_{dyn} < 1$). As a consequence of Eq.2.2, the turbulent pressure in our models can not exceed a value of one third of the local gas pressure.

2.3 Results

We computed a set of stellar models and stellar evolutionary tracks for non-rotating stars with Galactic metallicity in the initial mass range 7–80 $M_\odot$, including the physics described in Sect. 2. All input and physics parameters were chosen as in Brott et al. (2011).

2.3.1 Evolutionary Tracks

The evolutionary tracks of our newly computed models are plotted in Fig. 2.1 and superposed to those obtained by Brott et al. (2011). Throughout most of the evolution, the effect of turbulent pressure and energy on the luminosity and the surface temperature of the models is small, such that our new evolutionary tracks nearly coincide with those from Brott et al. (2011). According to the colour scheme in Fig. 2.1, which indicates the maximum fraction of turbulent pressure inside the stellar models, the HR-diagram can be roughly divided into three areas: the hot ($T_{\rm eff} > 10^4$ K) and luminous ($\log(L/L\odot) > 4.5$) stars, the cool stars ($T_{\rm eff} < 10^4$ K) of any luminosity, and the hot stars with $\log(L/L\odot) < 4.5$.

In the latter regime, the turbulent pressure does not exceed a fraction of the total pressure of a few tenths of a percent anywhere inside the stellar models. On one hand, the iron opacity peak in these models is located deep inside the envelope in nearly adiabatic layers, which leads to relatively low convection velocities. On the other hand, the models are too hot to contain a hydrogen ionisation zone. Finally, they do show a HeII partial ionisation zone close to the surface, which is, however, not vigorous enough to play a significant role (Cantiello et al. 2009).

In the cool supergiant region, the turbulent pressure fraction inside the star can be very significant. The maximum value is typically 25–30%, while the highest possible value, 33%, is reached for the most luminous models. The computed transonic convective velocities, of the order of 20–30 km/s, arise in the HCZ very close to the surface, where high opacities induce high local Eddington factors, density inversions, and high degrees of superadiabaticity (Sanyal et al. 2015). Such a high turbulent pressure fraction is possible here since ideal gas pressure is by far the dominant contribution to the total pressure in the envelopes of the cool supergiants. Even though a significant fraction of the total pressure arises from the turbulent motion, the evolutionary tracks are only shifted by few tens of Kelvin towards lower temperatures, compared to the tracks without turbulent pressure, which corresponds to a radius increase by a few percent. This is due to the fact that the region which contains high turbulent pressure contains very little mass (see below).

In the hot and very luminous stars, the turbulent pressure can account for up to ~5% of the total pressure. The evolutionary tracks are not significantly different from those of Brott et al. (2011), showing displacements of the order of hundreds of Kelvin towards lower effective temperatures. Turbulent pressure becomes more important as the stars expand during their main sequence evolution, as the convective velocities increase. It achieves a maximum in the O supergiant regime, and then decreases in the B supergiant regime as the iron opacity peak moves deeper inside, but turbulent pressure remains significant for surface temperature above ~10 000 K. The maximum turbulent pressure in these models occurs within the FeCZ, where high local Eddington-factors are achieved, giving rise to envelope inflation and density inversions (Sanyal et al. 2015). It does not reach as high fractions as in the cool supergiant because of the predominance of radiation pressure in the hot star envelopes.

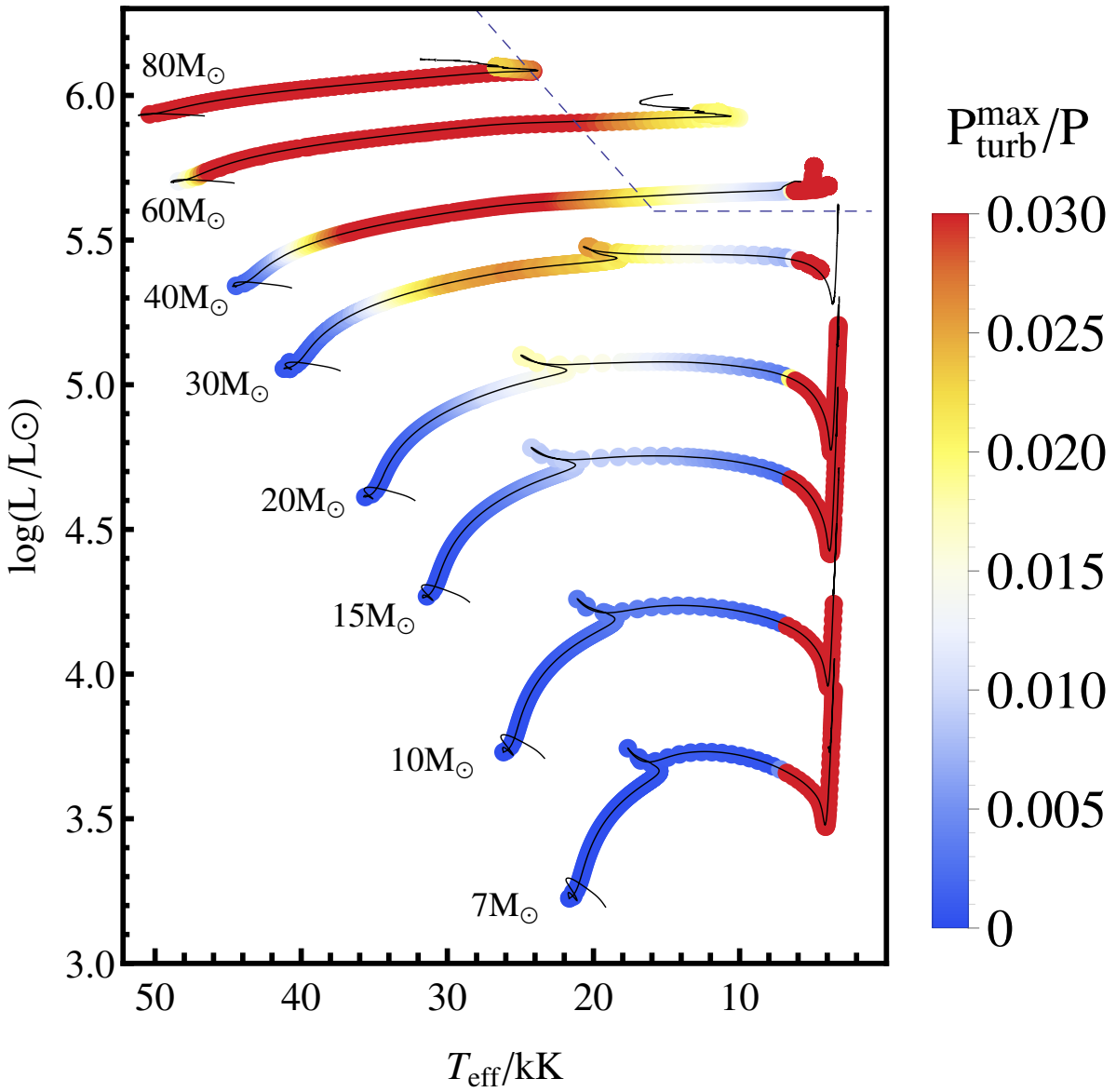

Figure 2.1: Stellar evolution tracks calculated including turbulent pressure and turbulent energy density, indicated by colored dots. Superposed are the tracks by Brott et al. (2011) (black lines). The colour indicates the maximum fraction of turbulent pressure occurring within each stellar model (see color bar to the right), where fractions above 3% are indicated in red. Stellar models at $T_{\rm eff} < 10$ kK coloured in red show contributions from $P_{\rm turb}$ up to $\approx 33\%$ and hot luminous OB stars coloured red up to $\approx 5\%$. The stellar masses next to the tracks indicate the initial mass of the models. The dashed line indicates the position of the HD-limit (Humphreys & Davidson 1979).

2.3.2 The structure of the outer layers

Following the results shown in Sec 3.1, we investigate the structure of the 20 $M_\odot$ and 60 $M_\odot$ models in more detail. Figs. 2.2 and 2.3 show the relative fraction of the turbulent pressure as function of the optical depth in the stellar envelopes of both models throughout the evolution.

In the 20 $M_\odot$ model (Fig. 2.2), we find that for $T_{\rm eff} \geq 10^4$ K the turbulent pressure fraction has its maximum in the FeCZ, located at an optical depth of $\log(\tau) \approx 2.5 - 4$. The turbulent pressure fraction is about 1.8% at $T_{\rm eff} \simeq 25\,000$ K, and the FeCZ moves deeper inside the star as the stellar model expands during its evolution. Once the stellar model reaches effective temperatures well below 10 000 K, the HCZ arises. This convective region, within which the maximum turbulent pressure fraction arrives at about 25–30%, reaches the stellar surface in stellar models with $T_{\rm eff} < 8000$ K, and covers an extended range of optical depths. The bottom panel of Fig. 2.2 compares the density profiles and the radial extent of the convection zones for a model with $T_{\rm eff} \simeq 7000$ K and turbulent pressure included to the same model where turbulent pressure was disregarded.

In the envelope of the 60 $M_\odot$ model, we find convective zones associated to the partial ionisation of iron and helium, while the model does not become cool enough to show hydrogen recombination.

As shown in Fig. 2.3, the FeCZ is located at an optical depth of $\log(\tau) > 1.5$, with $P_{\rm turb}/P$ rising to ~5% for $T_{\rm eff} \simeq 40\,000$ K. As the star evolves the convective region moves deeper inside the star. Figure 2.3 shows that due to the turbulent pressure, the star increases its radius by few percent, which leads to a slightly reduced density and an increase of the radial extent of the iron convection zone.

2.4 Comparison with observations

In particular the iron opacity peak at T ≈ 20 0000 K is known to induce a variety of dynamical phenomena at the stellar surface, e.g. pulsations in β-Cephei and slowly pulsating B stars (SPB, Miglio et al. 2007; Pamyatnykh 1999), and stochastically excited travelling waves generated by turbulent motions in the FeCZ (Goldreich & Kumar 1990; Cantiello et al. 2009; Belkacem et al. 2010; Samadi et al. 2010; Mathis et al. 2014) leading to a subsonic small scale velocity field at the surface that has been proposed to be the physical origin of the so called "microturbulence".

The spectra of luminous O-B stars is known to be also affected by the so called macroturbulent broadening, an extra line-broadening usually ad-hoc associated with large scale (compared to the line forming region) motions at the surface (see Markova et al. (2014), Simón-Díaz & Herrero (2014), and references therein). Similarly to the case of microturbulence, convection might play a significant role in the origin of macroturbulence as well. This view is supported by the work of Sundqvist et al. (2013), who showed that macroturbulence is suppressed in strongly magnetic massive stars, where the magnetic field is expected to at least partially inhibit convection. A similar effect was found for intermediate mass magnetic chemically peculiar stars (Ryabchikova et al. 1997) and for spots in late-type stars (Strassmeier 2009). In this context, vigorous envelope convection in the temperature range of the hydrogen recombination (Fig. 2.2) may be responsible for the non-thermal (macroturbulent) broadening observed in red supergiants (Collet et al. 2007; Carney et al. 2008).

With this motivation, we pursue the hypothesis that the relative strength of turbulent pressure in the sub-surface convective zones is related to the appearance and strength of macroturbulence at the stellar surface. We investigate the case of the luminous O-B stars, where the turbulent pressure constitutes up to ≈5% of the total pressure in the FeCZ.

We make use of the results from the quantitative spectroscopic analysis of the rich sample of spectra compiled by the IACOB project (Simón-Díaz et al. 2011a, 2015). In particular we benefit from the

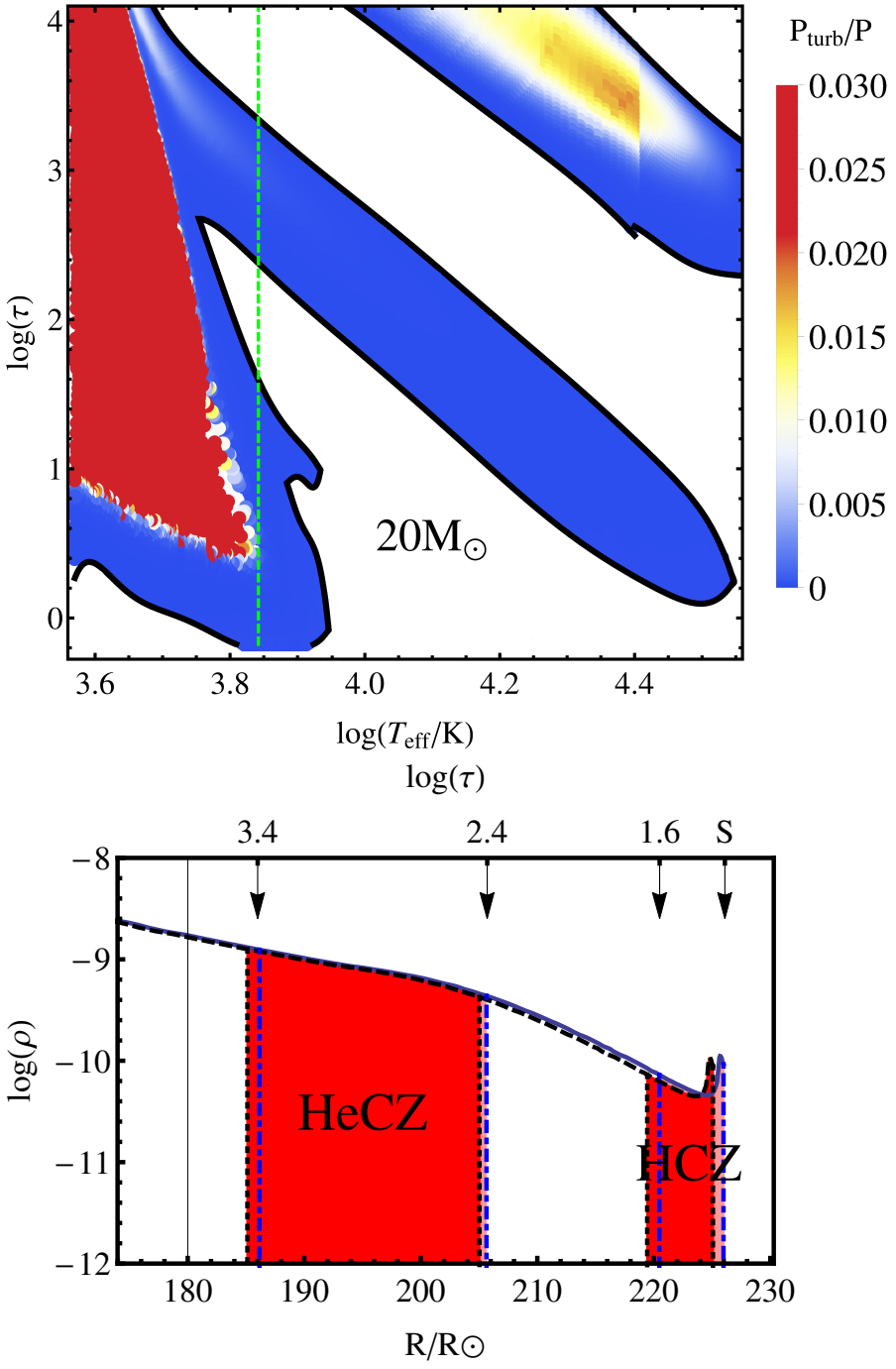

Figure 2.2: Top: ratio of turbulent-to-total pressure (color coded) as a function of effective temperature and optical depth throughout the evolution of the 20 $M_\odot$ model. The FeCZ is visible in the upper-right corner, the HeCZ lies across the diagram, and the HCZ appears for $T_{\rm eff}$ below ~10 000 K. The dashed line indicates the selected density profile shown in the bottom panel.
Bottom: Comparison of the density (in g cm^{-3}) as a function of the radial coordinate R in the outer layers of our 20 $M_\odot$ star at $T_{\rm eff} \simeq 7000$ K (blue solid line) with that in an identical model where the turbulent pressure term was switched off (black dashed line). The shaded dark-red regions confined within the dotted vertical lines denote the HeCZ and HCZ in the model calculated without $P_{\rm turb}$, while the light-red regions correspond to the same convection zones in the model calculated with $P_{\rm turb}$. The numbers associated to the arrows on the top of the figure indicate the optical depth $\log(\tau)$ of the borders of the convective zones in the case with $P_{\rm turb}$included (with S indicating the surface).

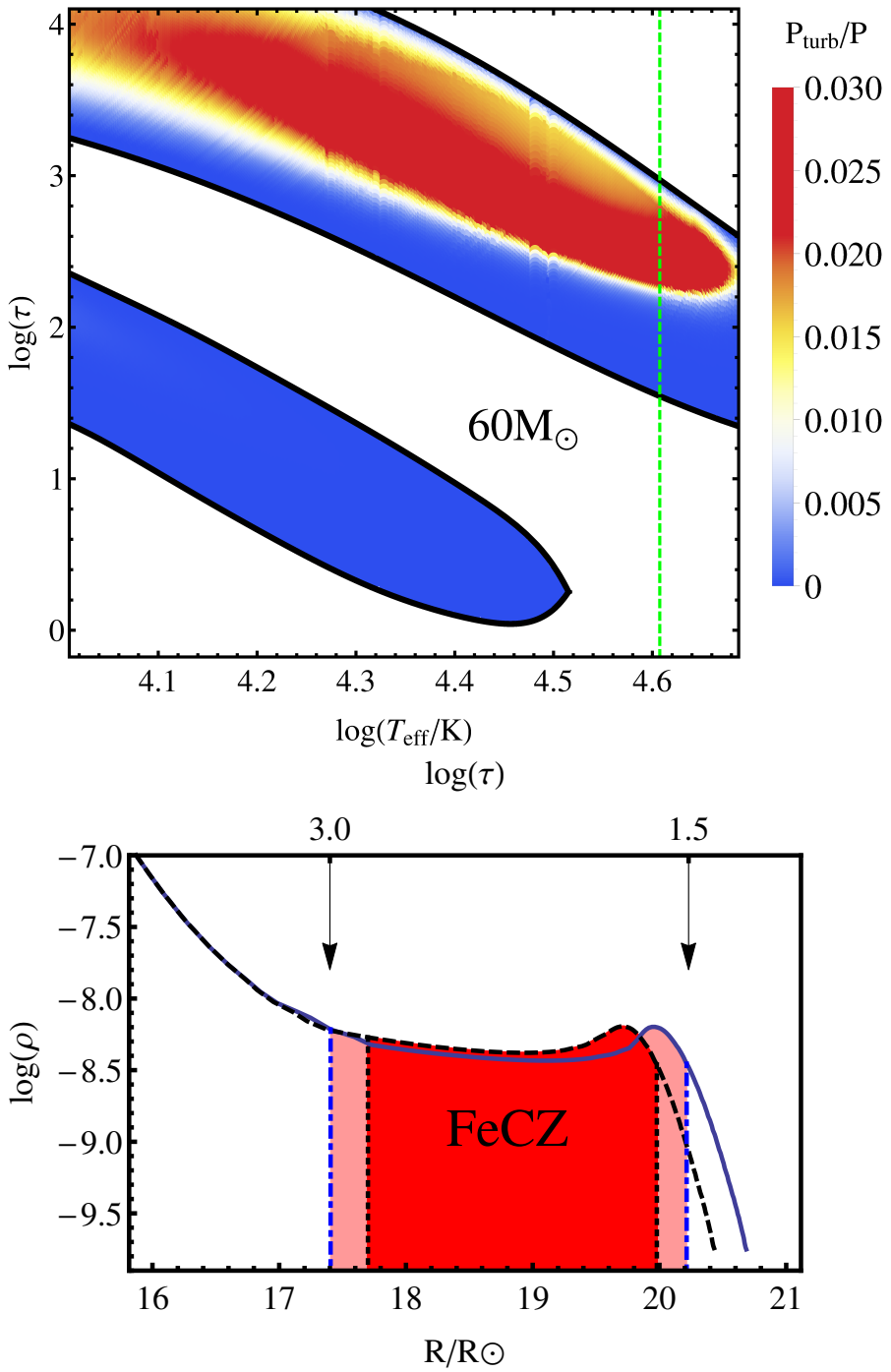

Figure 2.3: Same as Fig. 2.2, but for the 60 $M_\odot$ model. Top: ratio of turbulent-to-total pressure (color coded) as a function of effective temperature and optical depth during the evolution of the 60 $M_\odot$ model, showing the FeCZ and HeCZ are at higher and lower optical depths, respectively.
Bottom: density profile and extent of the FeCZ at $T_{\rm eff} \approx 40\,000$ K.

derived values of surface temperature ($T_{\rm eff}$), gravity (log(g)), projected rotational velocity (vsin(i)) and macroturbulent velocity (v_{macro}) for a sample of ~ 300 Galactic O-B stars used in Simón-Díaz (2015)[1].

In Fig. 2.4 we compare the observationally derived macroturbulent velocities to the maximum fraction of turbulent pressure in our models in the spectroscopic HRD (sHR, Langer & Kudritzki 2014). Stars presenting a clear signature of macroturbulence in their line profiles (i.e., a v_{macro} larger than 50 km/s) are marked by a bigger black circle in Fig. 2.4. Interestingly, those stars are located mainly in regions of the sHR where the turbulent pressure yields the highest contribution to the total pressure in the FeCZ. At places where the models predict a small contribution from the turbulent pressure only very few stars show an unambiguously high macroturbulent velocity. We discuss these exceptions at low $\mathscr{L}$ in the next section.

The agreement becomes even more striking looking at Fig. 2.5, where the observed macroturbulent velocities are directly plotted against the maximum fraction of turbulent pressure in our models. This plot reveals a clear correlation between macroturbulent velocity and turbulent pressure starting from $P^{max}_{turb}/P \approx 0.005$, with a Spearman's rank correlation coefficient of 0.812.

2.5 The connection to high-order pulsations

Figure 2.4 revealed about ten stars with $\log(\mathscr{L}/\mathscr{L}_\odot) < 3.3$ for which our models predict very small turbulent pressure contributions, but which unambiguously show macroturbulence at a level above 50 km/s (see also Fig. 2.5). Interestingly, we find that all these stars are located inside or very near to the region where stars are expected to be pulsationally unstable to high-order g-modes (Miglio et al. 2007; Pamyatnykh 1999, see also Simón-Díaz 2015), which is drawn as a gray band in Fig. 2.4. Indeed, Aerts et al. (2009) showed that the collective effect of high-order non-radial pulsations may produce a velocity field in the spectra of hot stars which resembles closely what is observed as macroturbulence in the stars discussed in Sect. 4.

Consequently, we interpret these stars as affected by a macroturbulent broadening that can be explained via a heat-driven pulsational origin. However, the homogeneity of the spectroscopic signatures of macroturbulence over the whole effective temperature range in the luminous stars calls for a single dominant mechanism to produce it (Simón-Díaz et al. in prep.). This is not the case when considering only classical (κ-mechanism) instability domains, which do not cover the full region where most of the stars showing a macroturbulent velocity field are observed (see Simón-Díaz 2015, Godart et al. in prep.). Shiode et al. (2013) and Aerts & Rogers (2015) consider gravity-waves originating in the convective core as the cause of macroturbulence. Whereas Shiode et al. (2013) based on their massive star models find that the surface velocity fluctuations do not exceed 10 m/s even in their most optimistic case, Aerts & Rogers (2015), based on 2-D non-linear simulations of convection-driven waves in a modified 3 $M_\odot$ model concluded that it might explain the macroturbulence observed in O-stars.

Within our scenario, the Reynolds stresses associated with turbulent pressure induce uncorrelated turbulent pressure fluctuations in the form

$$\delta P_{turb} \sim \rho v_c^2 \ , \tag{2.3}$$

(Goldreich & Kumar 1990; Grigahcène et al. 2005; Lecoanet & Quataert 2013; Shiode et al. 2013) where δP_{turb} is the Lagrangian pressure perturbation associated with the convective motions. Such stochastic fluctuations at the percent level can produce a strong local deviation from hydrostatic equilibrium, and

[1] The results of the analysis of a much larger dataset, along with a thorough empirical description of the behaviour of macroturbulent broadening in the whole O-B star domain will be presented in Simón-Díaz et al. (in prep).

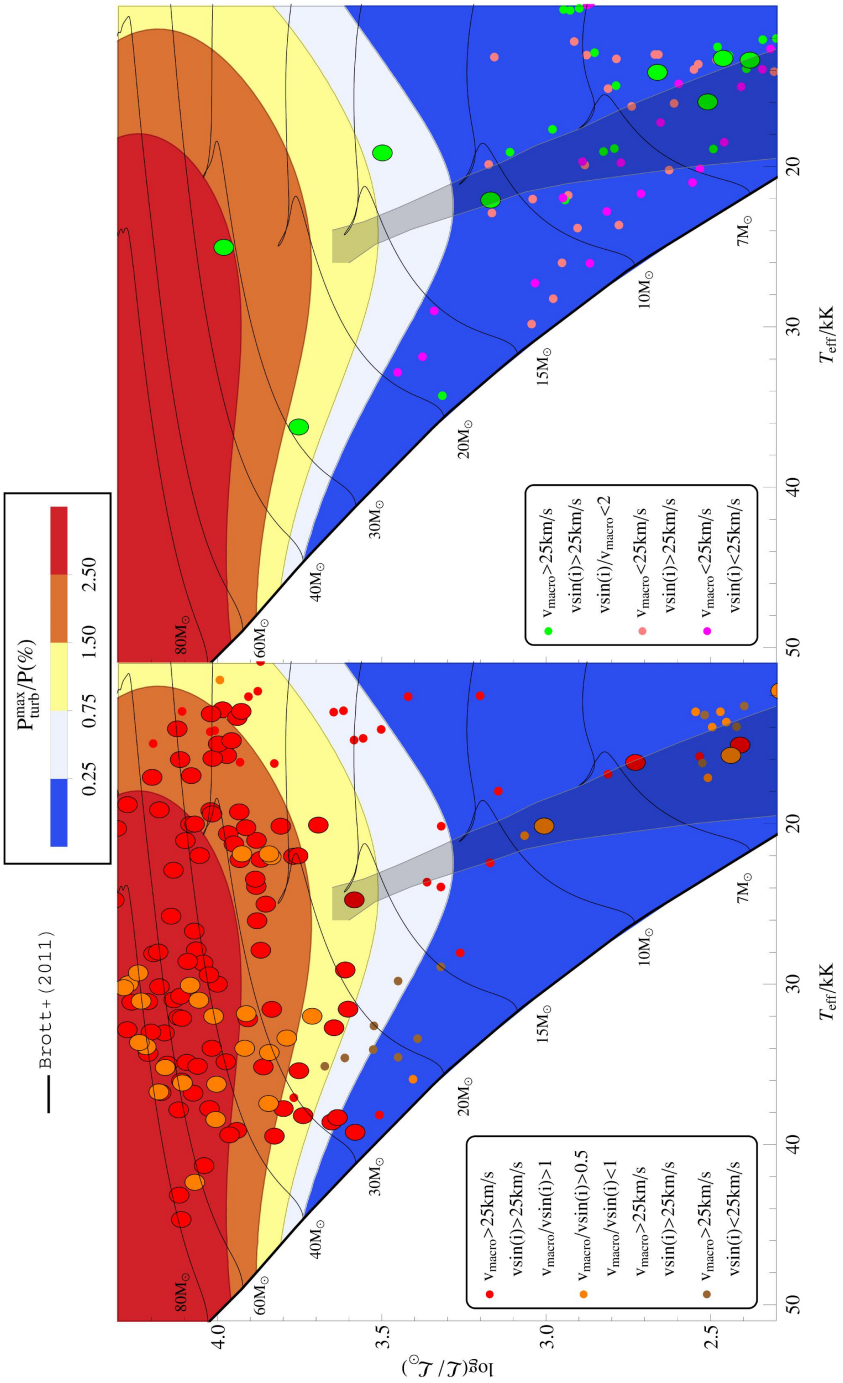

Figure 2.4: Spectroscopic HRD with coloured regions representing the maximum fraction of turbulent pressure as derived from a best-fit of the tracks in Fig. 2.1. Circles represent the observed O-B stars, colour coded according to their spectral line shape as in Simón-Díaz (2015), i.e. following the ratio between the projected rotational velocity $v \sin i$ and the macroturbulence velocity v_{macro}. In the left panel stars with line profiles showing a clear contribution from macroturbulence are located, while the right panel includes stars with line profile showing a dominant rotational broadening and a less clear contribution from macroturbulence. The bigger circles bordered in black indicate stars showing v_{macro} higher than 50 km/s. The gray bands indicate the $\kappa-$mechanism instability strip for SPB stars (Miglio et al. 2007).

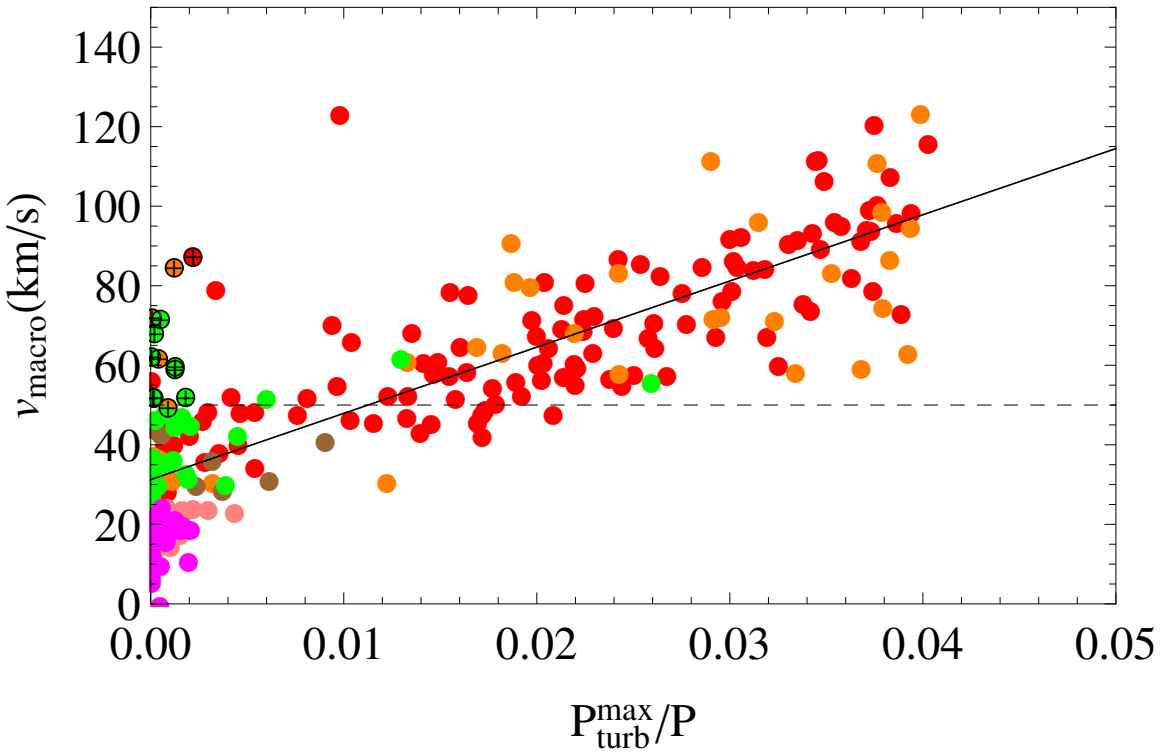

Figure 2.5: v_{macro} as a function of the maximum fraction of turbulent-to-total pressure derived from a fitting of the tracks described in Sect. 3. The circles are color coded as in Fig. 2.4 with the crossed-black circled dots indicating the stars with $v_{macro} > 50$ km/s and $\log(\mathscr{L}/\mathscr{L}_\odot) < 3.3$. The dashed line indicates the 50 km/s level (see Fig. 2.4).

will thus naturally excite high-order pulsations in the range of eigenmodes, which are closest to the spectrum of the fluctuations.

This would imply that also in the luminous stars with $\log(\mathscr{L}/\mathscr{L}_\odot) > 3.3$ in Fig. 2.4, the macroturbulence may be signifying high-order pulsations, which are, however, excited by turbulent pressure fluctuations rather than through the κ-mechanism or by strange mode instability. If so, we can on one hand expect that linear pulsation analyses which include the Reynolds stress tensor, as e.g., in Dupret et al. (2004, 2005) or Antoci et al. (2014), may uncover that stars in a large fraction of the red and orange coloured region in Fig. 2.4 are unstable to high-order g-mode pulsations. On the other hand, as the pressure fluctuations in these stars, as predicted by our simple analysis, can amount up to 5% of the total pressure, it is conceivable that in linear stability analyses, which require the growth of the instability from infinitesimal perturbations, an instability is not detected in all stellar models where high-order g-mode can be excited through finite amplitude pressure perturbations.

2.6 Conclusions

We implemented the effect of the turbulent motion of convective eddies in a simple formalism in the momentum and energy equations of our stellar evolution code. By comparing to previous computations (Brott et al. 2011), we find that the turbulent pressure does not alter the stellar structure significantly. However, we find maximum turbulent pressure contribution of up to 5% and 30% in our models for

O-B supergiants and cool red supergiants, respectively. By comparing the maximum turbulent pressure contribution in our models with spectroscopically derived macroturbulent velocities for a large sample of Galactic OB stars (Simón-Díaz 2015), we find both quantities to be strongly correlated.

Several less luminous stars, in which the turbulent pressure is thought to be small, show nevertheless high macroturbulent velocities. These are located close to or inside the region where linear pulsation analysis predicts high-order g-mode pulsations, arguing therefore for κ-mechanism pulsations, and not turbulent pressure fluctuations, as the origin of the macroturbulence phenomenon, in line with previous suggestions (Aerts et al. 2009; Simón-Díaz 2015).

We argue that the turbulent pressure fluctuations in hot luminous stars can excite such high-order pulsations, most likely non-radial g-modes, which may explain the occurrence of macroturbulence in stars which are found outside of the currently predicted pulsational instability domains. This view is in agreement with the indication that macroturbulence can be suppressed in strongly magnetic stars, given that such a field might effectively inhibit convective motions in the FeCZ (Sundqvist et al. 2013).

At the moment, turbulent pressure fluctuations appear to be the only mechanism which may excite high-order oscillations in luminous stars ($\log(L/L_\odot) > 4.5$) in the wide effective temperature regime for which strong macroturbulence is observed.

Acknowledgements: *LG is member of the International-Max-Planck-Research-School (IMPRS) for Astronomy and Astrophysics at the Universities of Bonn and Cologne. LF acknowledges financial support from the Alexander-von-Humboldt foundation. SS-D acknowledges funding by the Spanish Ministry of Economy and Competitiveness (MINECO) under the grants AYA2010-21697-C05-04, AYA2012-39364-C02-01, and Severo Ochoa SEV-2011-0187. Based on observations made with the Nordic Optical Telescope, operated by NOTSA, and the Mercator Telescope, operated by the Flemish Community, both at the Observatorio del Roque de los Muchachos (La Palma, Spain) of the Instituto de Astrofísica de Canarias. Moreover, LG and LF thank A. Miglio for useful discussions.*

CHAPTER 3

Relating turbulent pressure and macroturbulence across the HR diagram with a possible link to γ Dor stars

L. Grassitelli[1], L. Fossati[2,1], N. Langer[1], A. Miglio[3], A. G. Istrate[1], D. Sanyal[1]

[1]Argelander-Institut für Astronomie, Universität Bonn, auf dem Hügel 71, 53121 Bonn, Germany
[2]Space Research Institute, Austrian Academy of Sciences, Schmiedlstrasse 6, A-8042 Graz, Austria
[3]School of Physics & Astronomy, University of Birmingham, Edgbaston, Birmingham, B15 2TT, UK

Astronomy & Astrophysics Letters 2015, 584L, 2G

Abstract: A significant fraction of the envelope of low- and intermediate-mass stars is unstable to convection, leading to sub-surface turbulent motion. Here, we consider and include the effects of turbulence pressure in our stellar evolution calculations. In search of an observational signature, we compare the fractional contribution of turbulent pressure to the observed macroturbulent velocities in stars at different evolutionary stages. We find a strong correlation between the two quantities, similar to what was previously found for massive OB stars. We therefore argue that turbulent pressure fluctuations of finite amplitude may excite high-order, high-angular degree stellar oscillations, which manifest themselves at the surface an additional broadening of the spectral lines, i.e., macroturbulence, across most of the HR diagram. When considering the locations in the HR diagram where we expect high-order oscillations to be excited by stochastic turbulent pressure fluctuations, we find a close match with the observational γ Doradus instability strip, which indeed contains high-order, non-radial pulsators. We suggest that turbulent pressure fluctuations on a percentual level may contribute to the γ Dor phenomenon, calling for more detailed theoretical modelling in this direction.

3.1 Introduction

Stars transport energy mostly via two physical mechanisms: radiative diffusion and convection. Convection consists of upward and downward turbulent motion of material and consequently leads, strictly speaking, to local deviation from hydrostatic equilibrium. Grassitelli et al. (2015b) showed that the strength of turbulent pressure within the sub-surface convective zones (SSCZ) of hot massive stars may be related to the observationally derived macroturbulent velocities at the surface (Simón-Díaz & Herrero 2014), as a consequence of the local lack of hydrostatic equilibrium at the percent level due to stochastic turbulent pressure fluctuations. However, massive stars are not the only stars that show vigorous SSCZ.

Turbulent convection is known to play a decisive role in the stochastic forcing, self-excitation and damping of pulsation modes across the HR diagram (see, e.g., Houdek 2000, Dupret et al. 2004, Xiong & Deng 2007, Belkacem & Samadi 2013. Moreover, a recent study by Antoci et al. (2014) showed that turbulent pressure in the hydrogen ionization zone is likely to explain the high-frequency, coherent pulsation modes observed in the δ Scuti pulsator HD 187547. Hydrogen recombines at a temperature on the order of 10 000 K, leading to high values of the Rosseland opacity and to a high Eddington factor in the corresponding layers (Sanyal et al. 2015). This opacity bump could also play a role in the pulsational instability of the γ Doradus (γ Dor) class of stars (Handler & Shobbrook 2002).

Stars of the γ Dor class are intermediate mass stars showing periodic variability on a timescale of days. These A- and F-type stars are pulsating with high-order, non-radial g-modes (Guzik et al. 2000; Miglio et al. 2008). Theoretical stability analyses adopting time-dependent convection predict an instability strip (IS) to occur close to where γ Dor are observed, involving a flux-blocking excitation mechanism (Guzik et al. 2000; Dupret et al. 2005). However, Dupret et al. (2004) showed that the agreement between observations and theory depends very sensitively on the exact treatment of convection.

We investigate here the effects of turbulent pressure in intermediate mass stars, focusing on its observational fingerprints, and try to draw a global picture of these effects across the HR diagram.

3.2 Method

We have computed a set of stellar evolutionary models using the hydrodynamic Lagrangian one-dimensional Bonn evolutionary code (Heger et al. 2000; Yoon et al. 2006; Brott et al. 2011). For convection the models are computed using the Ledoux criterion (Kippenhahn & Weigert 1990), adopting the mixing length theory (MLT) with a mixing length parameter $\alpha = 1.5$ (Böhm-Vitense 1958; Brott et al. 2011). The opacities are computed from the OPAL opacity tables (Iglesias & Rogers 1996). No stellar wind mass loss was included in the calculations and we assumed a metallicity of $Z = 0.02$ (Brott et al. 2011).

We also used for comparison a modified version of BEC, which includes the turbulent pressure ($P_{\rm turb}$) and turbulent energy density ($e_{\rm turb}$) in the stellar structure equations (Grassitelli et al. 2015b). These quantities can be expressed as (Stothers 2003)

$$P_{turb} = \zeta \rho v_c^2 \quad , \quad e_{turb} = \frac{3}{2}\frac{P_{turb}}{\rho} \quad , \tag{3.1}$$

where ρ is the local density, ζ is a parameter chosen to be $\zeta = 1/3$ for isotropic turbulence (Stothers 2003), and v_c is the local convective velocity.

In Appendix A, Fig. 3.5 shows an HR diagram comparing two 1.5 $M_\odot$ tracks, with and without the inclusion of turbulent pressure and energy. We find that the structural effects arising from the inclusion of $e_{\rm turb}$ and $P_{\rm turb}$ do not significantly affect the evolutionary tracks, in agreement with Grassitelli et al.

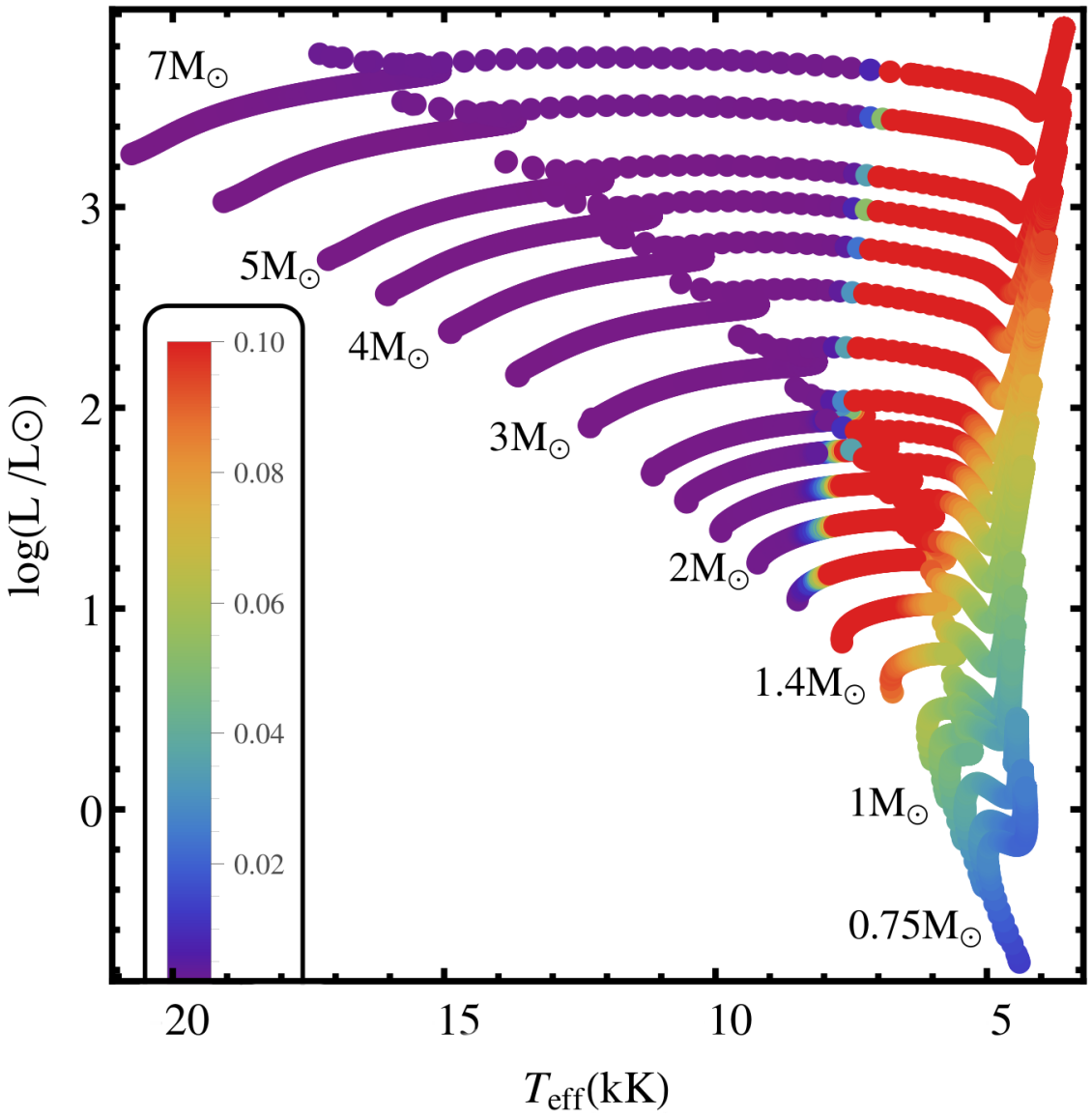

Figure 3.1: HR diagram showing the computed stellar evolution tracks. The colors of the dots indicate the maximum fraction of turbulent-to-total pressure occurring within the stellar envelopes (see framed color bar in the bottom left corner). Stellar models in red show $P_{turb}/P>10\%$. The masses of the models are indicated next to the tracks. For the upper HR diagram, see Fig.1 in Grassitelli et al. (2015b).

(2015b). Therefore, we study the contribution of the turbulent pressure to the equation of state *a posteriori*, using Eq. 3.1.

3.3 Results

Figure 3.1 shows the HR diagram with our newly computed evolutionary tracks for low- and intermediate-mass stars ($0.75-7\,M_{\odot}$), color coded according to the maximum ratio of turbulent-to-total pressure within

each stellar model. At $\log(L/L_\odot) \approx 1$ the models that show a significant P_{turb} fraction are confined within a rather narrow T_{eff} range of 6000–8000 K, while at T_{eff}<8000 K the P_{turb} contribution is small. Within this band, P_{turb} can account for up to ≈10–15% of the total pressure. The hot boundary at $T_{eff} \approx 8000$ K coincides with a sharp increase in opacity very close to the surface owing to hydrogen recombination. The maximum fraction of turbulent pressure reaches a peak at T_{eff}~7500 K, then followed by a gradual decrease with decreasing T_{eff}, where the maximum fraction of turbulent pressure is reduced to ≈ 5% at $T_{eff} \approx$ 4500 K.

At high luminosity, e.g., $\log(L/L_\odot) \approx 3$, the T_{eff} range within which the fraction of P_{turb} is larger than 10% has moved to the interval 4000–7000 K. This band forms a continuous region in the HR diagram with the higher luminosity red supergiants computed by Grassitelli et al. (2015b). Thus, it ranges from $\log(L/L_\odot) \approx 0.7$, where it crosses the zero-age main-sequence (ZAMS) at $M \sim 1.5\,M_\odot$, up to the most luminous supergiants with $\log(L/L_\odot) \approx 5.5$ irrespective of the evolutionary stage. Within this band, P_{turb}^{max} goes from 10% on the ZAMS to 33% at high luminosities.

The internal envelope structure can be seen in Fig. 3.2, where the outer layers of the $1.9\,M_\odot$ model are shown for part of its evolution. Figure 3.2 shows that the hydrogen convective zone (HCZ) becomes more and more extended (in terms of optical depth) as the star cools, moving toward the giant branch, although its radial extent is only ≈ 5% of the stellar radius for the coolest models. A steep increase of P_{turb} is present at $T_{eff} \approx 8000$ K as the inefficiency of convection causes the convective velocities to approach the sound speed (cf. Grassitelli et al. 2015b), followed by a smooth decrease as the superadiabaticity of the outer layers decreases (see Appendix 3.5 for a discussion of convective timescales and mixing length parameter α).

3.4 Observational consequences of turbulence pressure

3.4.1 Macroturbulence broadening

In the context of massive stars, Aerts et al. (2009) concluded that the joint effects of a large number of high-order, high-angular degree g-mode pulsations at the surface may mimic macroturbulent line broadening. Grassitelli et al. (2015b) found that in hot massive stars macroturbulence broadening is strongly correlated to the maximum fraction of P_{turb} within the stellar models. They suggested that stochastic turbulent pressure fluctuations may excite high-order g-modes that then give rise to the observed macroturbulence. We here consider the same possibility by looking at the same quantities at the opposite side of the HR diagram.

We collected observationally derived macroturbulent velocities (υ_{mac}) for low- and intermediate-mass chemically normal stars previously derived from high resolution spectra by Carney et al. (2008), Fossati et al. (2011), Doyle et al. (2014), and Ryabchikova et al. (2016). We further looked for additional intermediate-mass chemically normal apparent slow rotators in order to increase the sample, particularly in the range of the evolved stars. Given the relatively small υ_{mac} values (typically ~10 km s^{-1}), all stars for which it is possible to reliably measure υ_{mac} have a low projected rotational velocity ($\upsilon \sin i$) of at most 10–15 km s^{-1}. We therefore derived macroturbulent velocities for HD 167858 (Bruntt et al. 2008), KIC 8378079, KIC 9751996, and KIC 11754232 (Van Reeth et al. 2015), all reported to have a $\upsilon \sin i$ below 15 km s^{-1}.

For all stars, we analyzed the spectral lines as described in Fossati et al. (2011), and we adopted the atmospheric parameters listed in Bruntt et al. (2008) for HD 167858 and in Van Reeth et al. (2015) for KIC 8378079, KIC 9751996, and KIC 11754232. The results, listed in Table 3.1, show that for all stars we obtained a non-negligible υ_{mac} value. We also attempted to fit the spectral lines not accounting for

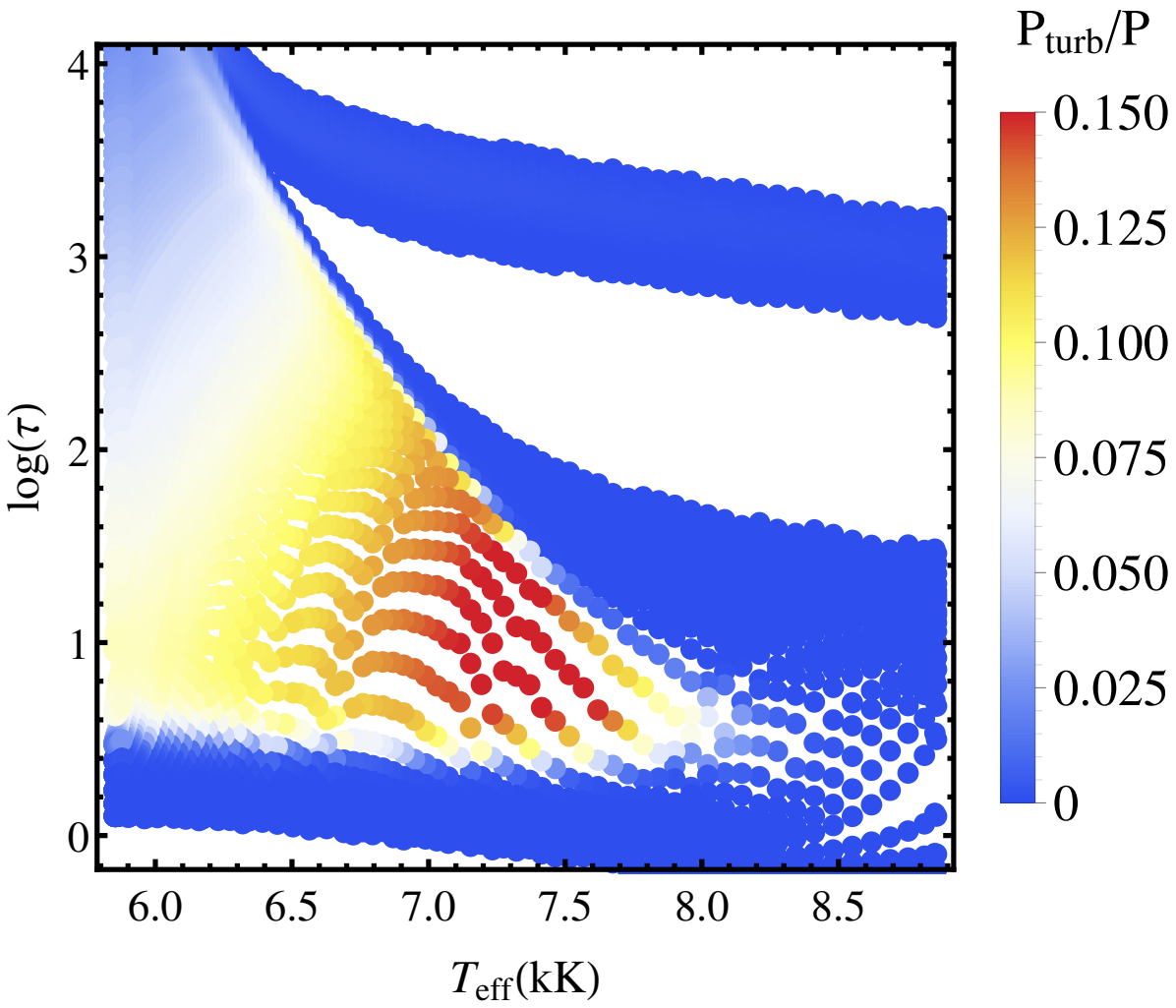

Figure 3.2: Ratio of turbulent-to-total pressure (color coded) as a function of the effective temperature and the optical depth throughout part of the evolution of a 1.9 $M_\odot$ model. Extended white areas are radiatively stable. The HeCZ is visible in the top right section of the plot. For $T_{\rm eff} > 7700$ K the HCZ is present from the surface up to $\log(\tau) \approx 2$. At lower $T_{\rm eff}$ the outer boundary of the HCZ is located at $\log(\tau) \approx 0$, while the inner boundary reaches $\log(\tau) > 3.5$ and merges with the HeCZ.

macroturbulent line broadening, which resulted in significantly worse fits compared to the case with macroturbulent broadening included.

Figure 3.3 shows the macroturbulent velocities as a function of the maximum fraction of turbulent pressure obtained from the stellar tracks at the position in the HR diagram of each observed star. The left panel of Fig. 3.4 shows the position of the stars considered here in the spectroscopic HR diagram (sHR; Langer & Kudritzki 2014) superposed on the computed stellar tracks.

Similar to the case of the massive stars (see Fig. 5 of Grassitelli et al. 2015b), we obtain a strong correlation between the two quantities: macroturbulent velocities increase with increasing P_{turb}^{max}/P. The relation is highly significant, with a Spearman-rank correlation coefficient of 0.96. In chemically normal slowly rotating MS late B- and A-type stars the spectral lines do not show the presence of macroturbulent broadening (e.g., Fossati et al. 2009a), and the stellar models consistently predict extremely small P_{turb}^{max} in that region. Moreover, Gray (1984), Valenti & Fischer (2005), and Ryabchikova et al. (2016) find a trend of increasing macroturbulent velocities for increasing effective temperatures in a sample of cool stars in the range 4500 K$<T_{\rm eff}<$6500 K. This is in a good agreement with our prediction as well, given that we expect an increase of P_{turb} with $T_{\rm eff}$ in that temperature range (see Sect.3 and Fig.3.2), providing additional evidence of a relation between $\upsilon_{\rm mac}$ and P_{turb} .

3.4.2 The γ Dor instability strip

Our results point toward the presence of a strong correlation between macroturbulent broadening and turbulent pressure across the whole HR diagram. In this picture, macroturbulent broadening may be the result of high-order modes excited by turbulent pressure fluctuations (Grassitelli et al. 2015b). Interestingly, the region of high P_{turb} shown in Fig. 3.1 broadly overlaps with the theoretical instability strips of γ Dor stars, which are indeed high-order, g-mode pulsators (Bouabid et al. 2011).

To further explore the possible P_{turb} -γ Dor connection, in the right panel of Fig. 3.4 we compare the position in the sHR diagram of observed γ Dor stars and hybrid γ Dor – δ Sct stars with the maximum value of P_{turb}/P as derived from the stellar models. This comparison shows that the observational γ Dor instability strip falls in the same area of the sHR diagram where we find the largest contribution of P_{turb} to the total pressure. In addition, the stars that present a non-negligible macroturbulent broadening lie predominantly along this same area of the sHR diagram. As a matter of fact, all the stars listed in Tab. 3.1 and HD 37594 are indeed bona fide γ Dor pulsators (Díaz-Fraile et al. 2014; Van Reeth et al. 2015).

If turbulent pressure fluctuations act as an excitation mechanism for high-order pulsation modes, it may well be that turbulent pressure fluctuations of finite amplitude play a role in the rise of the γ Dor phenomenon. Rigorous studies of the Reynolds stress tensor in connection with time-dependent convection (Grigahcène et al. 2005; Antoci et al. 2014) and eventually finite amplitude perturbations (Grassitelli et al. 2015b) are required to investigate the physical origin of the possible connection between high-order g-modes, $\upsilon_{\rm mac}$, and sub-surface turbulent pressure fluctuations.

3.5 Conclusions

We investigate the effects of convective turbulent pressure in late-type low- and intermediate-mass stars, focusing on their possible observational signatures. We find that stars with a major contribution from the turbulent pressure to the equation of state (i.e., $P_{turb}/P>10\%$) are confined to rather narrow band in the HR diagram (see Fig.3.1). This high contribution is found in models where the HCZ is located very close to the surface, irrespective of their evolutionary stages.

When comparing the maximum fraction of P_{turb} within the stellar models to observationally derived

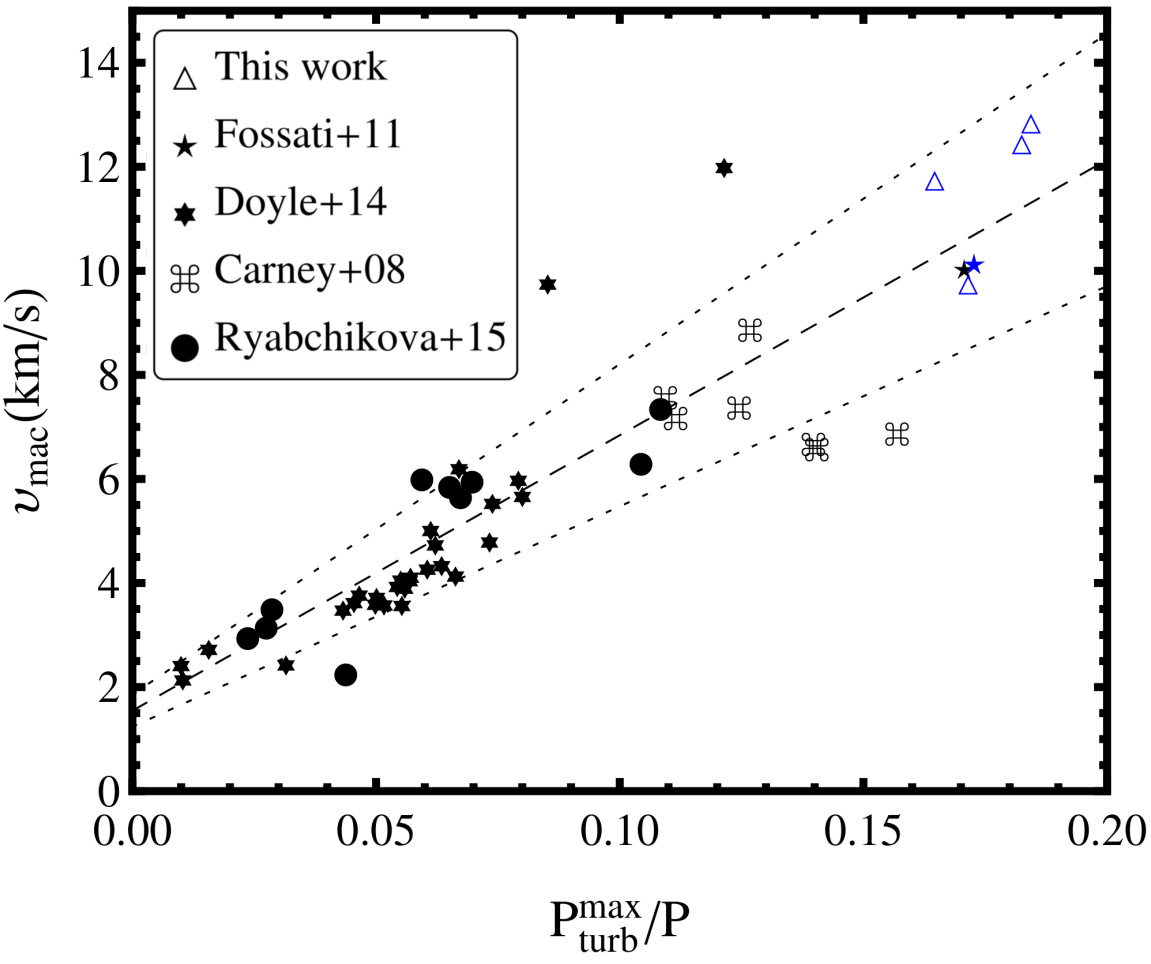

Figure 3.3: Observed macroturbulent velocities as a function of the estimated fraction of turbulent pressure from our calculations (via a fitting of the tracks). The data are from Carney et al. (2008), Fossati et al. (2011), Doyle et al. (2014), Ryabchikova et al. (2016), and this work. The dotted lines represent typical errors (i.e., 20% of υ_{mac}, equivalent to 1 standard deviation) inferred to the linear fit (dashed line). The five stars color coded in blue are bona fide γ Dor pulsators.

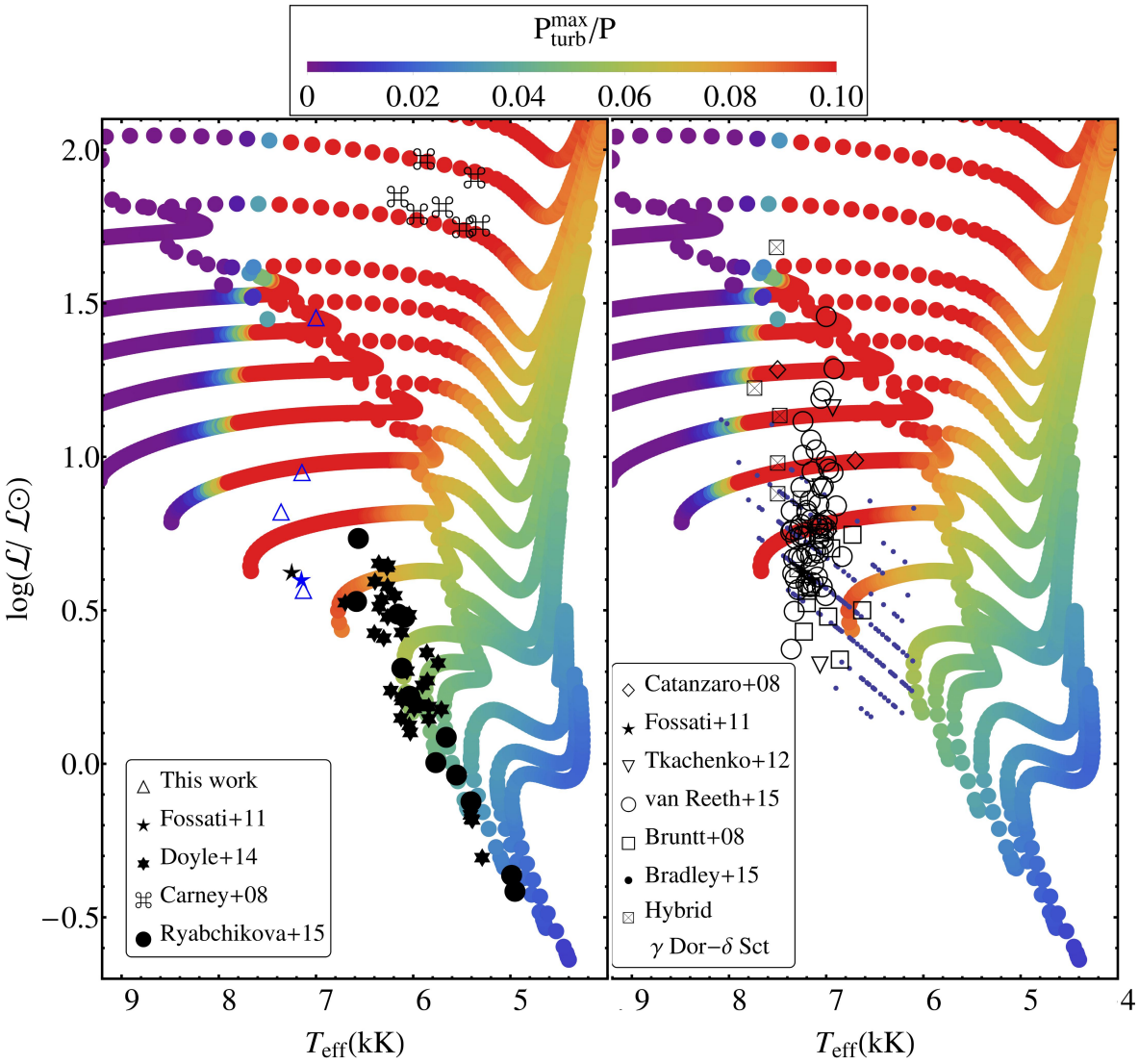

Figure 3.4: Left: stellar evolutionary tracks in a sHR diagram color coded according to the maximum fraction of P_{turb}/P (see top bar). Overplotted are the location of 56 stars analyzed by Carney et al. (2008), Fossati et al. (2011), Doyle et al. (2014), and Ryabchikova et al. (2016) for which macroturbulent velocities are available, in addition to those listed in Tab. 3.1. The five stars color coded in blue are bona fide γ Dor pulsators.
Right: As in left panel, with overplotted the location of $\approx$ 300 γ Dor stars analyzed by Bruntt et al. (2008), Catanzaro et al. (2011), Fossati et al. (2011), Tkachenko et al. (2012), Bradley et al. (2015), and Van Reeth et al. (2015) and some hybrid γ Dor–δ Sct stars from Catanzaro et al. (2011) and Tkachenko et al. (2012).

macroturbulent velocities, we find a strong correlation between these two quantities, analogous to the finding of Grassitelli et al. (2015b) for OB stars. Given that a similar strong correlation is found both in massive OB stars, where the high turbulent pressure appears in the iron convective zone, and in low- and intermediate-mass main- and post main-sequence stars, where the highest contribution from turbulent pressure lies within the HCZ, a physical connection of both phenomena appears likely.

This connection can be interpreted as a consequence of the local deviation from the hydrostatic equilibrium due to turbulent pressure fluctuations at a percent level. We argue that turbulent pressure fluctuations could lead to the excitation of high-order, non-radial pulsations, as observed in γ Dor stars and even in our Sun, which manifest themselves at the surface as macroturbulent broadening of spectral lines (Aerts et al. 2009). If indeed turbulent pressure fluctuations excite high-order modes, a connection with γ Dor may be present as well, which could involve finite amplitude pressure fluctuations in the HCZ.

Our results provide additional strong evidence for the connection between large-scale surface motions and the contribution of turbulent pressure, and calls for a revaluation, possibly inspired by 3D simulations, of the role of convection dynamics on the excitation and damping of both coherent and stochastically excited oscillation modes and waves. Rigorous studies should be performed to investigate the physical origin of the possible connection between sub-surface turbulent pressure fluctuations, macroturbulent broadening, and, e.g., the transition between δ Scuti (or the classical Cepheid instability strip), γ Dor, and stochastically-excited pulsators. This study appears particularly timely given the wealth of stringent observational constraints on photometric variability delivered, e.g., by CoRoT and *Kepler*.

Acknowledgements: *LG is part of the International Max Planck Research School (IMPRS), Max-Planck-Institut für Radioastronomie, and Universities of Bonn and Cologne. LF acknowledges financial support from the Alexander von Humboldt foundation. We thank Timothy Van Reeth for sharing the spectra of the Kepler stars and Konstanze Zwintz for useful discussions.*

Effects of P_{turb} on a 1.5 $M_\odot$ stellar model and derived stellar parameters

Table 3.1: $\upsilon \sin i$ and υ_{mac} values derived for the analysed stars.

Star	$\upsilon \sin i$ [km s^{-1}]	υ_{mac} [km s^{-1}]
HD 167858	6.2±1.0	9.8±1.5
KIC 8378079	1.5±2.6	12.5±1.1
KIC 9751996	3.9±3.4	12.9±1.5
KIC 11754232	2.4±2.5	11.8±1.1

In this section we discuss the comparison between tracks with and without the inclusion of P_{turb} and e_{turb} in the calculation of a 1.5 $M_\odot$ stellar models. We emphasize that, different from massive stars (Grassitelli et al. 2015b), the convective velocities for intermediate-mass stars do not exceed the local sound speed and no limitation of v_c is necessary.

During the main-sequence phase ($T_{eff} \gtrsim 5800$ K), the two tracks do not present appreciable differences; as the tracks approach the terminal-age main-sequence, the model with P_{turb} presents a displacement

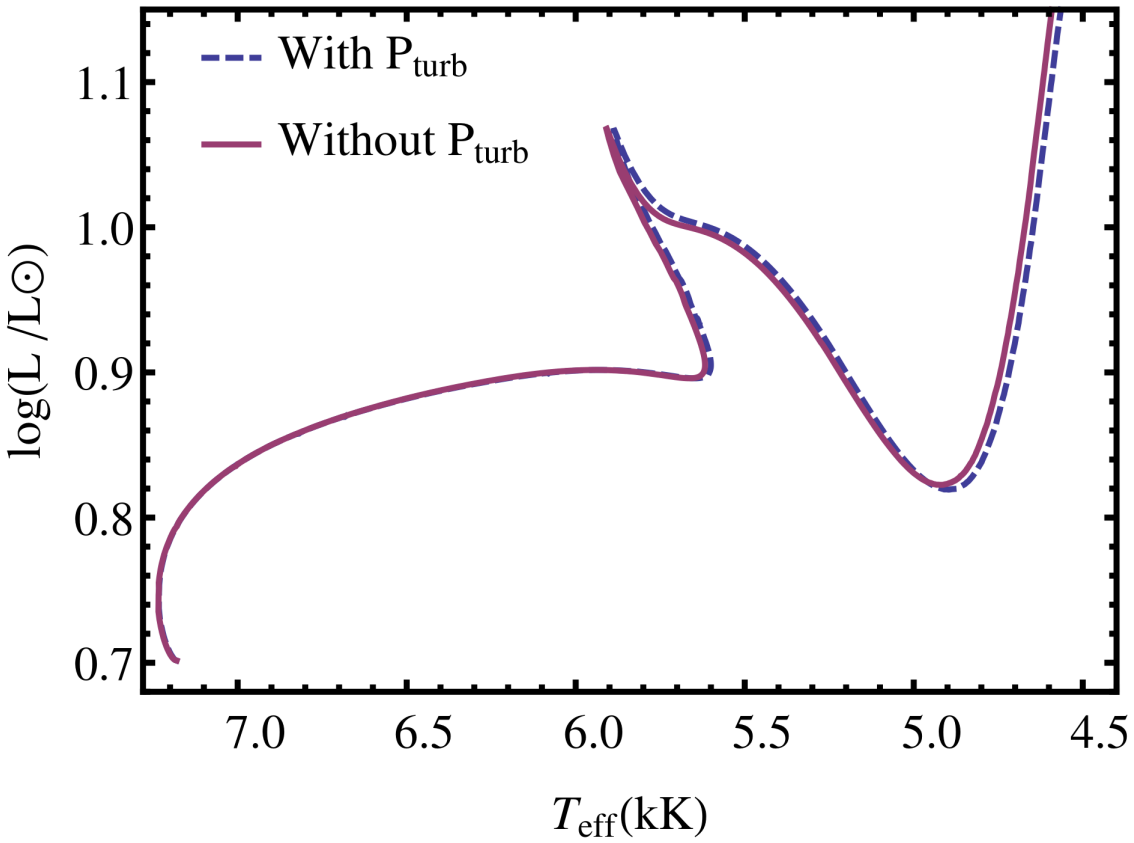

Figure 3.5: HR diagram showing evolutionary tracks of a 1.5 $M_\odot$ model with (blue dashed) and without (purple continuous) turbulent pressure.

on the order of ≈10 K toward lower effective temperatures. A similar behavior is also found for the post-main-sequence evolution, corresponding to a difference in radius on the order of ≈1% or less. In line with the results of Grassitelli et al. (2015b) for the massive stellar models (including a 7 $M_\odot$ stellar track), we consider the effects of turbulence on the hydrostatic models to be small, and do not directly include them in the calculations of the stellar tracks in Fig.3.1.

Convective timescales and mixing length

The results of an estimate of the convective timescales are shown in Fig. 3.6. The convective timescale τ_{conv} has been computed as

$$\tau_{conv} = \frac{\alpha H_p}{v_c}, \tag{3.2}$$

where H_p is the local pressure scale height. At the center of the hydrogen convective zone, where we obtain the highest convective velocities, the timescale for convection is on the order of five minutes. At the upper border instead (i.e., at the convective boundary close to the surface) the timescale increases from 1 up to ≈ 10 days or more. Thus the convective timescales vary by ≈ 4 orders of magnitude within the last mixing length of the convective zone. This makes a direct comparison with the observed periods

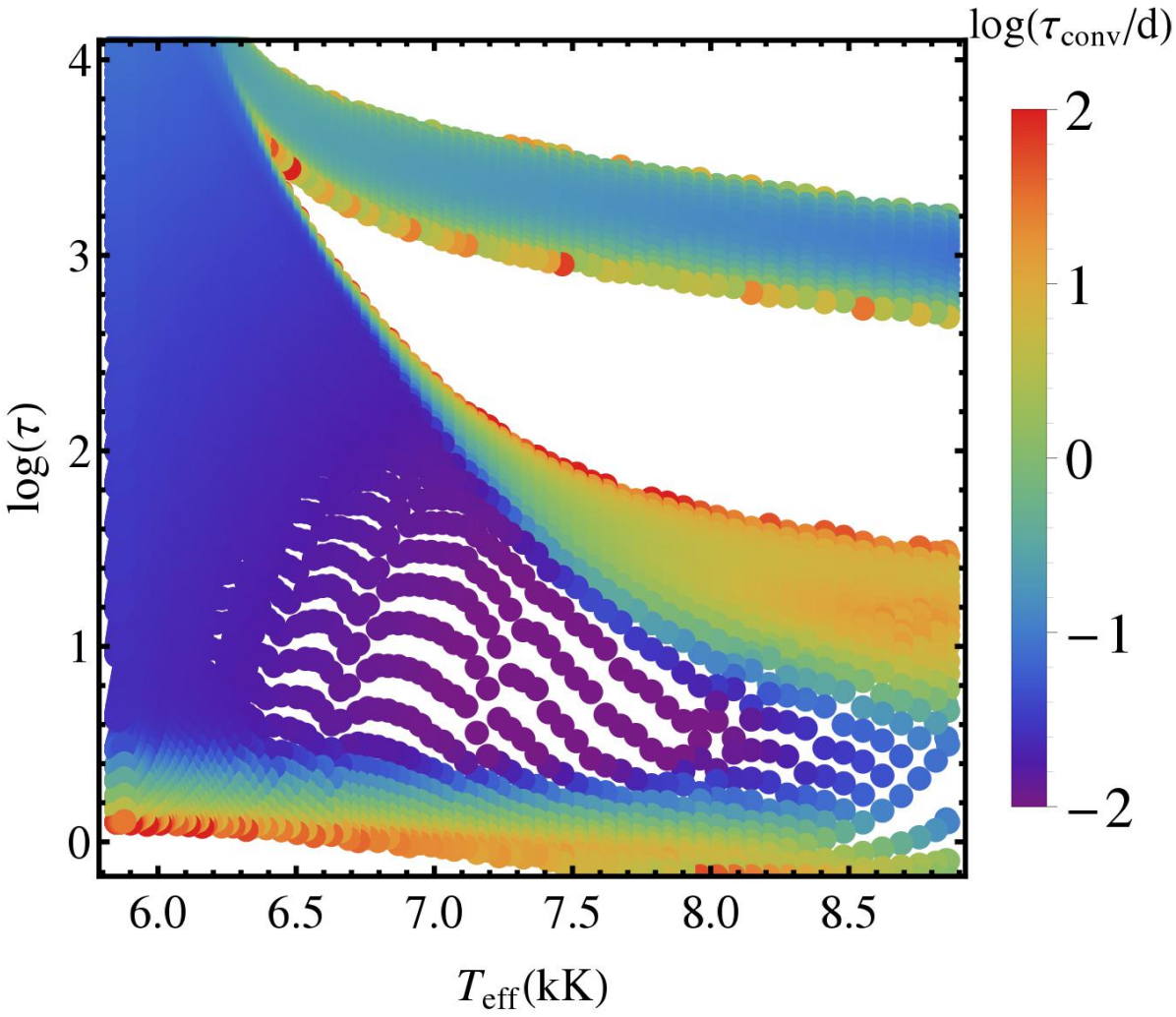

Figure 3.6: Convective timescale (color coded) as a function of the effective temperature and optical depth throughout part of the evolution of a 1.9 $M_\odot$ model (same as Fig.3.2). In the center of the hydrogen convective zone, where we find the higher contribution from P_{turb} , the convective timescales are $\approx 10^{-2}$ days, while at the edges of the hydrogen convective zone τ_{conv} increases up to $\approx 10^1 - 10^2$ days.

difficult. Numerical simulations are necessary in order to show whether observed mode lifetimes are compatible with stochastic excitation.

The absolute values given here and in Sect.3 depend upon the adopted value of the mixing-length parameter α. For $\alpha = 1$, the turbulent pressure fraction decreases to a maximum of 5% as a consequence of smaller convective velocities, while an increase of α (e.g., $\alpha = 1.8$) leads to transonic convective velocities. Changing α also changes the position of the local peak of P_{turb}^{max} , e.g., the position of the peak decreases by 300 K when adopting $\alpha = 1$.

CHAPTER 4

On the metallicity dependence of turbulent pressure and macroturbulence in stellar envelopes

L. Grassitelli[1], L. Fossati[1], N. Langer[1], S.Simón-Díaz [2,3], N.Castro [1], D. Sanyal[1]

[1]Argelander-Institut für Astronomie, Universität Bonn, auf dem Hügel 71, 53121 Bonn, Germany
[2]Instituto de Astrofísica de Canarias, 38200 La Laguna, Tenerife, Spain
[3]Departamento de Astrofisica, Universidad de La Laguna, 38205 La Laguna, Tenerife, Spain

Macroturbulence, once introduced as a fudge to reproduce the width of stellar absorption lines, reflects gas motions in stellar atmospheres. Whereas in cool stars, it is thought to be caused by convection zones immediately beneath the stellar surface, the origin of macroturbulence in hot stars is still under discussion. Recent works established a correlation between the turbulent-to-total pressure ratio inside the envelope of stellar models and the macroturbulent velocities observed in corresponding Galactic stars. In order to probe this connection further, we evaluate the turbulent pressure based on the mixing length theory arising in the envelope convective zones of stellar models in the mass range 1–125 $M_{\odot}$, computed for metallicities of the Large and Small Magellanic Cloud. We find that the turbulent pressure contributions in models located in the hot high-luminosity part of the HR-diagram is lower than in similar models with Solar metallicity, whereas the turbulent pressure in low metallicity models populating the cool part of the HR-diagram is not reduced. Based on our models, we find that the currently available observations of hot massive stars in the Magellanic Clouds appear to support a connection between macroturbulence and the turbulent pressure in stellar envelops. Multi-dimensional simulations of sub-surface convection zones, as well as a larger number of high quality observations are necessary to test this idea more rigorously.

4.1 Introduction

The Large and Small Magellanic Clouds (LMC & SMC) are two dwarf galaxies satellite of the Milky Way (MW). The close distance of these two galaxies makes possible to obtain high-quality spectra from individual stars (see e.g. Evans et al. 2011; Bestenlehner et al. 2014). This makes them great laboratories in which we can investigate several open questions in stellar physics, such as stellar evolution

in different environments (Yusof et al. 2013; Schneider et al. 2014; Köhler et al. 2015), the effects of different opacities on the structure of stars and its implications (Sasselov et al. 1997; Keller & Wood 2006; Cantiello et al. 2009), as well as the relation between the ambient metallicity and powerful events like long duration gamma-ray bursts or super-luminous supernovae (Graham & Fruchter 2013; Lunnan et al. 2014; Kozyreva et al. 2014). From this point of view, their main difference compared to our Galactic neighbourhood is their different metallicity (around half and a fifth of the solar metallicity for the LMC and SMC, respectively). The different chemical composition affects the opacity profile within the stars, of importance mostly in the sub-surface envelopes where temperatures are relatively low such that full ionization can not be sustained. Especially the recombination of the iron-group elements at about 200 000 K plays an important role in defining the structure of the outer layers of stars close to the Eddington limit, which is strongly influenced by the metallicity of the star (Langer 2012; Gräfener et al. 2012c; Jiang et al. 2015; Sanyal et al. 2015). The corresponding opacity bump, together with the opacity bumps due to hydrogen and helium recombination, often induces large scale turbulent motions of material, i.e. convection, in the sub-surface layers (Stothers & Chin 1993; Cantiello et al. 2009; Grassitelli et al. 2015b).

Recently, in the context of Galactic massive OB stars Grassitelli et al. (2015b) found a strong correlation between the strength of the pressure arising from turbulent motion in the iron convective zone (FeCZ) of their stellar models and the observational appearance of an extra broadening of the absorption lines in the spectra of corresponding stars. This extra broadening is usually called macroturbulence (Simón-Díaz et al. 2011b; Simón-Díaz 2015; Simón-Díaz et al. 2012, and reference therein), and it is thought to be due to large scale surface motion. The introduction of this extra-broadening of the spectral lines has been motivated and supported by the lack of apparent slow rotators and sharp-lined stars in the Galactic O-B stars (Howarth 2004; Simón-Díaz & Herrero 2014). Although the association between this extra-broadening and motion in the surface layers appears straightforward (Slettebak 1956; Conti & Ebbets 1977), the origin of this velocity field has not yet been fully understood.

However macroturbulence is not only a feature in the spectra of massive hot main-sequence stars and supergiants. The same kind of broadening is also present in other regions of the HR-diagram (Fossati et al. 2009b; Doyle et al. 2014). Grassitelli et al. (2015a) found a similar correlation between turbulent pressure ($P_{\rm turb}$) and macroturbulent velocities ($\upsilon_{\rm macro}$) in the context of late-type low- and intermediate-mass stars. In this case they considered the effects of turbulence in the hydrogen convective zone (HCZ), suggesting that a common mechanism across the HR-diagram might induce the surface velocity field observed as macroturbulent broadening. This mechanism was suggested to rely on the excitation of oscillations, as Aerts et al. (2009) showed that a high number of high-order non-radial g-mode pulsations can collectively reproduce the effects on the spectral lines which are typical for the macroturbulent broadening.

Therefore the relation between turbulent pressure and macroturbulent velocities has been interpreted as due to the broad spectrum of pulsations excited by the turbulent pressure fluctuations at the percent level (Grassitelli et al. 2015b). This dynamical mechanism to excite pulsations is expected to act effectively in the sub-surface convective zones in which convection is not an efficient mechanism to transport energy. This in fact leads to a turbulent flow with high convective velocities and consequently high Reynolds numbers (Canuto & Mazzitelli 1991; Arnett et al. 2015).

We investigate here the effects of the metallicity on the strength of the turbulent pressure in the sub-surface convective zones across the HR-diagram.

4.2 Method

We compute stellar models using BEC, a state-of-the-art implicit Lagrangian one-dimensional hydrodynamic stellar evolution code (Heger et al. 2000; Petrovic et al. 2005; Yoon et al. 2006; Brott et al. 2011; Köhler et al. 2015). It includes up-to-date physics, treating convection following the non-adiabatic standard Mixing Length Theory (MLT, Böhm-Vitense 1958), with a mixing-length parameter $\alpha = 1.5$ (Brott et al. 2011). It adopts the OPAL opacity tables in order to compute the Rosseland mean opacity of stellar matter (Iglesias & Rogers 1996), and includes mass-loss by stellar wind according to the prescription by Vink et al. (2001). Other physical parameters have been chosen as in Brott et al. (2011).

We estimate the strength of turbulent motion in the partial ionization zones by considering the turbulent pressure P_{turb} as in Grassitelli et al.(2015a, see also Canuto & Mazzitelli 1991; Jiang & Huang 1997; Stothers 2003; Maeder 2009):

$$P_{turb} = \zeta \rho v_c^2 \quad , \tag{4.1}$$

where ρ is the local density, ζ is a parameter chosen to be $\zeta = 1/3$ for isotropic turbulence (Stothers 2003; Maeder 2009), and v_c is the local convective velocity.

The regime of validity of the MLT is the subsonic regime, i.e. when the convective eddies move at a speed significantly smaller than the local sound speed. In fact the MLT does not take into account dissipation in case of transonic convective eddies and assumes pressure equilibrium with the medium (Böhm-Vitense 1958). Therefore, given that supersonic convection is unphysical, we limit v_c to the local isothermal sound speed (c_s) with the criteria (Grassitelli et al. 2015b,a)

$$v_c \leq c_s \quad , \quad c_s^2 = \frac{k_B T}{\mu m_H} = \frac{P_{gas}}{\rho} \quad , \tag{4.2}$$

where T is the local temperature, k_b is the Boltzmann constant, μ is the mean molecular weight, and m_H is the hydrogen mass. Consequently, the turbulent pressure can be at most equal to a fraction ζ of the gas pressure.

We do not directly include the effects of turbulent pressure and turbulent energy density in our calculations, estimating the turbulent pressure *a posteriori* via Eq.4.1, since Grassitelli et al. (2015b,a) showed that the structural differences as consequence of the inclusion of turbulent pressure and energy density are small. We expect these effects to be even smaller in low metallicity environments.

4.3 Results

We computed a set of stellar models and stellar evolutionary tracks for non-rotating main-sequence (MS) and post-MS stars with LMC and SMC metallicity (as defined in Brott et al. 2011) in the stellar mass range $1 - 125\,M_\odot$. The stellar evolutionary tracks in the HR-diagram are shown in Fig.4.1 and Fig.4.2, with each stellar model color coded according to the maximum fraction of turbulent pressure within the stellar envelopes, P_{turb}^{max}/P.

4.3.1 OB stellar models

Considering at first the hotter stellar models (i.e. $\log(T_{eff}/K) \gtrsim 4$), the computed evolutionary tracks show that at low luminosities ($\log(L/L_\odot) < 4$) P_{turb} is small ($P_{turb}^{max}/P \ll 1\%$). It tends to increase for higher luminosity, i.e. in the most massive models, for both LMC and SMC metallicity, reaching values of P_{turb}^{max}/P of the order of 3–4% at $\log(L/L_\odot) \approx 6$.

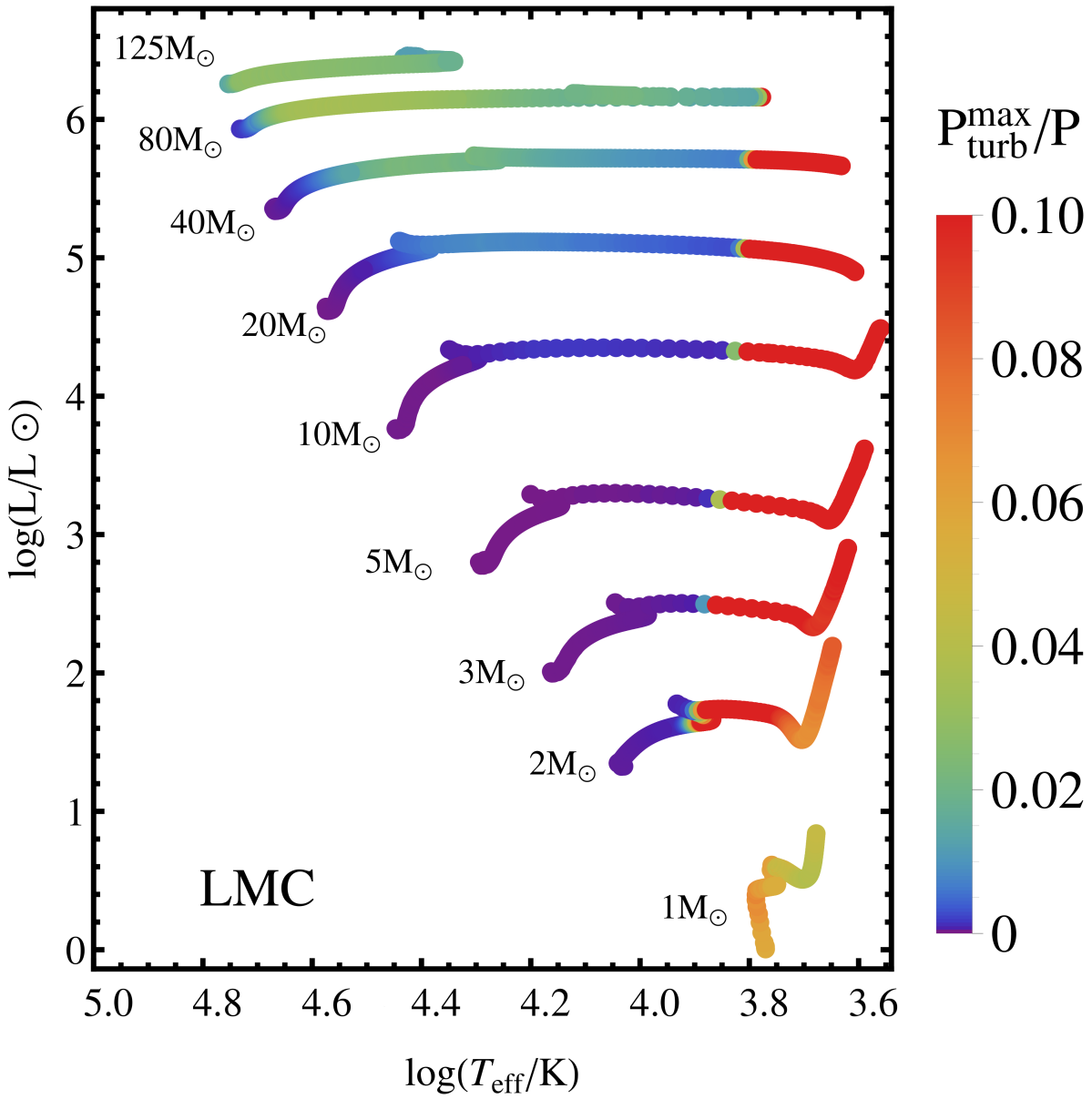

Figure 4.1: HR-diagram showing our stellar evolutionary tracks with LMC metallicity. Each dot indicates a stellar model color-coded according to the maximum fraction of turbulent-to-total pressure (see color bar on the right). The numbers close to the tracks indicate the zero-age-main-sequence mass of the models. Models with P_{turb}^{max}/P between 10% and 33% are colored red. The absolute maximum is found for the massive red supergiants.

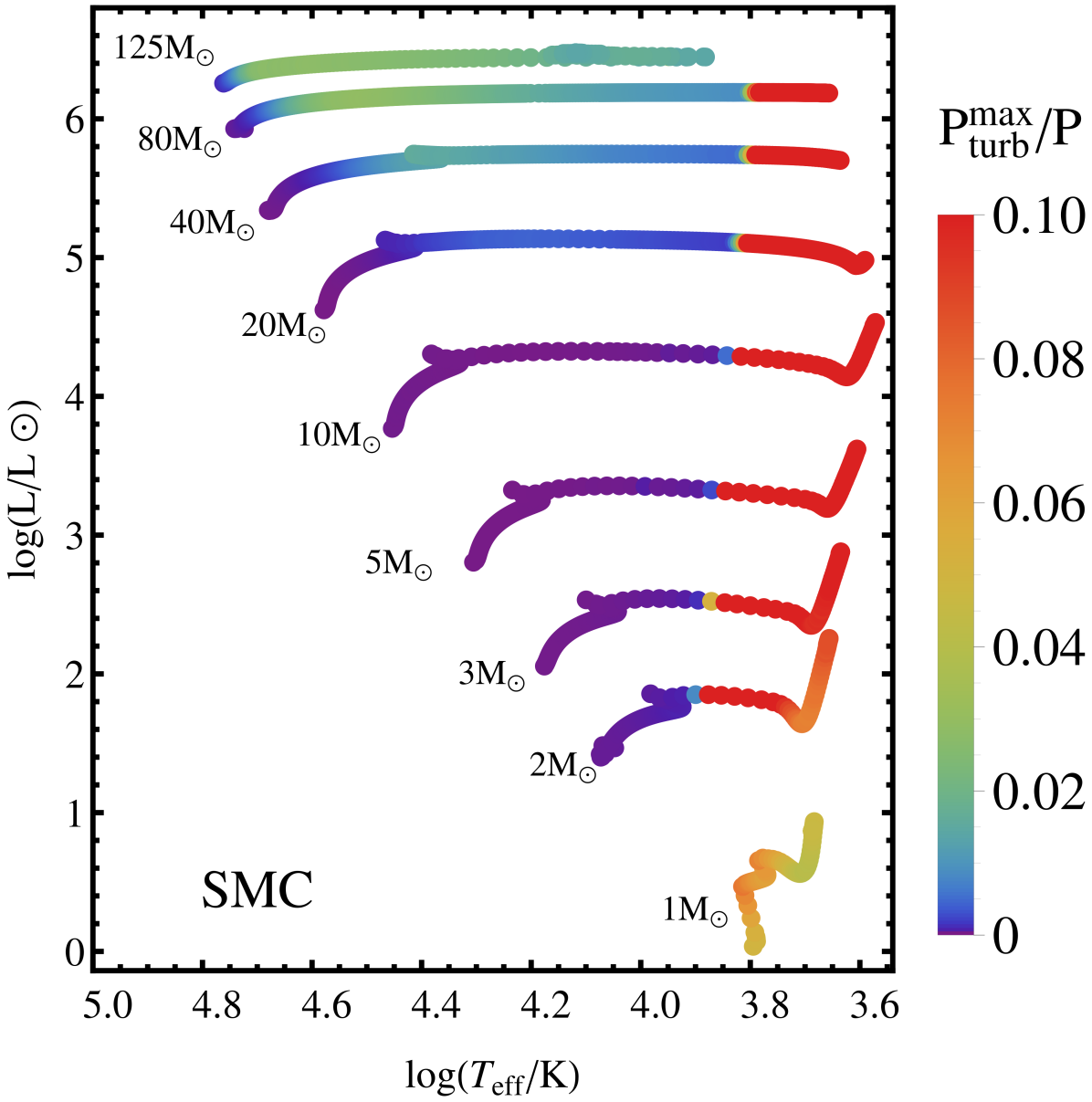

Figure 4.2: Same as Fig.4.1 but for SMC metallicity.

When comparing the stellar tracks in Figs. 4.1 and 4.2 with the Galactic ones in fig.1 of Grassitelli et al. (2015b), it appears that the maximum fraction of turbulent pressure for hot, massive stars is metallicity dependent. This can be seen more clearly in Fig.4.3, where the top part of the HR-diagram is shown for the three different metallicities. The differently coloured regions in the three panels (result of a best fit of the tracks) show that the same maximum contribution of turbulent pressure is located at higher luminosity as the metallicity decreases. Thus there is a trend of larger turbulent pressure fraction at higher metallicity, at either fix luminosity or fix initial stellar mass. This can be explained when considering that the iron opacity bump is less pronounced at metallicities lower than the Galactic one. Consequently the envelope of the stars inflate less for LMC and SMC metallicities compared to those of MW metallicity (Sanyal et al. in prep.). This leads in turn to higher densities in the FeCZ and thus, together with the lower opacities, to more efficient convection. Efficient convection implies low degrees of super-adiabaticity in the convective layers (and vice versa), which in turn imply low convective velocities and thus low pressure arising from the turbulent motion computed via Eq.4.1.

The ratio P_{turb}/P can be rewritten as

$$\frac{P_{turb}}{P} = \frac{\zeta \rho v_c^2}{P} = \frac{\zeta P_{gas} (v_c/c_s)^2}{P} \quad , \tag{4.3}$$

and therefore

$$\frac{P_{turb}}{P} = \zeta \beta M_c^2 \quad , \tag{4.4}$$

where M_c is the Mach number defined as the ratio v_c/c_s, and β is the local ratio of the gas-to-total pressure. In the hot, luminous part of the HR diagram Eq.4.4 leads to a local maximum of P_{turb}^{max}/P at $\log(L/L_\odot) \approx 6$ in both Fig.4.1 and Fig.4.2. This is because at first the Mach numbers increase moving from $\log(L/L_\odot) = 0$ to $\log(L/L_\odot) \approx 6$, until the convective velocities derived via the MLT reach the sound speed. As the convective velocities become transonic, Eq.4.2 limits the Mach number to 1, and therefore the only variable left in Eq.4.4 is β which, as already mentioned, decreases toward higher luminosities, leading consequently to a local maximum for P_{turb}^{max}/P (see Fig.4.6 in Sect.4).

4.3.2 Late-type main sequence stars and red giant models

Given that the metallicity is the fraction of mass of a star that is not in hydrogen or helium, we do not expect significant differences in comparison to the Galactic case for the convective zones arising at the temperatures where H and He recombine (where the helium convective zone is generally not expected to initiate transonic convective motion; Cantiello et al. 2009; Grassitelli et al. 2015b,a). This is the case for the cool stars (i.e. $\log(T_{\rm eff}/{\rm K}) \lesssim 4$) in Fig.4.1 and Fig.4.2. Hydrogen recombines at a temperature of $\approx 8\,000$ K, leading to a convective zone very close to the surface. The fraction of turbulent pressure arising in this convective zone is very high ($P_{turb}^{max}/P \approx 30\,\%$), especially in the more massive models. As it can be seen in Fig.4.1 and Fig.4.2, the HCZ leads to an almost vertical band of high contribution from the turbulent pressure in the HR diagram once the temperature for the recombination of hydrogen is met within the star, very similar to the one found by Grassitelli et al. (2015a). This band stretches from the zero-age-main-sequence of the models with about $\approx 1\,M_\odot$, with about a maximum fractional contribution equal to 10%, up to the most luminous models, where P_{turb}^{max}/P reaches 33%. While moving toward higher luminosities the band widens and its sharp hot edge moves toward slightly cooler temperatures (see Figs.4.1 and 4.2).

In this class of objects the high fraction of turbulent pressure it is not only due to the convective velocities approaching the sound speed (a characteristic shared with the hot luminous stellar models), but also due to the outer layers of the cool stars being gas pressure dominated. In fact the different β values

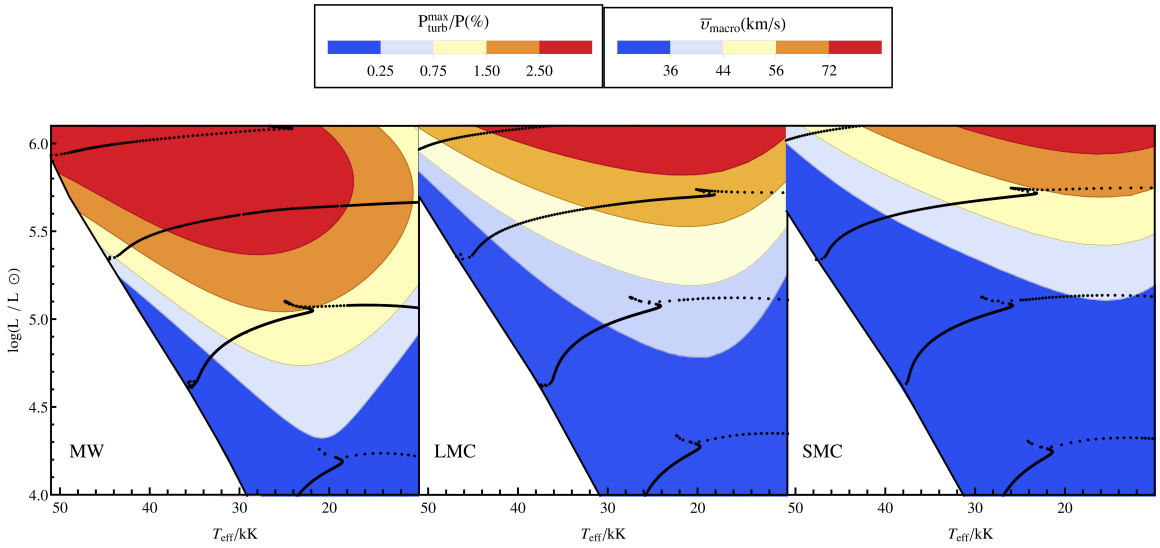

Figure 4.3: HR diagrams color-coded as a function of the maximum fraction of turbulent pressure as derived from a best fit of the tracks in Figure 4.1 (central pannel, LMC metallicity), Figure 4.2 (right pannel, SMC metallicity), and from figure 1 of Grassitelli et al. (2015b) (left pannel, MW metallicity). The values of the expected macroturbulent velocities ($\overline{\upsilon}_{\rm macro}$) given in the top bar were obtained adopting the linear relation between the observationally derived macroturbulent velocities of a sample of Galactic OB stars and the corresponding maximum fraction of turbulent pressure from figure 5 of Grassitelli et al. (2015b).

in the FeCZ of the massive stellar models (0.1 or less) and in the HCZ (close to 1) explain the differences in the contribution from $P_{\rm turb}$ in the cool and in the hot luminous parts of the HR-diagrams (see Eq.4.4).

The low luminosity low temperature corner of the HR-diagrams show instead a fractional contribution from $P^{\rm max}_{\rm turb}$ of a few percent, which is smaller compared to the value found in the slightly hotter models. In fact, once hydrogen recombines within the hydrostatic structure of the models (shown by the hot edge of the bands), a maximum for the ratio $P^{\rm max}_{\rm turb}/P$ is achieved throughout the evolution of a stellar model, followed by a gradual decrease (Grassitelli et al. 2015a). This is because, as stellar models evolve, the HCZ moves to higher optical depths, leading to more efficient convection and therefore lower Mach numbers associated to the convective eddies.

4.3.3 Evolution at 40 $M_\odot$

In Fig.4.4 and Fig.4.5 the outer layers of our 40 $M_\odot$ models for LMC and SMC metallicity are shown throughout their evolution, as a function of $\log(T_{\rm eff}/{\rm K})$ and logarithmic optical depth $\log(\tau)$. When the two models are close to the zero-age-main-sequence, only the FeCZ is present in an optical depth range $\log(\tau)\approx 2-3$, showing in both cases a turbulent-to-total pressure contribution of few percent. As the models evolve toward cooler effective temperature the FeCZ moves deeper inside the star up to an optical depth of $\log(\tau)\approx 4$, and the temperatures become low enough for the HeCZ to arise. In this convective zone however, the turbulent pressure constitutes, in general, only a small fraction of the local pressure ($\ll 1\,\%$). In the temperature range $\log(T_{\rm eff}/{\rm K})$=3.8–3.9 the hydrogen opacity bump induces convection at the surface which becomes more an more extended as the stellar model enters the red supergiant phase. Figures 4.4 and 4.5 show how, below $\log(T_{\rm eff}/{\rm K})$=3.8, the HCZ extends from $\log(\tau)\approx 0$ up to $\log(\tau)\gtrsim 4$, with $P_{\rm turb}$ accounting for up to 33% of the total pressure (limited by the criteria in Eq.4.2).

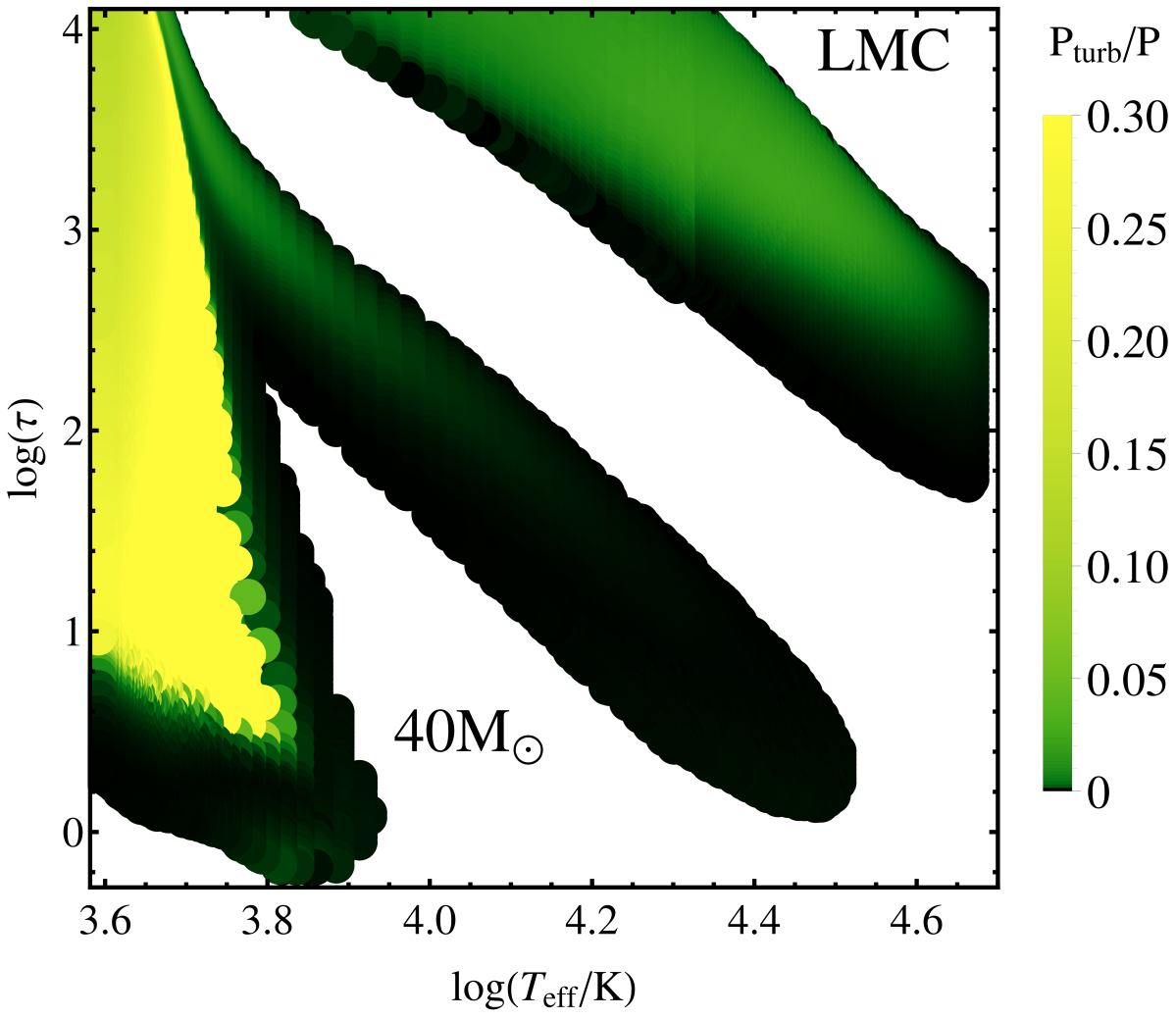

Figure 4.4: Ratio of turbulent-to-total pressure (color coded) as a function of effective temperature and optical depth throughout the evolution of our LMC 40 $M_\odot$ model. The FeCZ is visible in the upper right corner, the HeCZ stretches across the diagram, and the HCZ appears for $\log(T_{\rm eff}/{\rm K})$ below ~3.9. The extended white regions are layers which are radiatively stable.

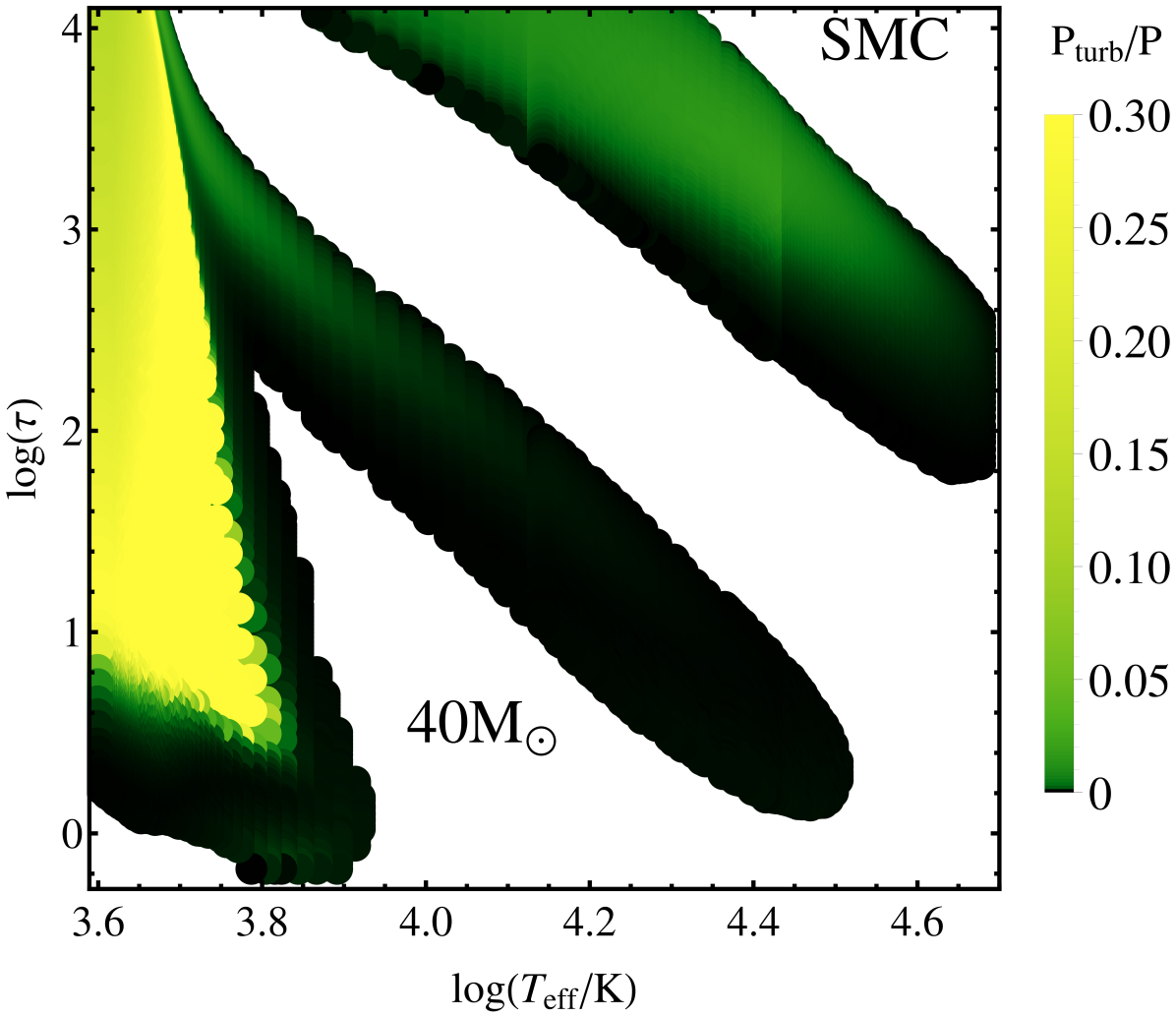

Figure 4.5: Same as Fig.4.4 but with SMC metallicity. Note that the temperature ranges are slightly different.

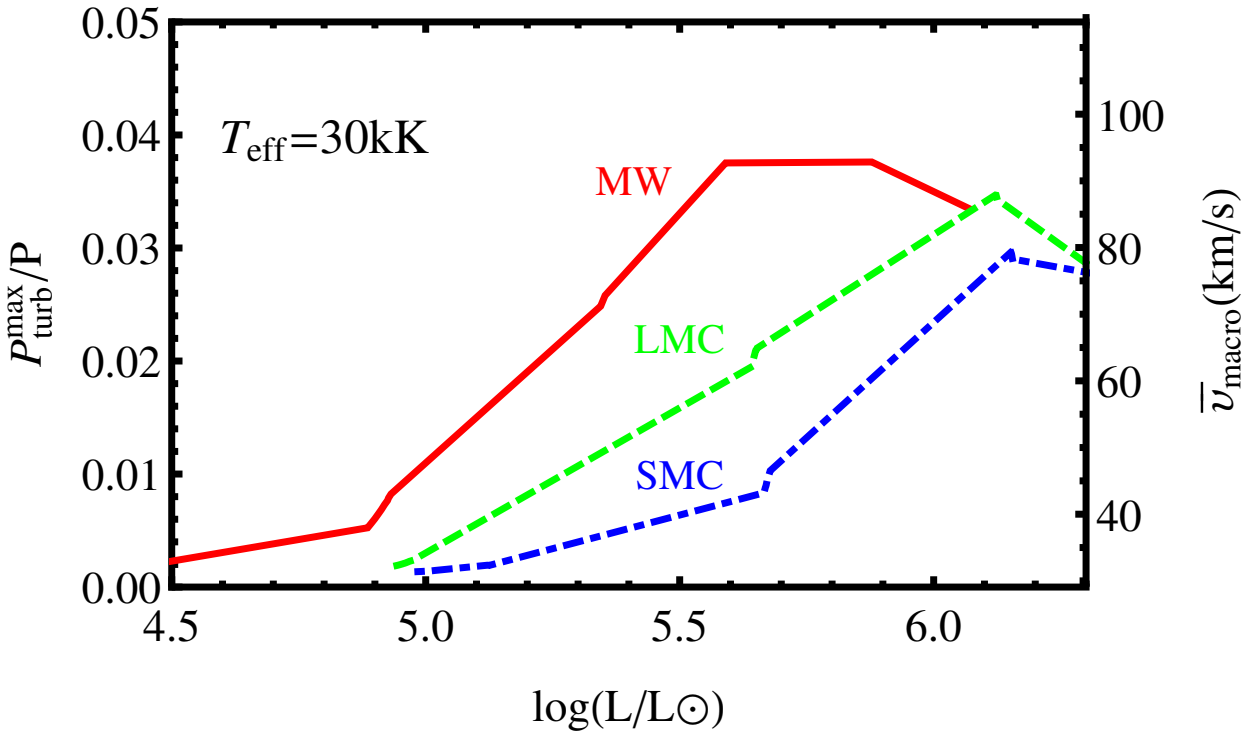

Figure 4.6: Maximum ratio of turbulent-to-total pressure in the case of stellar models at the effective temperature $T_{\rm eff}$=30000K, with MW (red, continouos line), LMC (green, dashed line), and SMC (blue, dot-dashed line) metallicity as a function of their luminosity. The scale on the right indicates the expected macroturbulent velocities ($\overline{\upsilon}_{\rm macro}$) derived via the use of the linear fit in fig.5 of Grassitelli et al. (2015b).

4.4 Observational diagnostic

Grassitelli et al. (2015b,a) showed that the fractional contribution of the turbulent pressure across the HR-diagram can be related to macroturbulent broadening. This is the case for the Galactic OB stars (cf. fig.5 by Grassitelli et al. 2015b) for which a tight correlation was found between the fraction of turbulent pressure and the observed macroturbulent velocities ($\upsilon_{\rm macro}$). In these massive stars the high contribution from the turbulent pressure was encountered in the iron sub-surface convective zone at the base of the envelope. Similarly, a set of late-type low- and intermediate-mass stars showed a linear relation between the observed macroturbulent velocities and the estimated fraction of turbulent pressure (cf. fig.3 by Grassitelli et al. 2015a) arising in this case in the hydrogen convective zone located very close to the surface.

Here, we investigate how macroturbulent broadening is expected to affect the atmosphere of stars with LMC and SMC metallicities. Unfortunately, unlike for the Galactic case (Simón-Díaz 2015), we lack a large sample of observationally derived macroturbulent velocity values for stars in the LMC and the SMC, and therefore a direct statistical comparison is not possible at the moment. However, we compare our predictions to the macroturbulent velocities of a small sample of early B-type stars derived by Dufton et al. (2006) in Sect.4.4.1. To the best of our knowledge this was the only sample of observationally derived macroturbulent velocities, together with $T_{\rm eff}$ and $\log g$, available in the literature.

Assuming a similar correlation between $P^{\rm max}_{\rm turb}$ and $\upsilon_{\rm macro}$ as found for the Galactic stars also for the Magellanic stars, we predict macroturbulence to become important at higher luminosities compared to the

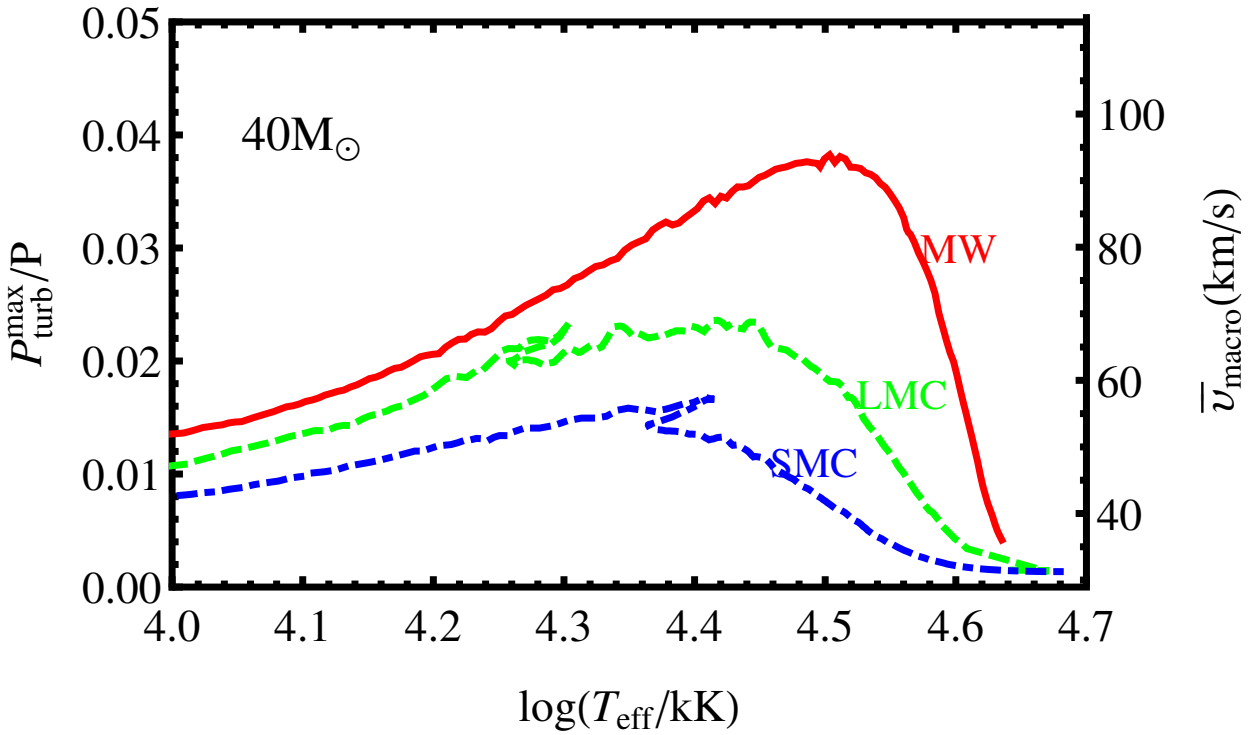

Figure 4.7: Maximum ratio of turbulent-to-total pressure in the envelopes of three 40 $M_\odot$ stellar models with MW (red, continouos line), LMC (green, dashed line), and SMC (blue, dot-dashed line) metallicity as a function of effective temperature throughtout part of their evolution. The scale on the right indicates the expected macroturbulent velocities ($\overline{\upsilon}_{macro}$) derived via the use of the linear relation in fig.5 of Grassitelli et al. (2015b).

Milky Way stars (see Fig.4.3). For example, in LMC and SMC we expect to find macroturbulent velocities induced by turbulent pressure higher than 50 km/s only above luminosities of $\log(L/L_\odot) \approx 5.3 - 5.5$, while at Solar metallicities we find this to happen starting from $\log(L/L_\odot) \approx 5$.

Figure 4.6 shows the maximum contribution from turbulent pressure as a function of luminosity and metallicity at a fixed effective temperature of T_{eff}=30 kK, and macroturbulent velocities are associated adopting the linear fit[1] of the Galactic stars of Grassitelli et al. (2015b). The fraction of turbulent pressure increases while moving to higher luminosity, and consequently the expected values for the macroturbulent velocities increase as a function of luminosity. Figure 4.6 also shows the local maximum of turbulent pressure discussed in Sect.3.1 which occurs due to the limitation of the convective velocities to the local sound speed (see Eq.4.2 and Eq.4.4).

We remark that it is not clear whether the linear correlation derived by Grassitelli et al. (2015b) for the Galactic OB stars applies to the stars of the Magellanic Clouds. This is mostly because the metallicity affects not only the derived values of the turbulent pressure, but also the whole structure of the envelope, potentially leading to a slightly different correlation for the macroturbulent velocities. Moreover, the observationally derived macroturbulent velocities include also the spectral broadening due to microturbulence (Simón-Díaz & Herrero 2014), and this is expected to be metallicity dependent (Cantiello et al. 2009). In any case, we expect stars in the Magellanic Clouds to show, in general, lower macroturbulent velocities.

Indeed, Penny & Gies (2009) proposed, following indirect arguments, that macroturbulent broadening

[1] The linear fit relating P^{max}_{turb} and υ_{macro} in fig.5 by Grassitelli et al. (2015b) writes $\upsilon_{macro} \simeq 31 + 1664 P^{max}_{turb}/P$.

is metallicity dependent. These authors reached this conclusion by investigating the projected rotational velocity distributions of stars in the different environments, finding a cumulative distribution function which differed between the Galaxy and the Magellanic Clouds, as the LMC and SMC stars were showing lower $\upsilon \sin i$ values. This indirect argument provides an empirical support for our scenario, as Penny & Gies (2009) interpreted this difference as a consequence of lower macroturbulent velocities in LMC and SMC. However, before reaching firm conclusions, our predictions should be compared with direct $\upsilon_{\rm macro}$ measurements of stars in the LMC and the SMC, ideally obtained following a similar approach as the one presented in the works by Simón-Díaz et al. (2011b); Simón-Díaz (2015) (i.e. considering a large sample of OB stars covering the whole region of the HRD above $\log(L/L_\odot) \approx 3$).

Figure 4.7 shows the evolution of the maximum fraction of turbulent pressure in the FeCZ as a function of effective temperature of three 40 $M_\odot$ stellar models with different metallicities. This shows how, in the early stages of the main sequence evolution, the ratio $P^{\rm max}_{\rm turb}/P$ tends to increase sharply for the MW metallicity ($\log(T_{\rm eff}) \approx 4.6$), slightly delayed and at lower effective temperature for the metallicities of the Magellanic Clouds (i.e. $\log(T_{\rm eff}) \approx 4.5$–4.6). A maximum is reached in the range $\log(T_{\rm eff}/{\rm K}) \approx 4.4$-4.5 (the exact value is a function of the metallicity and irrespective of the evolutionary phase), followed then by a decrease as the stellar models move toward the low temperatures. Consequently, we expect the macroturbulent velocities to increase sharply at first in the O-type phase, followed then by a decrease in the B-type phase until the red supergiant phase, where hydrogen recombines below the photosphere. This is in agreement with observations by Dufton et al. (2006), Fraser et al. (2010), and Simón-Díaz et al. (2010), who found a clear trend of decreasing macroturbulent velocities going from $T_{\rm eff}$=30 kK to $T_{\rm eff}$=10 kK in a sample of B-type supergiants in the SMC and the MW.

On the other side of the HR diagram, i.e. in the low temperature low luminosity part in Fig.4.1 and Fig.4.2, Grassitelli et al. (2015a) found a linear relation between $P^{\rm max}_{\rm turb}/P$ and $\upsilon_{\rm macro}$ independent of the evolutionary stage of the models, but in this case with the maximum turbulent pressure fraction found in the HCZ and not the FeCZ. In a recent work, Kitiashvili et al. (2016) found that the sub-surface convective motion indeed generates surface granulations and velocity fields of the order of tens of km/s, in line with the suggestion by Grassitelli et al. (2015a). This was done by performing 3D radiative hydrodynamic simulations of the envelopes of F-type stars. The agreement between the induced velocity field and the characteristic values of macroturbulence in these objects is another indication of the likely connection between the two phenomena. Given that the metallicity is not expected nor found to significantly influence the conditions in the HCZ, we predict a similar situation to occur also in the low metallicity environments. If the connection between finite amplitude turbulent pressure fluctuations and the γ-Doradus pulsating stars is confirmed, we expect to find this kind of pulsators also at metallicities other than the Galactic one.

4.4.1 Comparison to macroturbulence measurements

We collected the observationally derived values for the macroturbulent velocity from Dufton et al. (2006) for 13 B-type supergiants in SMC and, by locating them in the HR-diagram, we relate the observed macroturbulent velocities to the maximum fraction of turbulent pressure in our models. In order to do so, we need to take into account that these macroturbulent velocities have been derived using a Gaussian line profile, instead of a radial-tangential line profile (Gray 2005; Simón-Díaz & Herrero 2014) adopted in most of the recent literature. Therefore, to consistently compare the SMC stars to the Galactic ones, we make use of the strong empirical relation in Simón-Díaz & Herrero (2014) between the macroturbulent velocities derived via Gaussian and radial-tangential profiles, which means that all the macroturbulent velocities derived by Dufton et al. (2006) have been increased by a factor 1/0.65 (cf. fig.3 of Simón-Díaz & Herrero 2014).

Once this is taken into account, we can directly compare the macroturbulent velocities as a function of

P_{turb}^{max} /P for the stars in the SMC and the Galaxy. This is done in Fig.4.8, where the 13 B SMC stars are plotted superposed to the Galactic stars and their linear fit as shown in fig.5 of Grassitelli et al. (2015b). As in Grassitelli et al. (2015b,a), the two quantities appear linearly correlated, with a Spearman rank correlation coefficient of 0.74. Moreover, in Fig.4.8 we can see how most of the SMC stars seem to follow a similar relation as the Galactic OB stars.

Given the small sample of stars and the relatively large error bars in the derived stellar parameters (especially $\log g$, which can have error bars as high as 0.3 dex Dufton et al. 2005), we are limited in the interpretation of these results. However, a similar correlation (within the observational uncertainties of $\approx 20\%$ of υ_{macro}) between υ_{macro} and P_{turb}^{max} in SMC further supports the connection between turbulent convection and macroturbulence.

The fact that these SMC stars seem to follow a similar relation as the stars in the Galaxy suggests that a common relation exist between υ_{macro} and P_{turb}^{max} /P from the FeCZ, irrespective of the metallicity. To avoid confusion, we remark that the turbulent pressure does depend on the metallicity, as previously shown, while the relation between υ_{macro} and P_{turb}^{max} might not. We note also that the zero point of the linear relation at ≈ 30 km/s is due to the effects of microturbulence, given that this broadening mechanism (typically of the order of 10 km/s) is not taken into account separately when the macroturbulent velocities are derived. This is illustrated by Simón-Díaz & Herrero (2014), as microturbulence leads to an overestimate of the macroturbulent velocities especially when the relative contribution from microturbulence is important. Microturbulent velocities of the order of 10 km/s can lead to the erroneous interpretation of a macroturbulent velocity of the order of 15-40 km/s even in cases in which no macroturbulent broadening is present (Simón-Díaz & Herrero 2014).

We furthermore compare the macroturbulent velocities of a sub-sample of the B SMC stars in Dufton et al. (2006) to that of some of the Galactic B stars in Simón-Díaz (2015) as a function of $\mathcal{L} := T_{eff}^4/g$ (Langer & Kudritzki 2014) and constant effective temperature. We choose the temperature range where most of the SMC stars are located, i.e. in the range $T_{eff} = 17 - 23$ kK (see also fig.2 by Dufton et al. 2006), and thus restrict the samples in Dufton et al. (2006) and Simón-Díaz (2015) to the stars in this effective temperature range. From Fig.4.6 we predict the stars in the Magellanic Clouds to show in general lower values of υ_{macro} compared to the stars in the Milky Way at fixed luminosity (and also in the case of the same $\mathcal{L}$). This is indeed the case in Fig.4.9, where on average the SMC B stars show lower υ_{macro} values compared to the Galactic B stars in the same temperature range. Anyhow precise and systematic observations of a larger sample of stars in the Magellanic Clouds would make a good test case for the aforementioned hypotheses.

4.5 Conclusions

We computed a set of stellar evolution models with SMC and LMC metallicity in order to compare the fraction of the pressure due to convective turbulence within the stellar envelope to the Galactic case, in different regions of the HR-diagram. We find a trend of lower turbulent pressure fractions for lower metallicities in the OB stars, with contributions up to $\approx 3 - 4\%$ of the total pressure at $\log(L/L_\odot) \approx 6$. This is due to the lower opacities in the sub-surface convective zones induced by the recombination of iron and iron-group elements in the case of the SMC and LMC stellar models. Lower opacities lead to higher densities in the inflated envelopes, which also imply lower degrees of super-adiabaticity and thus lower convective velocities and lower turbulent pressure. No significant differences with the MW models are found in the case of the cool supergiants, for which the highest contribution from the turbulent pressure arises in the HCZ, accounting for up to 30% of the total pressure.

The highly significant correlation between turbulent pressure and macroturbulent velocities for the

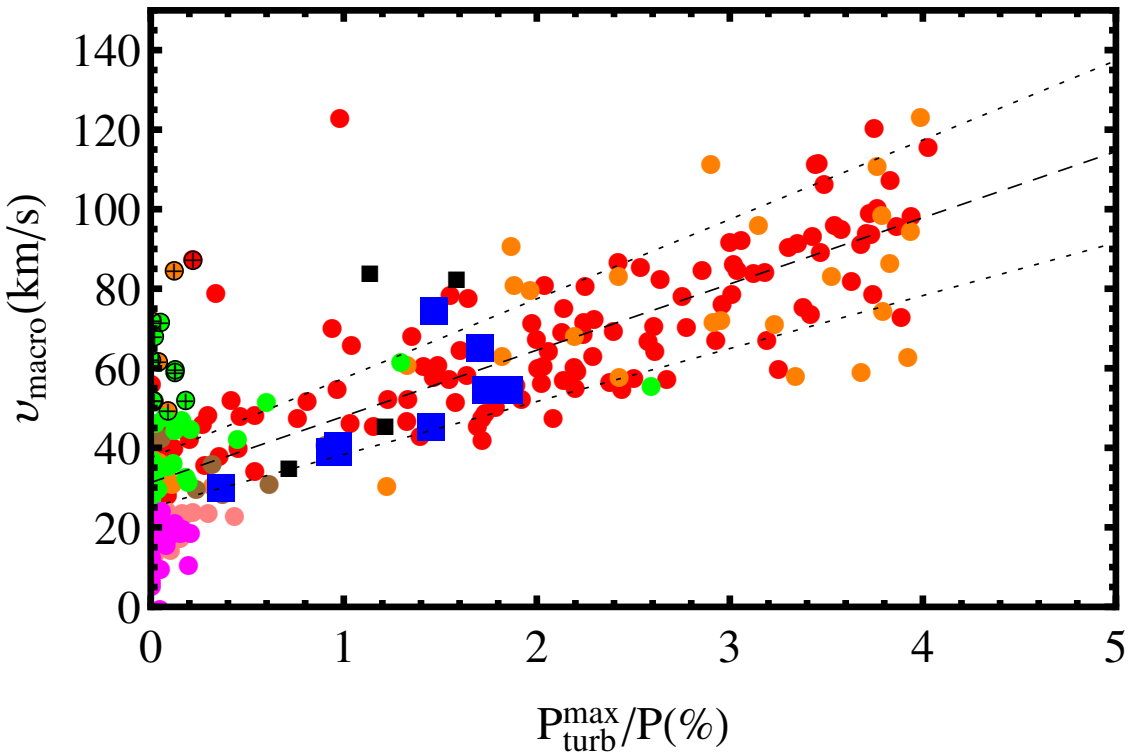

Figure 4.8: υ_{macro} as a function of the maximum fraction of turbulent-to-total pressure for the 13 B-type SMC stars (black and blue squares) in Dufton et al. (2006) compared to the set of Galactic OB stars (coloured circles) in fig.5 of Grassitelli et al.(2015a; for a description of the different colors, see Grassitelli et al. 2015b and Simón-Díaz 2015). Blue circles indicate the sub-sample of 9 stars used also in Fig.4.9. The dashed line indicates the linear best fit adopted to predict the theoretical macroturbulent velocities from fig.5 by Grassitelli et al. (2015b), while the dotted lines indicate standard error bars of $\approx 20\%$ of υ_{macro}.

Galactic stars found by Grassitelli et al. (2015b,a) has been interpreted considering that turbulent pressure fluctuations at the percent level may trigger high-order high-angular degree oscillations. A large number of high-order pulsations has been shown able to collectively mimic the effect of macroturbulence on the spectral lines by generating a velocity field at the surface on a scale larger than the size of the line forming region (Aerts et al. 2009).

Pulsations triggered by stochastic turbulent pressure fluctuations in the sub-surface convective zones, eventually together with classical κ-mechanism pulsations and strange mode pulsations, appear the only candidate at the moment able to explain the macroturbulent velocity fields observed in Galactic stars throughout the HR-diagram. Moreover, Grassitelli et al. (2015a) investigated a possible connection with some pulsating class of stars, namely the γ Doradus class of pulsators, given that the location of the observational instability strip lies within the band (similar to the ones in Fig.4.1 and 4.2) of high contribution from turbulent pressure in the HCZ, i.e. where $P^{max}_{turb} \geq 10\%$. Thus they suggested detailed asteroseismic calculations including the effects of eventually finite amplitude pressure fluctuations associated with time dependent turbulent convection (Dupret et al. 2004; Antoci et al. 2014; Grassitelli et al. 2015a).

Based on the results for the MW stars in the hot part of the HR-diagram we predict the Magellanic

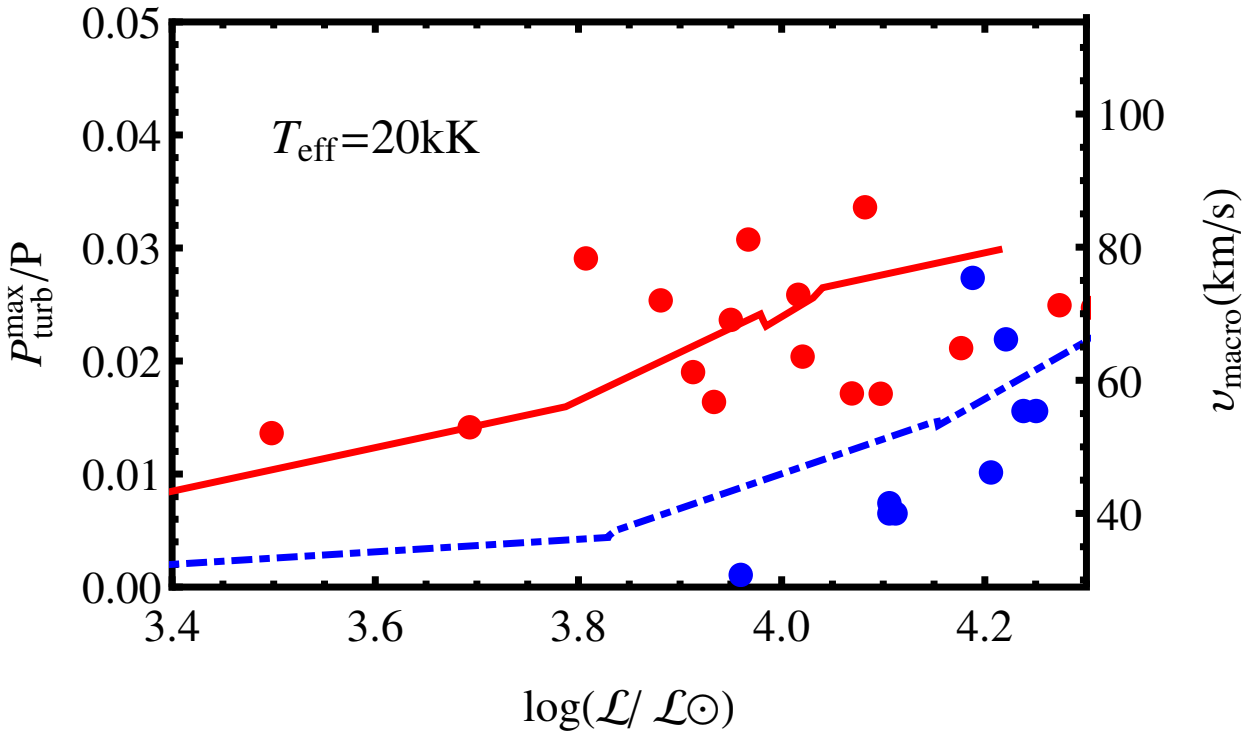

Figure 4.9: $\upsilon_{\rm macro}$ as a function of $\log(\mathcal{L}/\mathcal{L}_\odot)$, with $\mathcal{L} := T^4_{\rm eff}/g$, for the sub-set of SMC B-type stars from Dufton et al. (2006)(blue circles) and Galactic B-type stars from Simón-Díaz (2015)(red circles) in the effective temperature range $T_{\rm eff} \approx 17 - 23$ kK, superposed to the computed $P^{\rm max}_{\rm turb}/P$ (black continous line for the MW, red dashed for the SMC) as a function of $\log(\mathcal{L}/\mathcal{L}_\odot)$ at $T_{\rm eff}$=20kK.

Clouds to show, in general, lower macroturbulent velocities compared to the Galactic stars, as the turbulent pressure fraction is smaller for lower metallicities. This finds observational evidence in the results of Penny & Gies (2009), who found macroturbulent velocities to be function of metallicity in the O-star regime, given the lower $\upsilon \sin i$ found in the Magellanic Clouds. We also find support from the SMC B-type stars by Dufton et al. (2006), which are found with lower macroturbulent velocities compared to the Galactic stars by Simón-Díaz (2015).

When we directly relate the macroturbulent velocities from the SMC B-type stars by Dufton et al. (2006) to the corresponding fraction of turbulent pressure in the envelope of our stellar models, the two quantities appear to be linearly related, as in Grassitelli et al. (2015b,a), although with a lower statistical relevance of the result compared to the previous two cases. However, based on the results from the Galactic stars, the predicted macroturbulent velocities match observations fairly well (see Fig.4.9) and seem to follow the same relation found in the Galactic stars (see Fig.4.8). Also the trend of decreasing macroturbulent velocities in the effective temperatures range 10–30 kK found in the Galaxy and SMC by Simón-Díaz et al. (2010), Fraser et al. (2010), and Dufton et al. (2006) is in good agreement with our predictions. To interpret this trend we notice that, as the stars evolve, the iron convective zone moves deeper inside the star, thus yielding to more efficient convection and therefore lower convective velocities.

We conclude that evidence from this and previous works lead to an understanding of the origin of the macroturbulent broadening as connected to the inefficiency of convection and the consequent vigorous turbulent motion in the sub-surface convective zones. Although the turbulent pressure arising from this motion does not appear to have significant impact on the structure of 1D stellar models, it is intuitive

to imagine that local stochastic pressure fluctuations in the partial ionization zones at the base of the envelope might induce perturbations of the hydrostatic equilibrium which lead to variability at the surface (e.g., Stein & Nordlund 2001; Bedding et al. 2011). Radiation pressure dominated inflated envelopes close to the Eddington limit and inefficient convection are strictly related (Langer 2012; Sanyal et al. 2015; Owocki 2015), thus macroturbulence together with asteroseismic calculations might be used to infer the conditions deep inside the envelopes of massive stars as e.g., the strength and extent of inflation (Sanyal et al. 2015) or the mixing length parameter α (Castro et al. 2014; Grassitelli et al. 2015a). Additionally, inefficient convection might influence the wind of massive stars at its base, as the perturbations originated in the convective zones might induce the formation of structures at or above the photosphere, especially for transonic surface velocity fields (de Jager 1984; Cranmer & Owocki 1996; Prinja et al. 2002; Grassitelli et al. 2016). Given the interplay between large scale magnetic fields and convection, it is possible that strongly magnetic stars do not show vigorous convection, as the magnetic fields may damp or inhibit convection. Therefore we could expect that magnetic stars might be characterized by low macroturbulent velocities, as already noticed by Sundqvist et al. (2013).

CHAPTER 5

Diagnostics of the unstable envelopes of Wolf-Rayet stars

L. Grassitelli[1], A.-N. Chené[2], D.Sanyal[1], N.Langer[1], N. St.Louis[3], J.M. Bestenlehner[4,1], L. Fossati[5,1]

[1]Argelander-Institut für Astronomie, Universität Bonn, auf dem Hügel 71, 53121 Bonn, Germany
[2]Gemini Observatory, Northern Operations Center, 670 North A'ohoku Place, Hilo, HI 96720, USA
[3]Département de Physique, Pavillon Roger Gaudry, Université Montréal, CP 6128, Succ. Centre-Ville, Montréal, H3C 3J7 Quebec, Canada
[4] Max-Planck-Institute for Astronomy, Königstuhl 17, 69117 Heidelberg, Germany
[5]Space Research Institute, Austrian Academy of Sciences, Schmiedlstrasse 6, A-8042 Graz, Austria

Astronomy & Astrophysics 2016, 590, A12

Abstract: The envelopes of stars near the Eddington limit are prone to various instabilities. A high Eddington factor in connection with the iron opacity peak leads to convective instability, and a corresponding envelope inflation may induce pulsational instability. Here, we investigate the occurrence and consequences of both instabilities in models of Wolf-Rayet stars. We determine the convective velocities in the sub-surface convective zones to estimate the amplitude of the turbulent velocity at the base of the wind that potentially leads to the formation of small-scale wind structures, as observed in several Wolf-Rayet stars. We also investigate the effect of stellar wind mass loss on the pulsations of our stellar models. We approximated solar metallicity Wolf-Rayet stars in the range $2 - 17\,M_\odot$ by models of mass-losing helium stars, computed with the Bonn stellar evolution code. We characterized the properties of convection in the envelope of these stars adopting the standard mixing length theory. Our results show the occurrence of sub-surface convective regions in all studied models. Small (≈ 1 km/s) surface velocity amplitudes are predicted for models with masses below $\approx 10\,M_\odot$. For models with $M \gtrsim 10\,M_\odot$, the surface velocity amplitudes are of the order of 10 km/s. Moreover we find the occurrence of pulsations for stars in the mass range 9-14$M_\odot$, while mass loss appears to stabilize the more massive Wolf-Rayet stars. We confront our results with observationally derived line variabilities of 17 WN stars, of which we analysed eight here for the first time. The data suggest variability to occur for stars above $10\,M_\odot$, which is increasing linearly with mass above this value, in agreement with our results. We further find our models in the mass range 9-14 $M_\odot$ to be unstable to radial pulsations, and predict local magnetic fields of the order of hundreds of Gauss in Wolf-Rayet stars more massive than $\approx 10\,M_\odot$. Our study

relates the surface velocity fluctuations induced by sub-surface convection to the formation of clumping in the inner part of the wind. From this mechanism, we expect a stronger variability in more massive Wolf-Rayet stars, and a weaker variability in corresponding low metallicity Wolf-Rayet stars.

5.1 Introduction

Wolf-Rayet (WR) stars of spectral class WNE (nitrogen rich) are very hot, highly luminous stars that are thought to be the bare cores of evolved massive stars. Owing to strong stellar winds, these stars have lost almost all their hydrogen-rich envelope allowing us to model them as H-free helium stars (Chiosi & Maeder 1986; Langer 1989).

Such stars are expected to develop a convective core, due to the high central energy production, and a radiative envelope (Kippenhahn & Weigert 1990). In addition, the temperature in the outer layers decreases so much that another convective region arises because of a bump in opacity at log(T) ≅ 5.3, which is associated with iron and iron-group elements (FeCZ; Langer et al. 1994; Iglesias & Rogers 1996; Gräfener et al. 2012a; Langer 2012). As the opacity increases, the increased radiative acceleration brings the layers close to their local Eddington luminosity and, to avoid exceeding this luminosity, the star is forced to expand forming a low density inflated convective envelope (Petrovic et al. 2006; Gräfener et al. 2012a; Sanyal et al. 2015). This convective region is inefficient in transporting energy, but may lead to observable effects, such as turbulence in the surface layers, and may directly influence the wind at its base (Owocki & Rybicki 1986; Heger & Langer 1996; Glatzel 2005; Moffat 2008; Cantiello et al. 2009; Langer 2012; Gräfener & Vink 2013; Grassitelli et al. 2015b).

The mass-loss rate in massive stars is a crucial ingredient in determining correct stellar parameters, the evolutionary scenario, and consequently the fate of these stars (Langer 2012). In the WR phase the mass-loss rate and wind density are sufficiently high for the stellar winds to be optically thick, obscuring the hydrostatic layers from direct observations.

The spectra of WR stars of type WNE are dominated by broad emission lines of helium and, in part, nitrogen. Spectroscopic analysis of line profiles reveal the presence of systematic variability in the form of emission sub-peaks migrating from the line centre to the wings (Moffat et al. 1988; Lépine & Moffat 1999). Phenomenological investigations of these discrete wind emission elements involve the presence of a high number of randomly distributed stochastic density inhomogeneities, i.e. clumps in the wind of WR stars. The non-periodical nature of these radially propagating clumps and the migration of the sub-peaks have partially ruled out non-radial pulsation as the origin of these inhomogeneities (Cranmer & Owocki 1996; Lépine & Moffat 1999).

These structures in the outflow dynamically arise from instabilities that may be triggered at the base of the wind (Owocki 2015). Given the stochastic nature of this phenomenon, we investigate the conditions in which clumping can be triggered by sub-surface convection and can eventually be enhanced during the radial propagation in the wind by radiative instabilities (Owocki et al. 1988; Owocki 2015). In fact, observational evidence tends to show that clumps are formed at the base of the wind and do not develop when the wind is already significantly supersonic (Davies et al. 2005; Vink 2014; Owocki 2015). The phenomenon called clumping affects the parameters derived from model atmosphere analysis introducing further uncertainties in the observational analysis (Moffat & Robert 1994; Hillier 2008). Therefore an understanding of the origin of the observed variability and instabilities in the outer layers of these stars is fundamental for correctly estimating mass-loss rates and for understanding the physics of radiation pressure dominated winds (Hamann & Koesterke 1998).

As a result of the buoyancy force the convective elements move upwards and downwards and, in some cases, they may reach velocities of the order of the local sound speed. The interaction with the

material in the upper radiative layer may consequently generate gravity waves that propagate to the surface, potentially leading to observable phenomena such as turbulence or small-scale velocity fields, as in the case of micro- and macroturbulence (Goldreich & Kumar 1990; Cantiello et al. 2009; Grassitelli et al. 2015a,b). The appearance of a velocity field at the surface is connected with the outermost region of the sub-surface convective zone and the physical conditions in the low density envelope. However, observing these perturbations at the stellar surface is hampered by the optically thick wind and only indirect evidence might be inferred (Langer 1989; Gräfener & Vink 2013).

Another type of spectral variability is present in the wind of some WR stars. This variability is related to the presence of the corotating interaction regions (CIRs; Mullan 1984, 1986; Cranmer & Owocki 1996; Dessart & Chesneau 2002; St-Louis et al. 2009; Chené & St-Louis 2011), connected with the rotation of WR stars of the order of 50 km/s (Meynet & Maeder 2003; Yoon et al. 2006; Gräfener et al. 2012b). This large-scale variability in the wind of hot massive stars has a periodic behaviour, although this behaviour is epoch dependent, and is thought to be a signature for spiral-like structures appearing in the wind and carried around by rotation (Cranmer & Owocki 1996; Dessart & Chesneau 2002; St-Louis et al. 2009). The triggering mechanism at the base of the wind is probably not related to stochastic convective motions given the periodical stream-like nature of CIRs. Instead, studies have suggested that CIRs are analogous to the spiral structures in the solar corona and solar wind (Hundhausen & Gosling 1976; Gosling & Pizzo 1999; St-Louis et al. 2009), which are linked with magnetic fields and most likely also connected with shocks observed in the wind of hot luminous stars (Berghoefer et al. 1997; Marchenko et al. 2006; Lépine & Moffat 2008). In this paper we neglect to include both CIRs and large-scale variability in our direct analysis, but rather try to enlighten some aspects related to the observed small-scale variability in WR stars.

Furthermore, theoretical works (e.g. Glatzel et al. 1993; Glatzel 1994; Saio et al. 1998) predict the appearance of periodic variabilities arising from pulsations in the envelopes of stars with high luminosity-to-mass ratios. However, up to now, this periodical variability has not been clearly observed and identified, challenging both observations and models. In the context of WR stars, both observation and pulsational analysis need to take into account the effects of mass loss via stellar wind in the outer layers, a key feature in this class of objects. Therefore we also investigate the instability to pulsations of our helium star models in a hydrodynamically consistent way, including the effects of mass loss for the first time.

We present a set of helium star models computed with a state-of-the-art hydrodynamical stellar evolution code. We present the methods used to compute stellar models and to study the interaction between convective and radiative layers in Sect.2, and the results of our analysis are shown in Sect.3. In Sect.4 we present the results obtained from the pulsating models, in Sect.5 we discuss the possible observational signatures comparing our predictions to previously and newly analysed observations, and in Sect.6 we give our conclusions.

5.2 Method

We computed a set of chemically homogeneous helium star models with masses ranging from $2M_{\odot}$ to $17M_{\odot}$ with a one-dimensional (1-D) hydrodynamical stellar evolution code described in Heger et al. (2000), Petrovic et al. (2006), Brott et al. (2011), and references therein. The approach to use chemically homogeneous models is justified since the properties of H-free WN stars are insensitive to the internal chemical structure or evolutionary history (Langer 1989). The code adopts the standard non-adiabatic mixing length theory (MLT) to model the convective regions and physical quantities associated with the convective layers such as the convective velocities (Böhm-Vitense 1958; Kippenhahn & Weigert 1990; Heger et al. 2000). The mixing length parameter α is assumed to be equal to 1.5 as in Abbett et al. (1997).

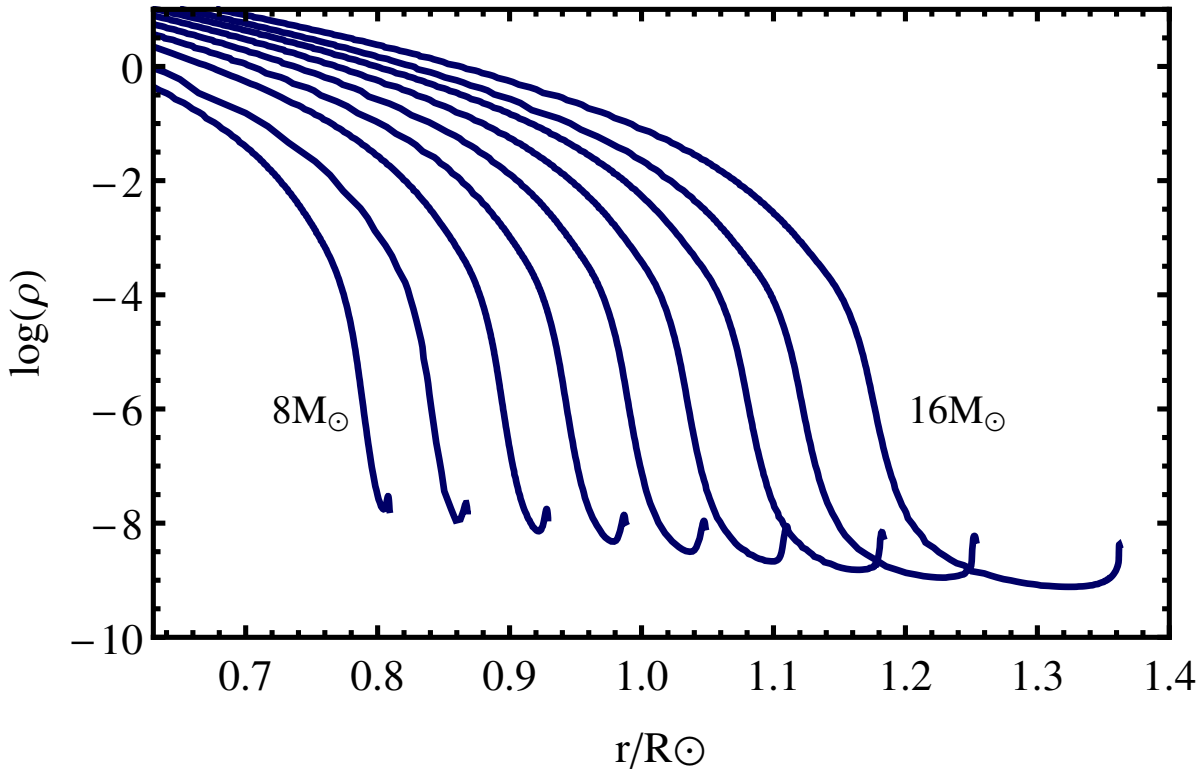

Figure 5.1: Density profiles (in g/cm^3) in the outer regions of our helium stars models with stellar masses ranging from 8 $M_\odot$ to 16 $M_\odot$. The extent of the inflated envelope increases while the density decreases with increasing mass.

The models are computed with outer boundary conditions derived from the assumption of a plane parallel grey atmosphere. A consequence of this assumption is that the feedback from an optically thick wind on the outer hydrostatic layers is neglected. The models are computed with OPAL opacity tables from Iglesias & Rogers (1996) and with a metallicity of Z = 0.02. We adopt the mass-loss rate prescription from Nugis & Lamers (2000) and neglect the effects of rotation and magnetic fields.

In order to determine whether a layer is unstable to convection, we adopt the Schwarzschild criterion, which can be expressed as

$$\Gamma = \frac{\kappa L}{4\pi c G M} \geq (1-\beta)\frac{32-24\beta}{32-24\beta-3\beta^2}, \tag{5.1}$$

where β is the ratio of gas pressure to total pressure, M is the stellar mass, L the luminosity of the star, G the gravitational constant, κ the Rosseland mean opacity, and Γ the local Eddington factor (Joss et al. 1973; Langer 1997).

Below, we compare the convective velocities v_c with the isothermal sound speed to define the Mach number M_c. The low density inflated envelope is defined as the layers above the point at which β is equal to 0.15 (Sanyal et al. 2015). The comparison with the isothermal sound speed in the envelope can be justified by analysing the timescales in the radiation pressure dominated envelopes. The thermal timescale is

$$\tau_{th} = \frac{GM\Delta M_{env}}{RL}, \tag{5.2}$$

where ΔM_{env} is the mass of the inflated envelope and R the stellar radius. This timescale is of the order

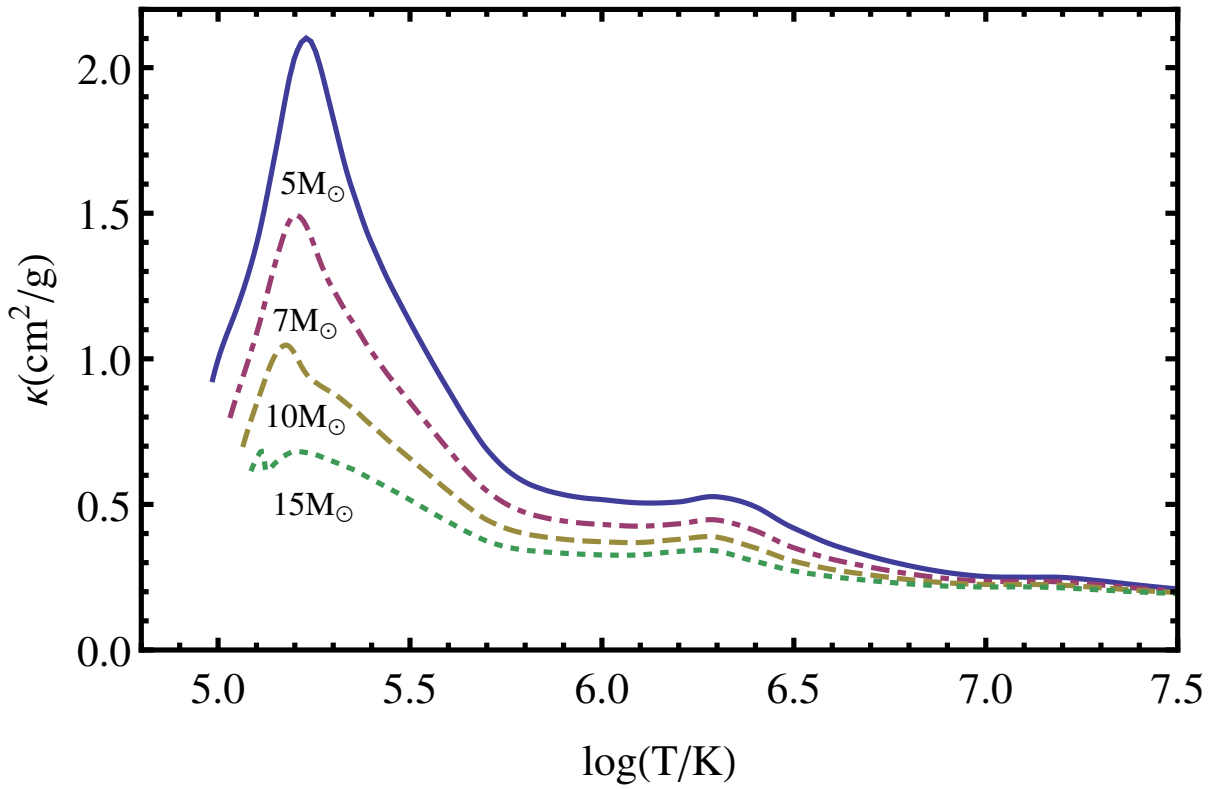

Figure 5.2: Opacity κ as a function of temperature for helium stars of different masses using OPAL opacity tables. The opacity bump from the iron group elements is clearly visible at log(T/K) ≅ 5.3.

of 100 s in our set of models (see Table 5.2), whereas the dynamical timescale $\tau_{\rm dyn}$, which is written as $\tau_{dyn} = \sqrt{R^3/GM}$, is one order of magnitude larger. This suggests that a perturbation would rapidly thermalize, therefore the isothermal sound speed is thought to be a better approximation for the real sound speed in these kinds of models.

Cantiello et al. (2009) presented a study of the convective regions in the outer envelopes of massive main-sequence stars and of the induced velocity field at the surface via propagation of uncorrelated gravity waves. Following Cantiello et al. (2009), we introduce $\langle v_c \rangle$ as the convective velocity averaged over one mixing length starting from the upper boundary of the sub-surface convective zone at r = R_c, defined as in Cantiello et al. (2009),

$$\langle v_c \rangle := \frac{1}{\alpha H_P} \int_{R_c - \alpha H_P}^{R_c} v_c(r)\, dr \quad , \tag{5.3}$$

where the mixing length αH_P is obtained by the product of the pressure scale height H_P (with the pressure given by the sum of gas and radiation pressure) and α. Gravity waves propagate typically with a frequency $\omega \sim M_c \omega_{ac}$, where ω_{ac} is the acoustic cut-off frequency, which is of the order of 10^{-2}Hz in our models, while acoustic waves are expected to have frequencies $\omega > \omega_{ac}$. Goldreich & Kumar (1990) showed that it is possible to estimate the fraction of convective energy flux going into acoustic and gravity waves from

$$F_g = M_c\, F_c \quad , \quad F_a = M_c^{\frac{15}{2}}\, F_c \quad , \tag{5.4}$$

where F_c is the total convective energy flux and F_a and F_g are the energy fluxes transported by acoustic and gravity waves, respectively. As a result, in the hydrostatic sub-sonic regime (where $M_c < 1$) we expect most of the convective energy to go into gravity waves.

In order to investigate the influence of the sub-surface convective zone in helium stars and relate the convective motion to observational phenomena at the surface without the ability to compute the energy dissipation by the gravity waves along the path exactly, we introduce an upper limit to the expected velocity amplitude at the surface based on the conservation of energy, namely

$$v_{surf} \leq \langle v_c \rangle \sqrt{M_c \frac{\rho_c}{\rho_s}} \quad , \tag{5.5}$$

where ρ_s and ρ_c are the densities at the surface and at the upper border of the convective zone and where the Mach number is defined as

$$M_c = \frac{\langle v_c \rangle}{c_T} \quad , \tag{5.6}$$

where c_T is the isothermal sound speed at the top of the FeCZ (Goldreich & Kumar 1990; Cantiello et al. 2009).

5.3 Sub-surface convection

Our helium star models with masses ranging from 2 to 17 $M_\odot$ are within the luminosity range $\log(L/L_\odot) \approx 4 - 5.5$ and the temperature range $\log(T_{\rm eff}/K) \approx 4.9 - 5.1$ (Table 5.1), which is very close to the helium zero age main-sequence computed by Petrovic et al. (2006) and by Gräfener et al. (2012a). We encounter numerical difficulties in treating models more massive than 17 $M_\odot$, especially in connection to mass loss by stellar wind and, therefore, we do not investigate them. We find inflated envelopes in the outer layers of models with $M \geq 6\,M_\odot$, which become more extended with increasing luminosity-to-mass ratios. For nearly all inflated regions we find $\Gamma(r) \approx 1$ (Gräfener et al. 2012a; Sanyal et al. 2015, see Fig.5.1).

All computed models have a convective region close to the surface extending over a significant fraction of the stellar radius ($\lesssim 10\%$) and that comprises a very small amount of mass, i.e. less than $10^{-8}\,M_\odot$ (see Table 5.1). This convective region arises because of the opacity bump at $\log(T/K) \cong 5.3$ (see Fig. 5.2). An estimate of the relative amount of flux carried by convection (Kippenhahn & Weigert 1990) in our models can be given via

$$\frac{F_c}{F_{tot}} = \frac{4\rho\, c_P T v_c^3}{\alpha H_P\, g\, F_{tot}} \quad , \tag{5.7}$$

where F_c and F_{tot} are the convective and total flux, respectively, c_P is the specific heat at constant pressure, T is the temperature, ρ is the density, and g is the gravitational acceleration. The fraction of convective flux decreases when the convective layers are increasingly radiation pressure dominated, i.e. with increasing stellar mass, going from 10^{-6} in the low mass to 10^{-10} in the more massive helium star models of our sample. The partial ionization zones due to helium and hydrogen recombination are absent as the surface temperatures of our models are $\log(T_{\rm eff}/K) \geq 4.9$ (see Fig.5.2).

Our models show that the convective velocities within the sub-surface convective zone are a function of the stellar mass and of the radial coordinate within the convective zone. Figure 5.3 shows the presence of a convective zone in all the investigated models, whose spatial extent gradually increase for higher masses.

The helium star models up to $10\,M_\odot$ display a convective zone that extends over less than 1% of the stellar radius and with convective elements that reach on average velocities not higher than few km/s.

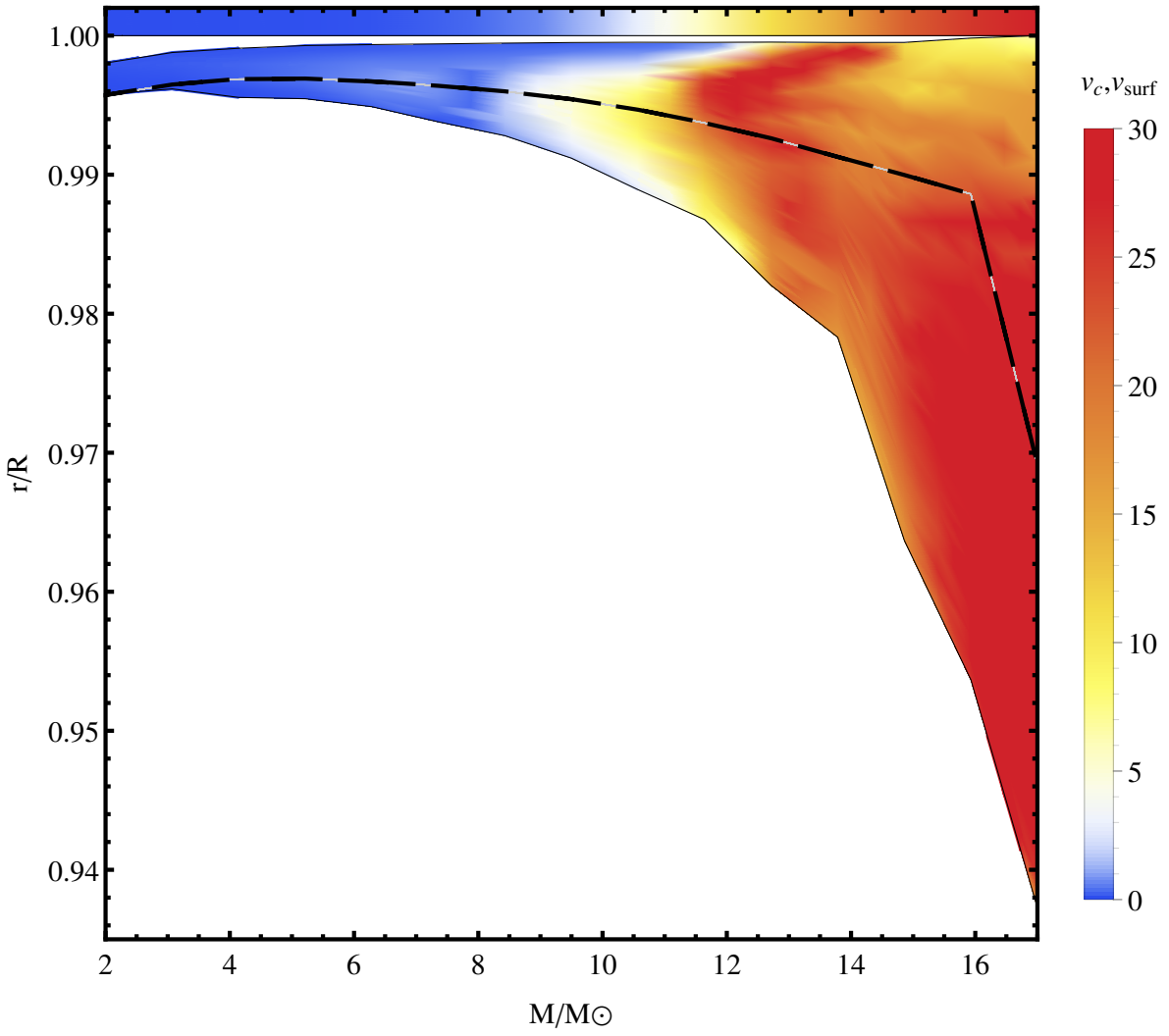

Figure 5.3: Normalized radial coordinate as a function of the mass of our helium star models for the outer 6.5% of the stellar radius. The white region represents radiative layers, while the coloured region denotes convection. The colours indicate the convective velocities within the FeCZ (in km/s); the black dashed line superposed lies one mixing-length away from the upper border of the convective region. The colours in the top bar indicate the expected velocity fluctuations at the surface (see also Fig.5.4 for a direct comparison between $\langle v_c \rangle$ and v_{surf}).

The models with $M \geq 10\,M_\odot$ have convective zones that show convective velocities of the same order as the local sound speed, i.e. velocities up to 30 km/s. Figure 5.3 shows how convection moves deeper inside in normalized radial coordinate as the envelope becomes larger, and, therefore, it occupies a larger fraction of the stellar radius. The convective region also moves closer to the surface, reaching it in the $17\,M_\odot$ model.

The increase in size of the convective zone is connected to the larger inflated envelope when moving towards higher luminosity-to-mass ratios (Petrovic et al. 2006; Sanyal et al. 2015, see Fig.5.1). The envelopes become more and more dominated by radiation pressure dominated for higher mass stellar models, density, and β decrease while $\Gamma(r)$ stays approximately equal to unity and the Schwarzschild criterion for convection (see Eq.5.1) is fulfilled in a larger region. The convective velocities also significantly increase for higher mass models, with the maximum occurring in the lowest density regions (see Fig.5.1), i.e. where β is at its minimum.

We compute the average velocity of the convective elements in the upper part of the sub-surface convective zone (Eq.5.3), assuming implicitly that only the elements in the last mixing length can interact with the upper radiative layer (Fig.5.3). The models show that these average velocities are smaller than 2 km/s for stars with masses below $10\,M_\odot$. For models with $M \geq 10\,M_\odot$, $\langle v_c \rangle$ becomes larger with values of the order of 20 km/s in the case of $15\,M_\odot$ (Fig. 5.4). This result can be related again with the fact that when we approach higher stellar masses, the luminosity-to-mass ratios increase. This inflates further the stellar envelope which in turn increases the mixing length and, combined with the higher luminosities, increases the convective velocities (see Fig. 5.1, Kippenhahn & Weigert 1990; Sanyal et al. 2015). This is in agreement with Cantiello et al. (2009) and Grassitelli et al. (2015b), who find that convective velocities in the FeCZ are higher for higher luminosities, while here, conversely from main-sequence stellar models, the convective velocities are in general higher for higher effective temperatures.

Figure 5.4 shows the average convective velocities at the top of the iron convective zone and the expected velocity perturbation at the surface. We can see how the velocities are attenuated in the radiative zones, i.e. the expected velocity fields at the surface are smaller than $\langle v_c \rangle$. This is due to the factor $\sqrt{M_c\,\rho_c/\rho_s} < 1$ in Eq.5.5. However the expected v_{surf} roughly follow the increase of the convective velocities in the case of the most massive models. Moreover in the models computed with a stellar mass larger than $12\,M_\odot$, the relative attenuation becomes lower and the difference between the average convective velocities and surface velocity fields is reduced. In fact the convective layers approach the surface and the radiative layers are less extended. Both the Mach number and ratio ρ_c/ρ_s approach unity in the models more massive than $15M_\odot$ with the convective zone reaching the surface in the $17M_\odot$ model. In this configuration one can forsake the assumption made in Eq.5.5 concerning the propagation of the waves, given the absence of a radiative layer separating the convective region from the surface.

We thus infer from Fig.5.3 and Fig.5.4 that low-mass helium stars are not expected to show strong velocity fields originating in the iron convective zone at the base of the wind. A steeper trend of increasing surface velocity fluctuations is expected for helium stars with higher luminosity-to-mass ratios due to the higher convective velocities in the region of the iron bump and the lower distance from the surface. An extrapolation of these results to higher masses ($\geq 17M_\odot$) needs to be performed with caution. This is because the computed convective velocities are expected to become supersonic and the standard MLT may not apply anymore (Goldreich & Kumar 1990; Canuto & Mazzitelli 1991).

The number of clumps expected to be triggered by these perturbations may be roughly estimated, assuming a transversal correlation length at the surface of the order of the local pressure scale height (Cantiello et al. 2009). This is usually of the order of 10^9 cm in our massive models, a scale that is very similar to the lateral coherence scale of few degrees that is able to reproduce observations by Dessart & Owocki (2002) while investigating the line profile variability of small-scale structures in the wind of WR

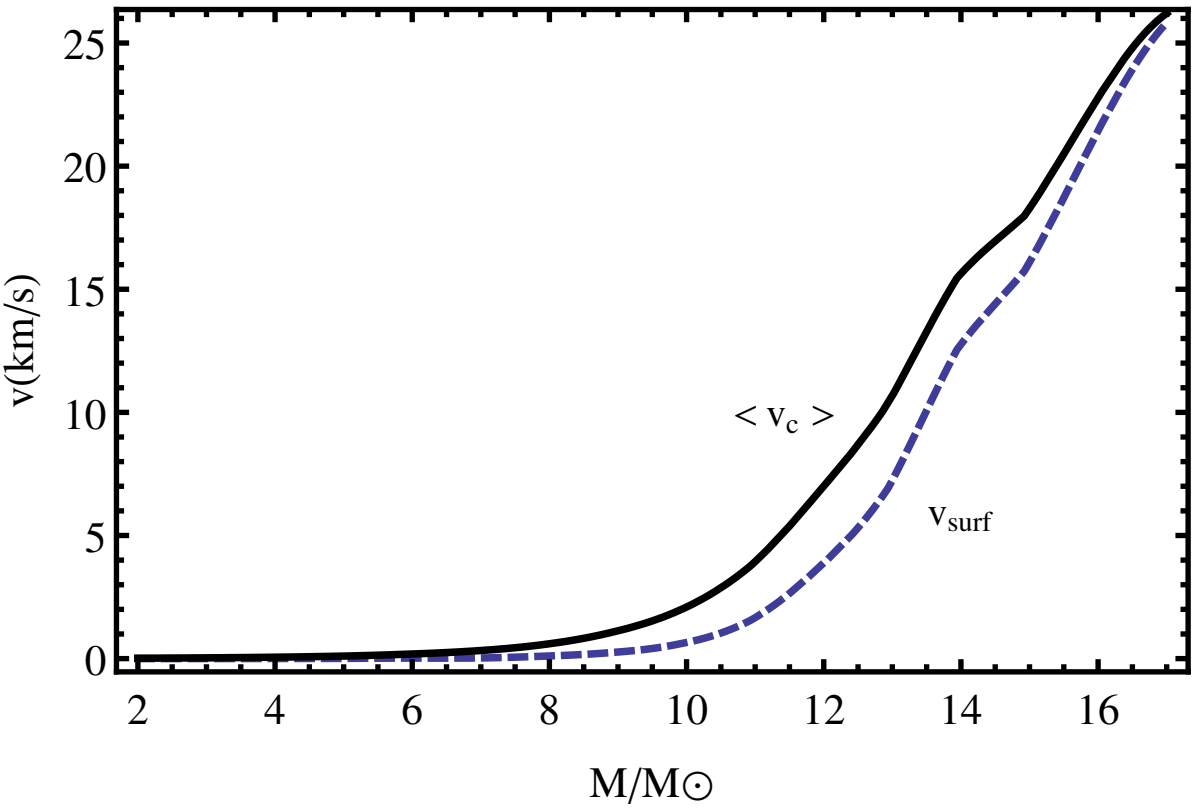

Figure 5.4: Average velocity (black solid line, $\langle v_c \rangle$) of the convective elements at the top of the convective zone and expected surface velocity fluctuations (blue dashed line, v_{surf}) as a function of stellar masses.

stars. With this approach, we estimate a number of clumps N_{Clumps},

$$N_{Clumps} = \frac{4\pi H_P^2}{4\pi R^2} \approx 10^3 - 10^4, \tag{5.8}$$

with a decrease in number for the more massive models.

In summary, convective velocities of the order of the local sound speed have been found in the case of the highest mass models considered here. A steep increase in $\langle v_c \rangle$ has been found starting from $\approx 10\,M_\odot$. Similarly, the expected velocity field at the surface sharply increases for $M > 10\,M_\odot$, approaching the local sound speed for the most massive models.

5.4 Pulsations

In low density extended envelopes of stars with high luminosity-to-mass ratio, such as the envelopes of our massive helium main-sequence stars (Fig.5.1), the appearance of so-called strange mode pulsations is expected (Glatzel et al. 1993; Saio et al. 1998; Owocki 2015). The main characteristic of these pulsations is their occurrence in regions where the ratio of the local thermal-to-dynamical timescale is small ($\tau_{th}/\tau_{dyn} \ll 1$, see also Sect.2 and Table 5.2). This is the case for WR stars and makes them good candidates for the appearence of pulsational instabilities in their radiation pressure dominated envelopes. The short thermal timescales exclude a thermal origin for these kind of pulsations, unlike κ and ϵ mechanisms (Glatzel 1994; Saio et al. 1998; Blaes & Socrates 2003).

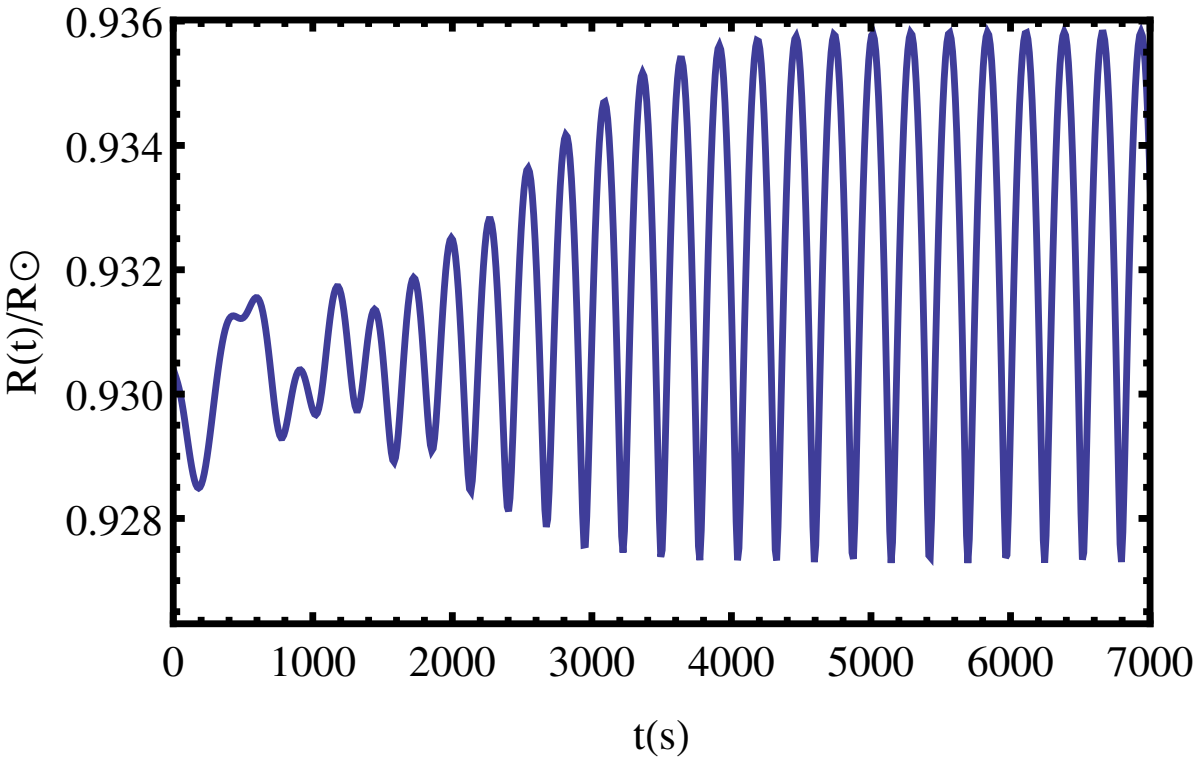

Figure 5.5: Evolution of the radius as a function of time for a $10 M_{\odot}$ radially pulsating helium star model. The pulsation amplitude grows rapidly before saturating.

We use the same hydrodynamical stellar evolution code introduced in Sect. 2 to analyse the pulsational properties of our models. This code has already been used to investigate pulsations in the red supergiant phase by Yoon & Cantiello (2010) and is tested against linear pulsation analysis for basic pulsational properties in Heger et al. (1997). The code adopted here is fully implicit and therefore numerical damping may be present (Appenzeller 1970).

Radial pulsations in our models were found to be excited in the mass range 9-14 $M_{\odot}$. They show a short growth time of the order of few dynamical timescales, which is a characteristic feature of strange mode instabilities (see Fig.5.5 and Glatzel 1994). After the growth phase, all these models reach saturation. Stability tests with respect to radial perturbations for helium main-sequence models have been investigated in Glatzel et al. (1993), who identified the set of unstable modes as strange modes. We find that our pulsation periods are in good agreement with those of the lowest order unstable modes in Glatzel et al. (1993). The periods obtained with our models are plotted in Fig.5.6 and listed in Table 5.2. The pulsation periods almost linearly increases with stellar mass (Fig.5.6). This is related to the larger spatial extent of the envelope and increased dynamical timescale in the high mass models. No pulsations are found for models below 9 $M_{\odot}$ in contrast to the stability analysis performed by Glatzel et al. (1993), where modes are excited for stellar masses as small as 5 $M_{\odot}$.

From Fig.5.7 we can see how the extent and position of the convective zone within the stellar model evolves during a pulsation cycle. The convective zone in Fig.5.7 is no longer strictly shaped by the iron opacity bump, but follows the perturbed layers where the density, and therefore the opacity, is higher. It moves periodically from deeper inside the star where the convective zone forms during the contraction of the envelope, up to the surface when the compression wave reaches the surface and forces the envelope

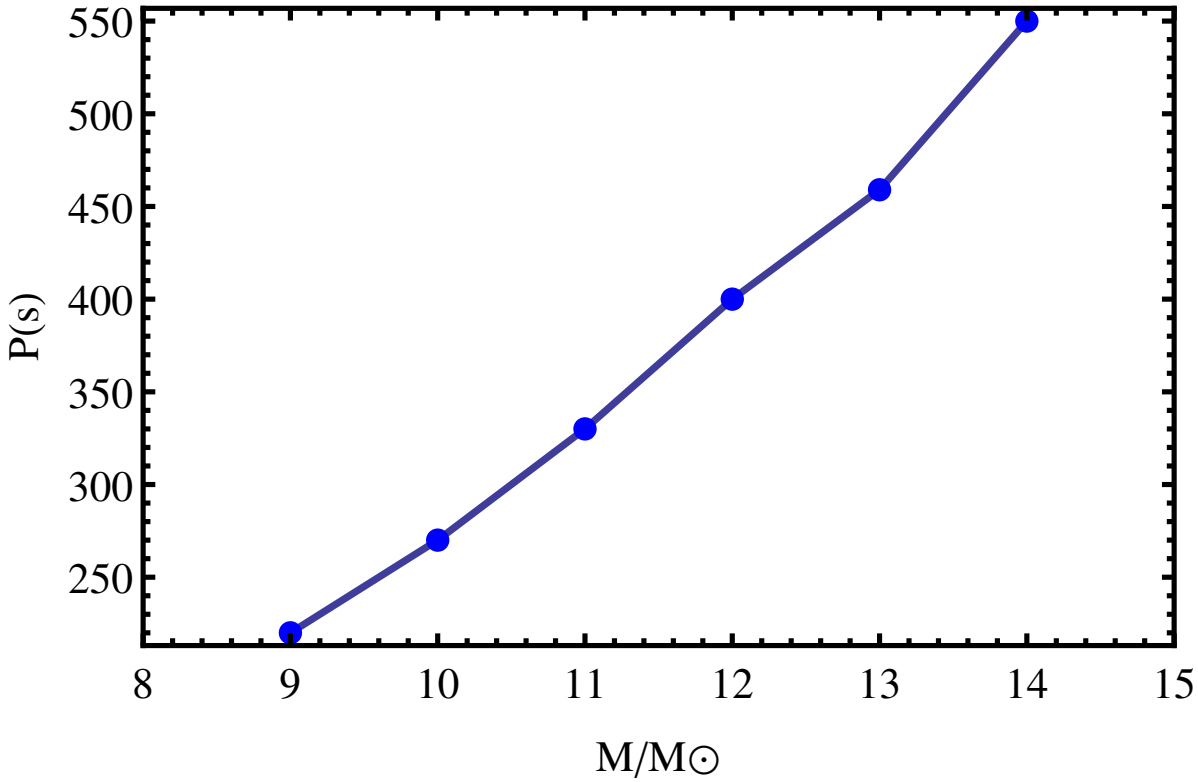

Figure 5.6: Period of a saturated pulsational cycle for different pulsating model masses.

to expand. During a pulsation cycle part of the envelope shows significantly high values of the local Eddington factor, up to $\Gamma \approx 1.5 - 2$ in the contraction phase.

The saturated amplitude of the pulsations ΔR is plotted in Fig.5.8. The amplitude is defined as the difference between the minimum and maximum radius in a saturated pulsation cycle. In Fig.5.9 we show the maximum surface radial velocity amplitude due to the radial pulsations ($v_{\rm osc}^{\rm max}$). Figure 5.8 shows an increase of the maximum pulsation amplitude from 9 to 13 $M_\odot$, which is connected to the higher radial velocity (see Fig.5.9). In contrast, the 14 $M_\odot$ model has a lower maximum amplitude and maximum velocity than lower mass models. No other pulsating model has been found for masses $M > 14\,M_\odot$, when mass loss was applied. Conversely, we find that higher mass models without mass loss are also unstable to more than one mode. We therefore interpret the decrease of the amplitude for the models with higher masses as the result of the higher mass-loss rate. For the pulsating 14 $M_\odot$ model, which shows $\Delta R/R$ of the order of 0.03 with no mass loss applied, the pulsation amplitude is smaller when mass loss is applied ($\Delta R/R = 0.0085$). In these cases the amount of mass depleted from the inflated envelope during a pulsation cycle becomes larger than 5%, which is equivalent to 40% of the envelope radial extent in a hydrostatic non-pulsating configuration.

Although the WR mass-loss rates proposed by Nugis & Lamers (2000) are approximately 2 orders of magnitude smaller than the critical mass-loss rate necessary to remove the inflated envelope (Petrovic et al. 2006), the absence of radial pulsations for masses $M > 14\,M_\odot$ can be explained as a stabilizing influence of mass loss on the strange modes instability. These models are in fact expected to be unstable in the context of the analysis carried out by Glatzel et al. (1993). However, neither Glatzel et al. (1993) nor any other author (at the best of our knowledge) included mass loss in their stability analysis.

From Fig.5.9 we notice that pulsations occur with supersonic velocities with values up to a factor 4

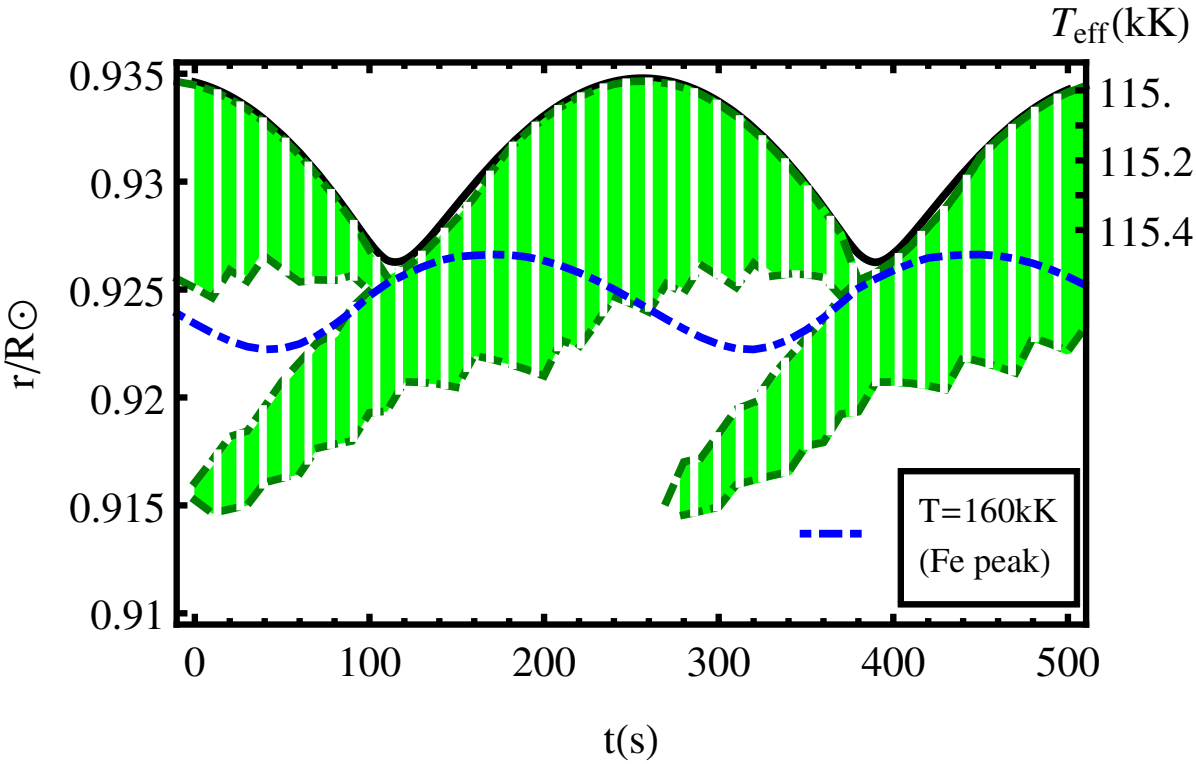

Figure 5.7: Radial coordinate and surface temperature as a function of time for a 10 $M_\odot$ pulsating stellar model. The black thick line is the surface of the stellar model and the green striped region shows the layers unstable to convection during a pulsation cycle. The blue dot-dashed line tracks the location as a function of time of the temperature at which the iron opacity peak is maximum in a static configuration, i.e. log(T/K) ≈ 5.3 (see also Fig.5.2).

higher than the isothermal sound speed. This is another peculiar feature of the strange mode instability (Glatzel 1994, 2005). Instead, the luminosity variations during a saturated pulsation cycle are very small (see Tab.5.2), corresponding to a variability of the order of 10^{-7} bolometric magnitudes. The results obtained here show that strange modes in mass-losing, H-free WR stars occur in the mass range 9-14$M_\odot$ with periods of the order of minutes, amplitude of the order of 1% of the stellar radius, and supersonic radial velocities. The amplitude of the pulsations increases as a function of mass in the range 9-13 $M_\odot$, while pulsations are damped or inhibited for the more massive models considered here, i.e. $M \gtrsim 13\,M_\odot$ and with $\dot{M} \gtrsim -10^{-5}\,M_\odot$/yr. Consequently, the most massive H-free WR stars may not be unstable against pulsations. Therefore, the role of pulsations in driving the wind or in inducing instabilities in WR stars may not be crucial, or their importance can be restricted to the mass range 9-14 $M_\odot$.

5.5 Comparison with observations

One of the dominant features characterizing WR stars is their strong, partly optically thick wind. Such a feature shrouds the hydrostatic surface of the star and we are only able to have indirect evidence of the physical conditions at the base of the wind.

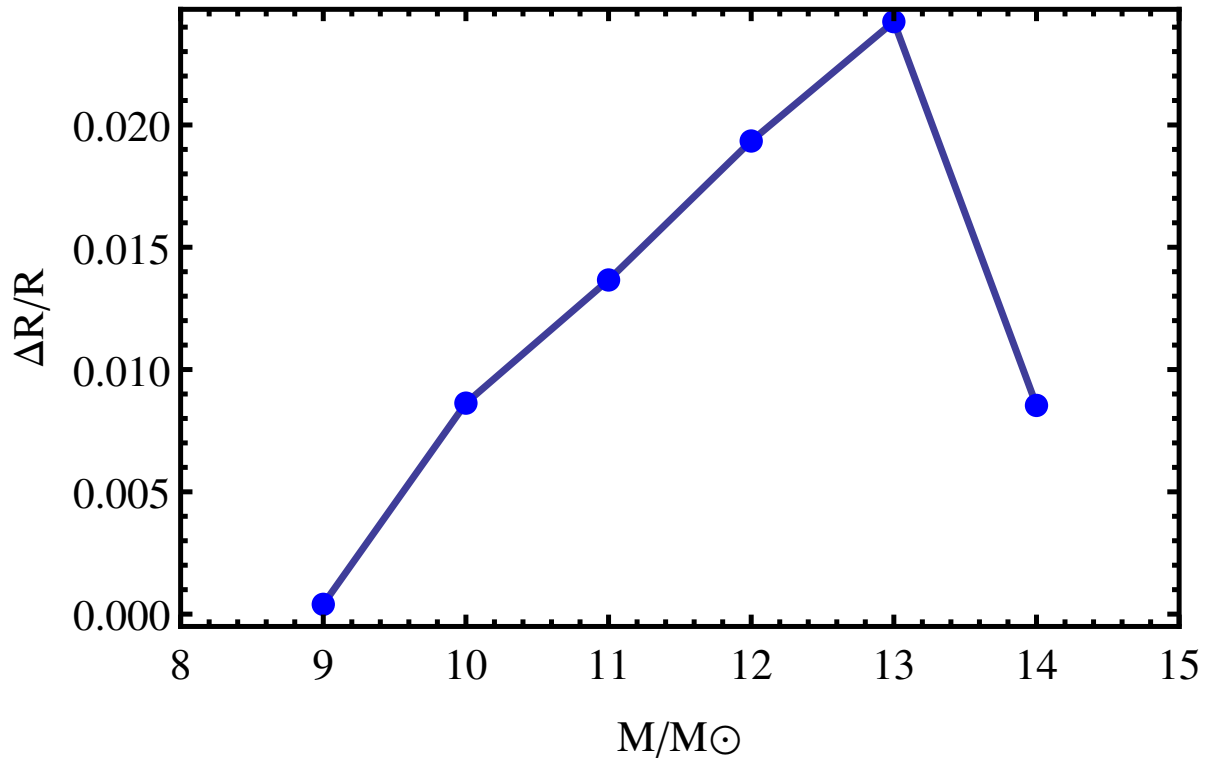

Figure 5.8: Saturated amplitude of the pulsations appearing in the helium star models. The decreasing amplitude above $13M_{\odot}$ is believed to be an effect of the increased mass-loss rate.

5.5.1 Spectral variability

Seeking to test the influence of the velocity field generated by the sub-surface convective zone and to relate it to the formation of clumps, we compare our results with the recent studies by Michaux et al. (2014), Chené & St-Louis (2011), and St-Louis et al. (2009). These works focus on WR stars and the variability of WR spectral lines and are based on atmosphere models from Sander et al. (2012) and Hamann et al. (2006). Additionally, we analyse the spectra of eight WR stars of the WN spectral type as described in Appendix A.

Our goal is to verify whether an increasing small-scale variability level as a function of the estimated mass can be found in some spectral lines, as expected from Fig.5.4. Following St-Louis et al. (2009), Chené & St-Louis (2011), Michaux et al. (2014), and the formalism of Fullerton et al. (1996), we consider the rms variation across the HeII wind spectral lines relative to the local continuum strength identified as variable σ. We did this to investigate the spectroscopic variability in the sub-sample of H-free WR stars of the WN subtype (see Chené & St-Louis 2011, and reference therein for further details). The degrees of spectral variability σ were derived in general from only four to five spectra per star, which does not allow a direct distinction between stochastic and periodic variability. This in turn does not always allow for a direct distinction between WR stars showing CIRs and WR stars with only clumping, which is achieved by characterizing the kinematics of the excess emission on top of the emission lines that either move from one line edge to the other in the case of CIRs, or from the line centre to the line edges in the case of clumps.

From Michaux et al. (2014), which is mostly a compilation of the data of St-Louis et al. (2009) and Chené & St-Louis (2011) for the WN class, we exclude the objects showing to some extent hydrogen

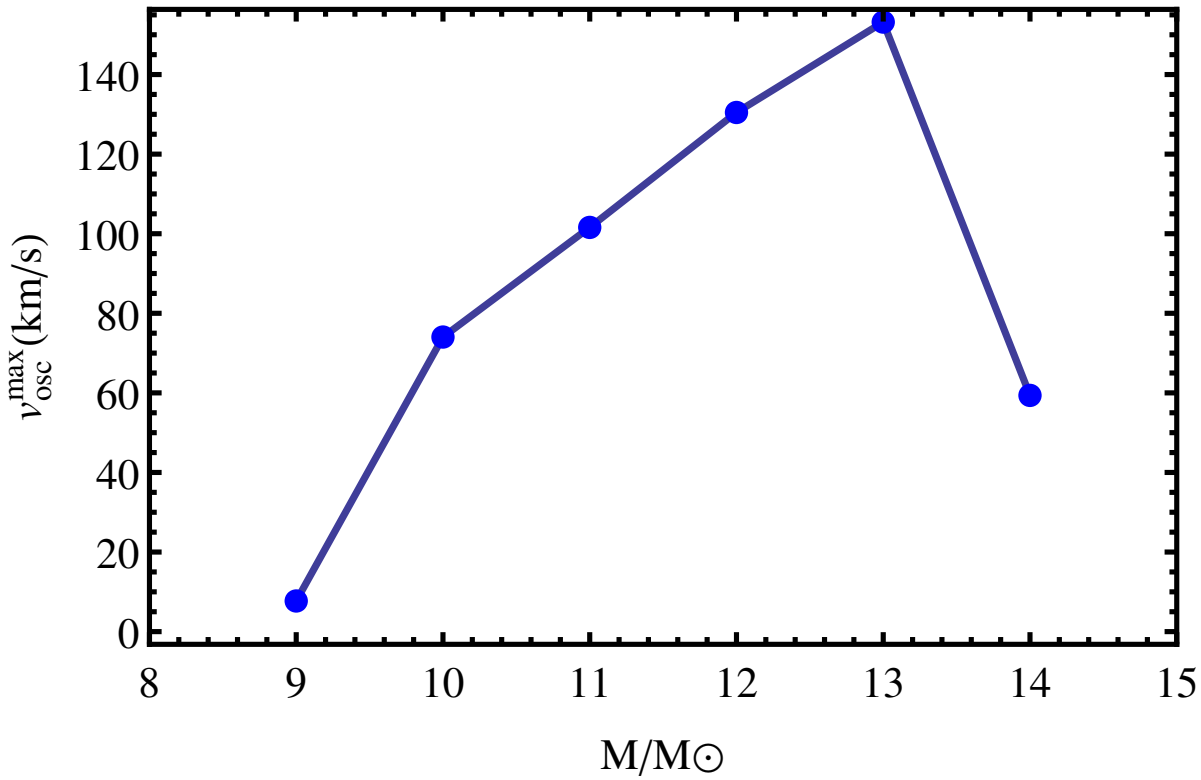

Figure 5.9: Maximum radial velocity reached at the surface during a saturated pulsation cycle in the helium star models. The sound speed in these models is of the order of 30 km/s.

lines. In fact, H-rich WN stars can be structurally different from the H-free models that have been computed in this work. Additionally, we exclude stars that have been reported to most likely have CIR-type variability (St-Louis et al. 2009; Chené & St-Louis 2011; St-Louis 2013). The CIR-type variable spectra are associated with large-scale variability, which most likely does not find its origin in the small-scale inhomogeneity investigated here. Therefore these objects are not included in the linear fit in Fig.5.10 (empty circles) and in the following analysis. In other words, only the sample of single[1] H-free WN stars has been plotted in Fig.5.10 as a function of the estimated mass.

Most of the spectral variability studies on which the σ values are extracted are presented in the works of St-Louis et al. (2009) and Chené & St-Louis (2011). An additional eight WN stars, however, partially presented in Chené et al. (2012) were also included (pink dots in Fig.5.10). They are the Galactic stars WR 7 (WN4b), WR 20 (WN5O), WR 34 (WN5o), WR 37 (WN4b), WR 51 (WN4o), WR 62 (WN6b), WR 84 (WN7o), and WR 91 (WN7b). Each of these stars was observed four to eight times with the Gemini Multi-Object Spectrograph (GMOS) at Gemini South, under programme numbers GS-2008B-Q-87, GS-2010B-Q-58, GS-2014A-Q-42, and GS-2014A-Q-73. In Appendix A, we present the spectra and a detailed variability analysis comparable to what is available in the literature for other WN stars.

The observed WR stars only partially fall in the mass range presented in Fig. 5.4. However, the linear fit in Fig.5.10 shows larger variability at higher stellar masses. This trend is in agreement with the results shown in Fig.5.4. In addition the zero point of the linear fit at 10 $M_\odot$ matches our prediction. Moreover, we do not find any correlation when the degrees of spectral variability are compared to the terminal wind

[1] Some WR stars might have an O-B companion, which in any case does not significantly affect the WR spectrum and derived physical quantities, according to Hamann et al. (2006).

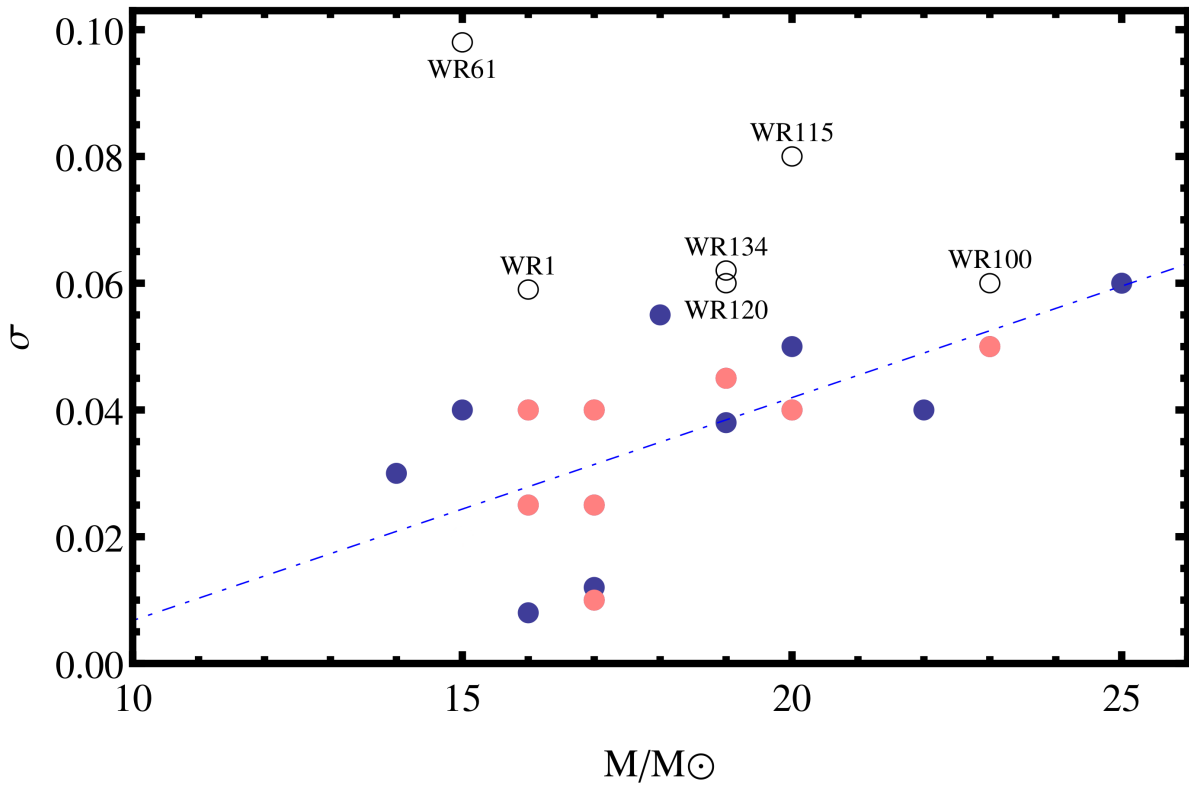

Figure 5.10: Variability of rms relative to the line strength σ as a function of mass of the Galactic H-free WN stars. The blue dots correspond to the small-scale variability in WN stars from St-Louis et al. (2009); Chené & St-Louis (2011); Michaux et al. (2014), while the pink dots correspond to the variability for the stars analysed in this work (see Appendix A). Empty black circles correspond to CIR-type variability (St-Louis et al. 2009; Chené & St-Louis 2011; St-Louis 2013). The stellar masses are derived by Hamann et al. (2006). The linear fit in blue dashed is computed considering only the blue and pink dots. The Spearman's rank correlation coefficient is ≈ 0.7.

velocities tabulated by Hamann et al. (2006), suggesting that the spectral variability is not related to the specific wind structure but rather by the conditions in the deeper hydrostatic structure of the WR stars.

While these results have to be taken with caution given the small sample and the associated uncertainties, we conclude that our results are supporting the idea that sub-surface convection may trigger the formation of clumps in the wind of Wolf-Rayet stars.

5.5.2 Characteristic timescale and number of clumps

A further comparison with observational data could involve the characteristic timescale associated with convection, $\tau_{\rm conv}$, defined as

$$\tau_{conv} = \frac{\alpha H_P(R_c)}{\langle v_c \rangle} \quad . \tag{5.9}$$

This timescale is of the order of $10^2 - 10^3$ seconds in our models with $M \geq 10\,M_\odot$ (Table 5.1). Clumping could be detected by means of linear polarimetry (see Davies et al. 2005, 2007; Vink 2012; St-Louis 2013) and a Fourier analysis of its variability could lead to the direct detection of the sub-surface convection in WR stars where the optical depth of the wind is sufficiently low.

The derived timescale appears to be in good agreement with spectroscopic variations associated with small-scale structures in the wind of WR stars. Lépine et al. (1999) obtained a time series of

high-resolution and high signal-to-noise ratio spectra of the WC8 star γ^2 Velorum with a relatively high sampling rate of one spectrum every 300s. From these observations, they concluded that the temporal variability of the sub-peaks associated with clumps in the wind took place on a timescale of the order of minutes to hours [2].

The timescale might also be observable by detecting short time variations in different parameters of linear polarimetry such as the total linear polarization or the angle of maximum polarization. The detection of the stochastic variability on such a short timescale requires the use of extremely short exposures and readout times, therefore limiting both the number of usable instruments and observable targets. In this respect it might be best to use instruments capable of obtaining both linear polarimetry Stokes parameters Q and U simultaneously to halve the observing time.

Furthermore, we can compare the estimated order of magnitude for the number of clumps as from Eq.5.8, i.e. about $10^3 - 10^4$ clumps, with observations. The wind crossing time, usually of the order of hours (Lepine et al. 1996; Chené et al. 2008), is comparable to the excitation timescale above, therefore even if our estimate shall be considered as a lower limit, we do not expect this to differ significantly compared to the integrated number of clumps throughout the stellar outflow. We find that indeed our estimate is in agreement with the number of clumps observed by Lépine & Moffat (1999) for WR stars ($\approx 10^4$) as well as with Davies et al. (2007) for O and LBV stars.

5.5.3 Magnetic fields

The formation of magnetic flux tubes could also be connected to sub-surface convection in hot rotating stars (Prinja et al. 2002; MacGregor & Cassinelli 2003; Cantiello et al. 2009, 2011; Cantiello & Braithwaite 2011). A magnetic field can be generated from a dynamo mechanism taking place in the FeCZ and propagate through the outer layers of WR stars, affecting their winds and eventually the structures in these winds. The presence of extended FeCZs in the most massive WR models could be associated with different phenomena as was successfully accomplished in the case of O-stars (e.g. Prinja et al. 1995; Prinja & Crowther 1998; Cantiello & Braithwaite 2011). These phenomena are discrete absorption components (e.g. Cranmer & Owocki 1996), i.e. X-ray emission (e.g. Kramer et al. 2003; Oskinova et al. 2009) and large-scale variability induced by corotating interaction regions (e.g. Cranmer & Owocki 1996; Chené & St-Louis 2011; Chené et al. 2011b), which appear in several WR star winds.

Based on the model for the rise of toroidal magnetic flux tubes generated by a dynamo mechanism in the convective zone proposed by MacGregor & Cassinelli (2003), who investigated the buoyant transport of magnetic flux through the interior of hot stars, we estimate the field strength of the magnetic flux tubes in the sub-surface convective zone. Assuming equipartition between the magnetic and kinetic turbulent energy as in Cantiello et al. (2009), we can write the magnetic field strength B as

$$B \simeq \langle v_c \rangle \sqrt{4\pi\rho_c} \quad . \tag{5.10}$$

From Eq.5.10 we derive a magnetic field at the interface between the convective and overlying radiative zone of the order of tens of Gauss for the low-mass ($\lesssim 10\,M_\odot$) helium stars , while for the more massive models we find magnetic fields of up to 500 G (cf. Tab.5.1). If we assume conservation of the magnetic flux for the magnetic flux tubes (MacGregor & Cassinelli 2003), we find that the strength of the magnetic field arising at the surface is roughly the same as that at the interface between the convective and radiative layers, i.e. of the order of hundreds of Gauss in the models with $M \gtrsim 10\,M_\odot$. However the magnetic pressure at the surface is still only a fraction of the surface gas pressure, i.e. at maximum a third of it in

[2] The variability timescale does not have to be confused with the time necessary for a sub-peak to migrate from the line centre to the line edges.

the most massive model. This implies that the gas and radiation pressure most likely dominate and define the global structure of the outflow at the base of the wind (Gary 2001), but local twisting of the magnetic field lines might lead to locally enhanced magnetic field strength such that the magnetic pressure may exceed the local gas pressure with potential observational effects, such as CIRs.

Despite the simplified method and assumptions, and the observational difficulties in detecting and estimating the magnetic fields of WRs, we find that the predicted values are of the same order of magnitude as the most probable values determined for a sub-sample of WR stars by de la Chevrotière et al. (2013, 2014). These are marginal detections of the field in the observable region of the wind and that the field configuration was assumed to have a split monopole configuration.

5.5.4 Pulsations

It has been suggested that violent mass-loss events and large-scale variabilities may be connected with strange mode instabilities in hot massive stars (Glatzel et al. 1993; Glatzel & Kaltschmidt 2002). A clear observational signature for fast pulsating WR stars has not yet been found. After the non-confirmation of the presence of fast pulsations in WR40 of spectral sub-type WN8 (Blecha et al. 1992; Martinez et al. 1994), the only candidate at the moment is the H-depleted WR123 of the spectral sub-type WN8, which shows a 9.8 hours period. This period however does not match the period range of the lowest order unstable modes in Fig. 5.6 (Balona 2010; Lefèvre et al. 2005; Chené et al. 2011a). However, WR123 is expected to be considerably more massive then the mass range considered here. Previous attempts to reproduce this 9.8h period have been unsuccessful (see Chené et al. 2011a, and reference therein).

The predicted bolometric magnitude change of our models during a pulsation cycle is of the order of $\Delta m \propto log(L_{min}/L_{max}) \approx 10^{-7}$ (see Tab.5.2). However, the associated changes in effective temperature imply a variability as high as 0.1 mag in the X-ray and visible bands. While this may be above the level of non-periodical variability of WRs at the mmag level (Gosset & Rauw 2009; Balona 2010; Chené & Moffat 2011; David-Uraz et al. 2012), a periodic variability in the frequency range we predict has not been detected in the bright Galactic WC5 star WR111 by Moffat et al. (2008) (see also Lefèvre et al. 2005; Chené et al. 2011b). The pulsations may be generally hidden by other types of variability appearing in WR outflows and by the optically thick winds, given the high optical depth of the hydrostatic layers. Whether any variability induced by the pulsations is detectable depends on how pulsations affect the stellar outflow and whether coherence is preserved throughout the wind. From Fig.5.8 and the discussion in Sect.4, it is suggested that the wind has a stabilizing effect on strange modes instability and inhibits them in most cases. This might explain why, even if expected, there has been no match between the theoretical predictions and observations of strange modes pulsations in H-free WR stars, as previous models neglected the effect of mass loss to the stability of strange modes.

A different explanation for small- or large-scale variability might instead involve the effects of turbulent pressure fluctuations and finite amplitude high order non-radial pulsations of non-thermal origin. These are expected to appear in the case of transonic convective velocities and inefficient convection, as has been suggested to connect the strength of turbulent pressure in the partial ionization zones to the appearence of the macroturbulent broadening in OB and late-type stars; this is a broadening of spectral lines on a scale larger than the line forming region (Grassitelli et al. 2015a,b). In our models the turbulent pressure contributes less then 1% to the equation of state, but the Mach numbers are close to unity in the more massive models.

5.6 Conclusions

The purpose of this work was to study the condition in the envelopes of massive helium stars and analyse the instabilities appearing in these radiation pressure dominated regions. These models correspond to H-free Wolf-Rayet stars, which are located close to the Eddington limit. These instabilities can possibly provoke or influence the formation of structures observed at the surface or in the wind. We find that sub-surface convective zones are present in all the investigated models. Their spatial extent increases for higher stellar masses. The convective zones arise as a result of the iron opacity peak and they are inefficient in transporting energy. Convection reaches the surface in the $17\,M_\odot$ model. In our models the iron opacity bump is also responsible for the envelope inflation (Sanyal et al. 2015) starting from the $6\,M_\odot$ model. These envelopes are characterized by their proximity to the local Eddingont limit (i.e. $\Gamma \approx 1$).

The convective motion may trigger velocity and density fluctuations at the stellar surface. An upper border for the surface turbulent velocity is estimated by considering the energy transported via gravity waves from the upper limit of the sub-surface convective zone to the surface. We find that the expected surface velocity amplitudes are small ($\lesssim 1$ km/s) for stellar models with masses below $M \lesssim 10\,M_\odot$, but are more than 20 km/s for the more massive stellar models ($M \gtrsim 10\,M_\odot$). Therefore if clumping is triggered at the base of the wind by these fluctuations, we expect that the formation of structures should be inhibited or spatially delayed (Gayley & Owocki 1995; Owocki 2015) in the case of low-mass WNE stars. However, our models predict strong small-scale variability for higher WR masses. A trend of stronger variability for higher stellar masses was identified from the observational data of St-Louis et al. (2009), Chené & St-Louis (2011), and from this work (see Sect.5.1 and Appendix A) for single H-free WNE stars. We also conclude that if wind clumping is triggered by sub-surface convection, the assumption of a constant clumping factor as a function of mass may not be appropriate. We find also that the timescales associated with convection, of the order of hours, are supported by observations by Lépine et al. (1999). Moreover, the number of clumps that we estimate by considering the size of the biggest convective eddies and the correlation lengths associated with the gravity waves, i.e. $10^3 - 10^4$, is also supported by observations by Lépine & Moffat (1999).

We find that the envelopes of the helium star models are unstable to pulsations in the range $9 - 14\,M_\odot$. The periods of the pulsations are in agreement with a low order mode in Glatzel et al. (1993). The variations in bolometric magnitude connected with these pulsations are very small (less than micromagnitudes), i.e. below the observable photometric variability and the observed variabilities connected with structures in the wind. However the supersonic radial velocities could give rise to observable periodical effects apparently not yet observed in the context of WR stars. Moreover, the strong mass loss applied to our stellar models has a stabilizing effect on the pulsations. It appears that mass loss has an inhibiting effect on the pulsational instability in the most massive cases. This may help to explain the lack of observational evidence for periodical variability in WR stars of the WNE type, which is in contrast to previous direct theoretical predictions that did not include mass loss.

We also find that the strength of the magnetic fields rising from the convective zone to the surface of our most massive models, of the order of hundreds of Gauss, is comparable to the most probable values determined in some WR stars by de la Chevrotière et al. (2013, 2014). The pressure induced by the buoyant magnetic flux tubes is, however, globally not enough to define the structure of the wind, but local enhancement of the magnetic field might lead to or trigger the formation of CIRs.

Acknowledgements: *L.G. is part of the International Max Planck Research School (IMPRS), Max-Planck-Institut für Radioastronomie and University of Bonn and Cologne. L.F. acknowledges financial*

support from the Alexander von Humboldt foundation. Based on observations obtained at the Gemini Observatory, processed using the Gemini IRAF package, which is operated by the Association of Universities for Research in Astronomy, Inc., under a cooperative agreement with the NSF on behalf of the Gemini partnership: the National Science Foundation (United States), the National Research Council (Canada), CONICYT (Chile), the Australian Research Council (Australia), Ministério da Ciência, Tecnologia e Inovação (Brazil) and Ministerio de Ciencia, Tecnología e Innovación Productiva (Argentina). Further, L.G. thanks T.Moffat, Y.Michaux, G.Gräfener, J.-C.Passy, and the referee S.P.Owocki for precious discussions and comments on this manuscript.

5.7 Variability study of eight additional WN stars

5.7.1 Data extraction and analysis

The bias subtraction, flat fielding, spectrum extraction, sky subtraction, and wavelength calibration of all spectra were executed in the usual way using the gemini packages of the IRAF[3] software. Calibration lamp spectra were taken during the night after each spectrum. Special care was taken for the normalization of the spectra. First, a mean was made for each run. Then, each spectrum of a given star was divided by the mean spectrum and the ratio fitted with a low-order Legendre polynomial (between fourth and eighth order). The original individual spectrum was divided by this fit, and was therefore at the same level as the mean spectrum. This allowed us to put all individual spectra at the same level. The mean spectrum was then fitted in selected pseudo-continuum regions, i.e. wavelength regions where large emission lines do not dominate. Finally, the fitted continuum function is applied to each individual spectrum. The error on the continuum normalization measured as the standard deviation of individual spectra around the continuum function is typically of 0.5

5.7.2 Determining the σ-value

The final spectra are shown in the top panels of Figures A1-A2 for the three strongest lines present in our wavelength interval, i.e. the HeIIλ4686, HeIIλ5411, and HeIλ5876.

To determine the level of line-profile variability, we first identify at which wavelengths the spectrum may be significantly variable, using the temporal variance spectrum (TVS) of each data set. The TVS was calculated using the formalism of Fullerton et al. (1996) and the quantity $\Sigma_j(99\%) = \sqrt{(\frac{(TVS)_j}{\sigma_0^2 \chi^2_{N-1}(99\%)})}$ was obtained, where σ_0 is the reciprocal of the rms of the noise level in the continuum in a time series of N spectra. The value of $\Sigma_j(99\%)$ quantifies the level of variability at each wavelength: a spectrum that reaches a value of n varies with an amplitude n times higher than the variability measured in the continuum (which is assumed to be pure noise) with a confidence level of 99%. The spectrum of a given star is considered significantly variable at a given wavelength j if the value of $\Sigma_j(99\%)$ is significantly greater than 1. When a line is identified as significantly variable, it is possible to calculate the amplitude of its variability relative to its intensity. To accomplish this, we calculated for each wavelength j a modified $TVS_j^{1/2}$ as defined in Chene (2007) and divided it by the line flux $(\bar{S}_j - 1)$, where $\bar{S}_j$ is the weighted mean flux at wavelength j. This ratio is named the σ spectrum. One should note that the calculation of σ does not take into account instrumental variations due to the noise level. Thus, when the variation level of a given line is too close to the noise, which is the case for weaker lines, σ is artificially

[3] IRAF is distributed by the National Optical Astronomy Observatories (NOAO), which is operated by the Association of Universities for Research in Astronomy, Inc. (AURA) under cooperative agreement with the National Science Foundation (NSF).

high. That is why we manually set $\sigma_j = 0$ when the variability at a given wavelength j is not clearly significant according to the value of $\Sigma_j(99\%)$ or when the line has a relative intensity that is lower than 1.5, which is the intensity limit of a spectral line from which we can investigate the variability for the present data set.

Figures A1 and A2 show our results for the eight additional WN stars. The bottom panels show a superposition of all the observed spectra with the average spectrum overplotted in red. The line intensity is normalized to ease the comparison with the different lines. The normalizing factor of the lines is written on the top left. The second panels from the bottom show the $\Sigma(99\%)$ spectrum. The dotted line marks the threshold of significant variability. The third panels from the bottom show the σ spectrum. The most reliable values are extracted from the central region of the line, as the edges tend to be more sensitive to instrumental effects. Finally, the top panels show the montage of the residuals (individual spectra - average). The residuals of the HeII λ 4686 line are divided by a factor 2 for a better visibility. The residuals are in chronological order, with the bottom to the top. The heliocentric Julian date corrected to start on 1 Jan 2000 is written on the far left of the plot. All the spectra and associated values ($\Sigma(99\%), \sigma$) are masked at the interstellar medium Na I D lines at 5885 and 5890Å.

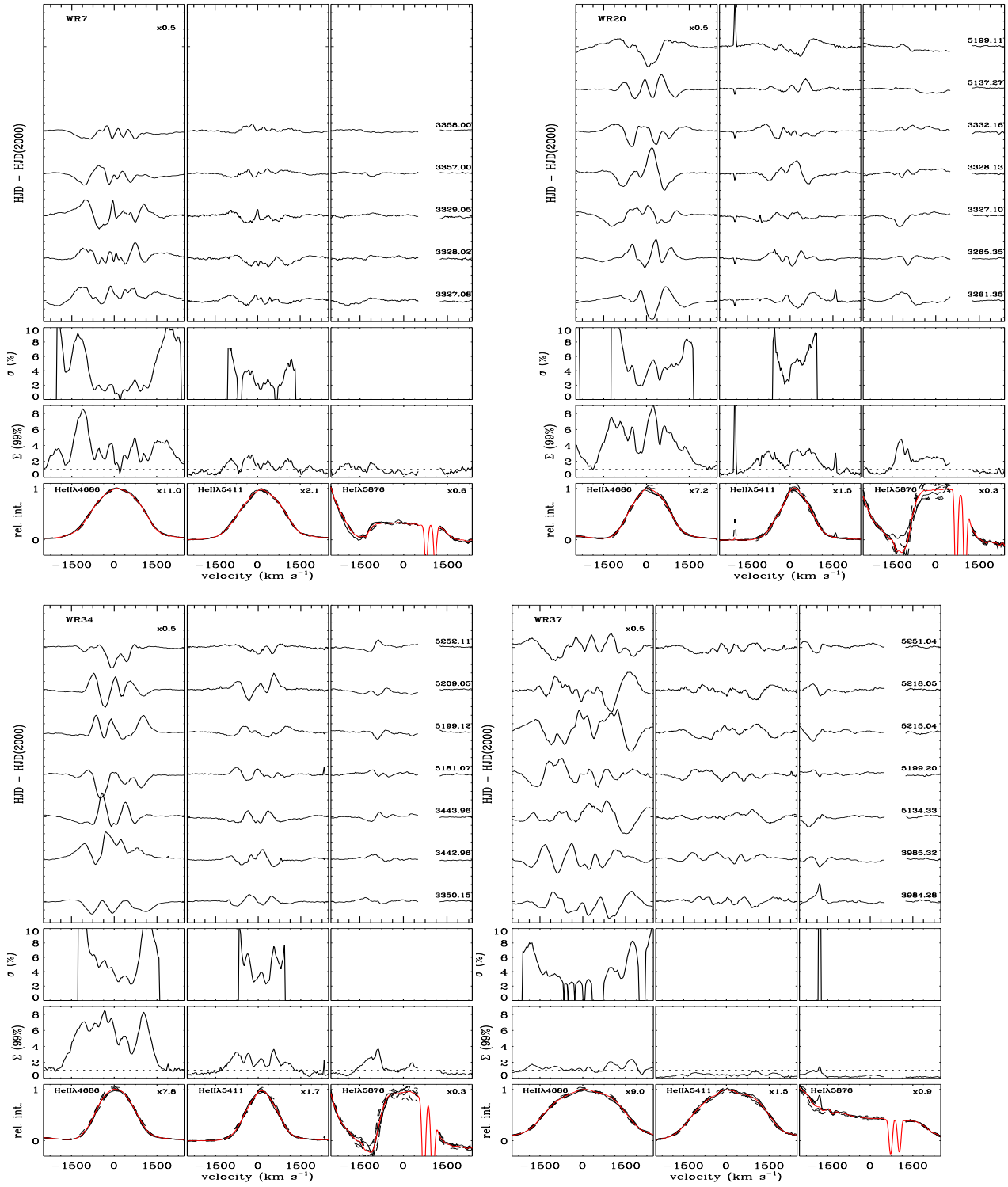

Figure 5.11: a)top: Montage of the He II λ4686 (left), He II λ5411 (centre), and He I λ5876 (right) residuals (individual spectra mean) for WR7, WR20, WR34, and WR37 (as indicated in the top left section of the top panel). For all cases, the scale factor of the ordinate is indicated in the top right-hand corner of the left column. HJD - HJD(2000) is indicated in the y-axis. Second from top: σ spectrum. Second from bottom: Σ (99%) spectrum. Bottom: Mean spectrum.

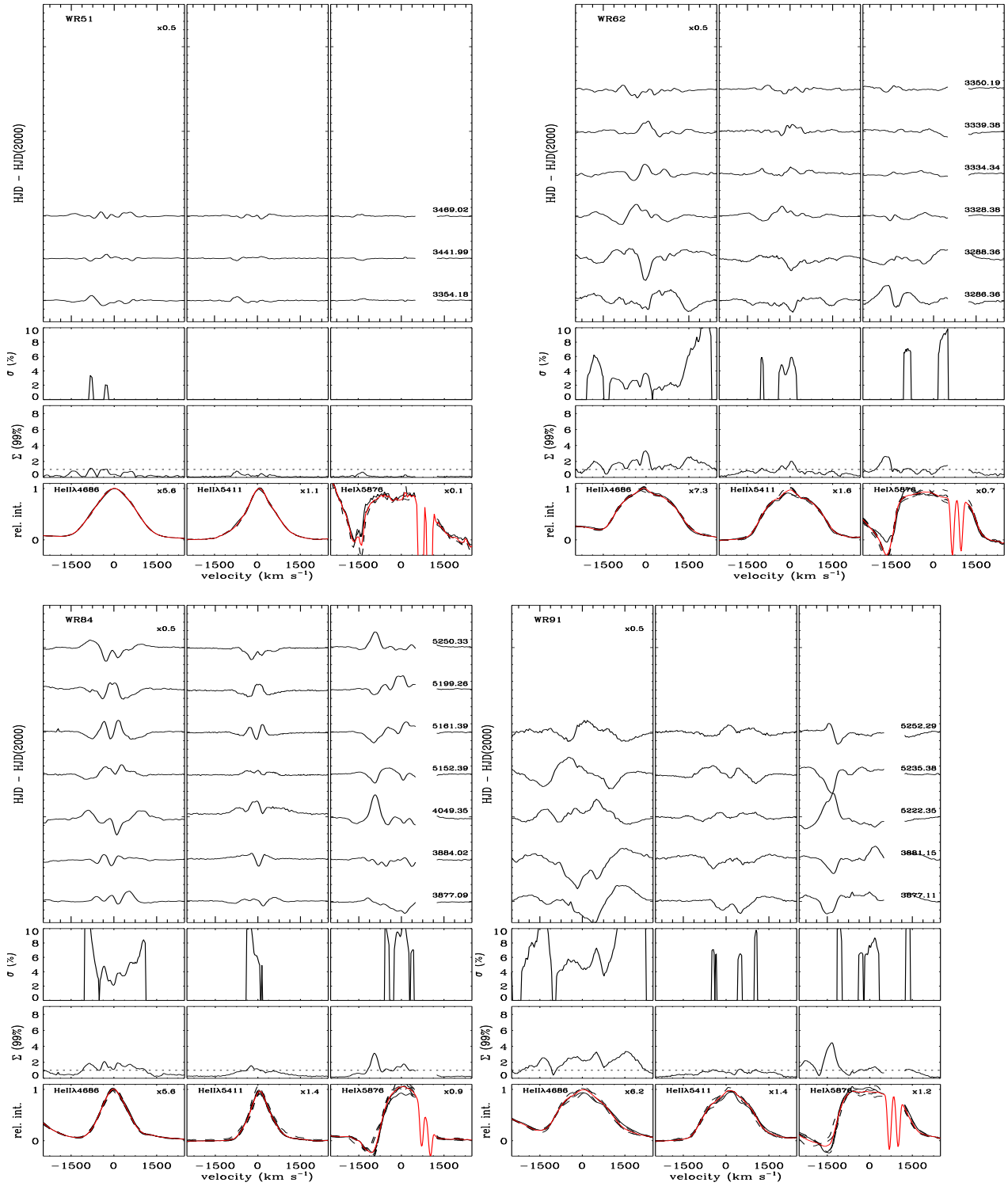

Figure 5.12: Same as Fig.A.1, but for WR51, WR62, WR84, and WR91.

Table 5.1: Properties of our set of helium zero age main-sequence models with Z=0.02. ΔM_{env} mass of the envelope, $\langle v_c \rangle$ averaged convective velocity over the last mixing length of the FeCZ, v_{surf} surface velocity fluctuation, ΔR_{conv} spatial extent of the convective zone, M_c Mach number for the averaged convective velocity, τ_{conv} convective timescale, B magnetic field strength.

M	$\log L/L_\odot$	$\log T_{eff}/K$	R	$\log \dot{M}$	ΔM_{env}	$\langle v_c \rangle$	v_{surf}	ΔR_{conv}	M_c	τ_{conv}	B
$M_\odot$			$R_\odot$	$M_\odot/yr$	$10^{-9} M_\odot$	km/s	km/s	$R_\odot$		s	G
2	3.36	4.84	0.34	-6.44		0.01	$1.\times10^{-3}$	7.70×10^{-4}	$5.\times10^{-4}$	51284	0.31
3	4.07	4.93	0.49	-6.37		0.03	$2.\times10^{-3}$	1.47×10^{-3}	$1.\times10^{-3}$	35047	1.45
4	4.22	4.95	0.53	-6.33		0.06	$4.\times10^{-3}$	1.84×10^{-3}	$2.\times10^{-3}$	20930	2.10
5	4.46	4.98	0.61	-6.03		0.10	$9.\times10^{-3}$	2.28×10^{-3}	$4.\times10^{-3}$	14328	4.07
6	4.66	5.00	0.68	-5.79	0.21	0.19	0.02	2.85×10^{-3}	0.02	9670	7.49
7	4.81	5.03	0.75	-5.64	0.43	0.33	0.03	3.88×10^{-3}	0.01	6788	12.7
8	4.94	5.04	0.81	-5.50	0.63	0.60	0.11	5.08×10^{-3}	0.02	4553	22.8
9	5.03	5.05	0.87	-5.36	1.15	1.13	0.27	6.29×10^{-3}	0.04	3003	40.7
10	5.13	5.06	0.93	-5.34	1.32	2.09	0.66	8.68×10^{-3}	0.07	2017	70.5
11	5.21	5.07	0.99	-5.13	1.68	3.94	1.66	1.12×10^{-2}	0.13	1343	122
12	5.29	5.07	1.05	-5.04	2.23	7.01	3.89	1.42×10^{-2}	0.25	949	203
13	5.35	5.08	1.11	-4.95	2.71	10.7	7.25	2.07×10^{-2}	0.37	779	284
14	5.41	5.08	1.18	-4.87	3.52	15.6	12.7	2.61×10^{-2}	0.56	663	387
15	5.46	5.08	1.25	-4.81	4.11	18.3	16.1	4.62×10^{-2}	0.65	687	415
16	5.53	5.08	1.36	-4.72	5.33	22.8	21.4	6.80×10^{-2}	0.88	732	532
17	5.56	5.08	1.42	-4.68	5.80	26.2	25.8	8.64×10^{-2}	0.96	1619	369

Table 5.2: Physical parameters of the models that are unstable to pulsations. Luminosity difference, ΔL, between the maximum and minimum radii, Δm bolometric magnitude difference between maximum and minimum radii, P pulsation period, ΔR difference between maximum and minimum radii, v_{osc}^{max} maximum velocity achieved during a pulsation cycle, τ_{dyn} dynamical timescales, τ_{th} thermal timescales, and ω_{dyn} frequency of the pulsations normalized by the dynamical timescale as defined in Glatzel et al. (1993).

M	ΔL	Δm	P	ΔR	v_{osc}^{max}	τ_{dyn}	τ_{th}	ω_{dyn}
$M_\odot$	$L_\odot$	$10^{-7} mag$	s	$R_\odot$	km/s	s	s	
9	0.00038	0.03	220	4×10^{-4}	7.74	429	109	7.08
10	0.01694	1.33	270	8×10^{-3}	74.0	451	101	6.06
11	0.04082	2.67	330	0.01	101	471	112	5.18
12	0.08167	4.52	400	0.02	130	493	130	4.47
13	0.05357	2.55	459	0.03	153	517	138	4.09
14	0.02262	0.94	550	0.01	59.3	545	159	3.60

Outlook

42
Hitchhikers guide to the Galaxy

Stellar physics is a fascinating branch of astrophysics of utmost importance for our understanding of the Universe we experience. Stars do not only fill the night sky with immense beauty and leave us with an indescribable sense of humility, our Sun provides the energy for life on this planet, and numerous events of stellar origin could instead destroy the natural equilibrium on this planet.

Over the last century the effort of brilliant minds pushed the boundary of our knowledge of stars, the building blocks of galaxies, to an exciting level. Thanks to this progress we now have a consistent and firm knowledge of the fundamental physical mechanisms taking place in stars. However, despite the great progresses, numerous open questions still puzzle astrophysicists, some of which have been partially investigated in this thesis.

One of the challenges in modern days stellar physics concerns the detailed mechanism for the transport of energy throughout the interior of a star. Radiative transport and turbulent convection are the two main mechanism to transport energy in a star. Especially stars with envelopes close to their Eddington limit, however, tend to struggle while transporting the enormous energy flux. The high opacity and the low densities favour high degrees of super-adiabaticity in the convective zones, leading to turbulent "boiling" where the recombination of some elements takes place and the temperature is not high enough to sustain a fully ionized plasma. Even if the global and long-lasting stability of star is a clear empirical evidence, numerous instabilities can be connected to the conditions in the low density outer layers, affecting both observational results and theoretical modelling. The motion of the convective eddies intrinsically leads to turbulence in the extended envelopes, the physics of which is an extremely difficult challenge, given that the precise dynamics requires the solution of the non-local time dependent full set of Navier-Stokes equations. This is not possible in the context of the 1D stellar evolution calculations, and even in the most sophisticated calculations requires a lot of computational time and has numerous uncertainties. The uncertainties in this context have often led astrophysicists to address them as a possible reason for numerous discrepancies in the comparison between observations and numerical calculations (see e.g. de Jager 1984; Blomme et al. 1991; Maeder 2009).

Motivated by this, we studied the structural effects arising due to the turbulent pressure contribution in the convective zones. Our results pointed to the inadequacy of these effects to explain the theoretical and observational discrepancies regarding the position of the stars in the HR diagram (Castro et al. 2014), especially concerning the "mass-discrepancy problem" and the Humphreys-Davidson limit (Humphreys & Davidson 1984; Markova et al. 2014). Differently, the study of the conditions in the sub-surface convective zones proved very favourable while investigating atmospheric phenomena such as surface motion. In fact, already the Sun suggests that the turbulent sub-surface motion can lead to observational effects as, e.g., the "5 minutes" oscillations (Stein & Nordlund 2001).

Since several decades there have been observational evidences for an important extra-broadening

mechanism acting on the spectral lines, prominently in the massive OB stars regime, but common also in other locations of the HR diagram (Slettebak 1976; Simón-Díaz & Herrero 2014). Despite the long time, no convincing theory was able to explain the origin of this phenomenon. Neglecting this effect can have a major impact on the derived stellar parameters, especially the projected rotational velocities which are one of the most important quantities affecting stellar evolution, second only to the stellar mass (Maeder & Meynet 2012).

Chapter 2, 3, and 4 of this thesis compared the fraction of turbulent pressure encountered in the envelope of our stellar models to the estimated macroturbulent velocities of a vast sample of stars of different masses, evolutionary stages, and metallicities. The linear relation encountered independent of the location in the HR diagram clearly suggests a connection between the turbulent motion in the sub-surface convective zones and the appearance of this extra broadening. The connection has then been interpreted as evidence that turbulent pressure fluctuations due to the stochastic deviation from local hydrostatic equilibrium can lead to the excitation of high order non-radial pulsations. In fact it is likely that when the fraction of total pressure arising from turbulent motion in the sub-surface convective zones is of the order of some percent or higher, stochastic variability in the local pressure could induce perturbations and consequently a velocity field at the surface, which manifests as extra broadening of the spectral lines. Further comparison between theoretical predictions and observationally derived macroturbulent velocities might strengthen the results of this approach. It is intuitive to think that transonic convective motion can induce perturbations, influencing not only the atmosphere, but eventually also the whole structure of stars as well as their outflows. This suggests that state-of-the-art asteroseismic calculations which do not include a time-dependent treatment of convection, the inclusion of the full Reynold stress tensor, and eventually non-infinitesimal fluctuations of the thermodynamic quantities, might most likely do not fully capture the complex physics behind the excitation of pulsations in convective zones and of the induced velocity fields at the surface. If this is true, a new door could be opened on the treatment of pulsations in stellar physics, leading to a new way to constrain the internal structure of stars throughout the HR diagram. Additionally, this could explain the good agreement between the observational instability strip for γ-Dor stars and the location in the HR Diagram where strong turbulent motion is encountered due to the recombination of hydrogen close to the surface. Such an agreement could be extended to other conditions, widening the concept of, e.g. solar-like oscillations or stochastically excited oscillations.

Not only in the context of standing waves the turbulent motion could lead to observational effects at the surface. In the case of WR stars instead the propagation of waves excited at the interface between the convective and radiative layers seems able to trigger a velocity field at the surface that could explain the appearance of density inhomogeneities in the extended partially optically thick outflows characteristic of WR stars (Moffat et al. 1988; Owocki 2015). These inhomogeneities, which appear as emission sub-peaks in the spectral lines, are thought to have important effects in the estimated mass loss rates by stellar wind, key feature of WR stars but common also in some less evolved massive stars (Hamann et al. 2006; Vink 2015). The apparent agreement between observations and our theoretical predictions (based on the mass dependence of the phenomenon and the estimated number of clumps) shows again that inefficient convection and transonic convective motion are most likely key agents in provoking perturbations and, indirectly, other phenomena. In this case, perturbations due to the interaction between the convective blobs and the radiative zones could act as triggering mechanism for the formations of instabilities which propagate also into the supersonic outflow. Our results also suggest that the usual choice of a constant clumping factor in stellar wind models might not be appropriate when deriving mass loss by stellar wind, as the mass, luminosity, and metallicity of the star is expected to influence the triggering mechanism.

On the other side, the wind can inhibit another class of instability, the pulsational instability theoretically expected to be present in the extended envelopes of stars with high luminosities (Glatzel et al. 1993). This would reconcile the theoretical expectation of pulsating WR stars with the lack of observations

supporting this prediction. Moreover, this result points at the importance of including the effects of the stellar wind mass loss when performing stability analyses against pulsation, of importance mostly in the case of high mass loss rates.

Summarizing, the results of this thesis point toward the important effects which can arise in the presence of inefficient convective energy transport. In fact, when convection is not able to transport efficiently the energy flux of the star, i.e. in presence of high super-adiabaticity in the low density envelopes close to the Eddington limit, the convective eddies are forced to move faster, with velocities even comparable to the local sound speed. The consequent drastic fluctuations in the thermodynamic quantities or the interaction with the surrounding medium due to the turbulent motion can drive dynamical instabilities which can lead to a velocity field at the surface and eventually to the formation of structures in the stellar outflow.

This work suggests that the effects of turbulence might be of key importance when performing stability analyses, as well as when instabilities appear at the photosphere or in the stellar wind. In this direction, future improvements in the understanding of these effects shall investigate the metallicity dependency of the relation between the macroturbulent broadening of the spectral lines and convective motion, as well as the metallicity dependence of the clumping in WR stars in the framework of a "balistic" model.

The inclusion of the full time dependent Reynold's stress tensor and of the finite amplitude fluctuations associated to a turbulent flow might help to better understand the origin of apparently different kind of oscillations, from the "solar-like" oscillations to the γ-Dor class of pulsators, up to the very massive stars showing velocity fields and density inhomogeneities at their surface. This should also possibly take into account the although small structural differences due to the inclusion of the terms associated to turbulence in the stellar structure equations and therefore in the computation of the stellar models, as for the fact that even small structural differences in the very outer layers might have important effects on the period spacing of the excited modes, the exact frequencies of the modes, etc..

Following these improvements, the use of the macroturbulent broadening as a tool to be coupled to asteroseismic analysis in order to investigate the inner sub-surface structure of the envelopes might considerably help understanding the physics of inflation, the efficiency of convection, and help constrain the mixing length parameter (or in general the theory of convective energy transport) in contexts other than the Sun. Moreover, the understanding of the origin of structures in the stellar winds is a matter of fundamental importance in deriving mass-loss rates, thus affecting the evolutionary models of massive stars, the nature of the progenitors of Supernovae and Gamma Ray Bursts, as well as the theory of stellar winds itself.

This work appears timely as the Kepler satellite and other forthcoming surveys will allow for very precise spectral analyses, which can be used to constrain even more the aforementioned connections, enlightening the origin of some instabilities in the envelope of stars.

APPENDIX A

Other Publications

Massive main-sequence stars evolving at the Eddington limit

D. Sanyal[1] **L. Grassitelli**[1], N. Langer[1], J.M. Bestenlehner[1],

[1]Argelander-Institut für Astronomie, Universität Bonn, auf dem Hügel 71, 53121 Bonn, Germany

Astronomy & Astrophysics 2015, 580A, 20S

Abstract: Context. Massive stars play a vital role in the Universe, however, their evolution even on the main-sequence is not yet well understood. Aims: Because of the steep mass-luminosity relation, massive main-sequence stars become extremely luminous. This brings their envelopes very close to the Eddington limit. We analyse stellar evolutionary models in which the Eddington limit is reached and exceeded, explore the rich diversity of physical phenomena that take place in their envelopes, and investigate their observational consequences. Methods: We use published grids of detailed stellar models, computed with a state-of-the-art, one-dimensional hydrodynamic stellar evolution code using LMC composition, to investigate the envelope properties of core hydrogen burning massive stars. Results: We find that the Eddington limit is almost never reached at the stellar surface, even for stars up to 500 $M_{\odot}$. When we define an appropriate Eddington limit locally in the stellar envelope, we can show that most stars more massive than 40 $M_{\odot}$ actually exceed this limit, in particular, in the partial ionisation zones of iron, helium, or hydrogen. While most models adjust their structure such that the local Eddington limit is exceeded at most by a few per cent, our most extreme models do so by a factor of more than seven. We find that the local violation of the Eddington limit has severe consequences for the envelope structure, as it leads to envelope inflation, convection, density inversions, and, possibly to, pulsations. We find that all models with luminosities higher than $4 \times 105 L_{\odot}$, i.e. stars above 40 $M_{\odot}$ show inflation, with a radius increase of up to a factor of about 40. We find that the hot edge of the S Dor variability region coincides with a line beyond which our models are inflated by more than a factor of two, indicating a possible connection between S Dor variability and inflation. Furthermore, our coolest models show highly inflated envelopes with masses of up to several solar masses, and appear to be candidates for producing major luminous blue variable eruptions. Conclusions: Our models show that the Eddington limit is expected to be reached in all stars above 40 $M_{\odot}$ in the LMC, even in lower mass stars in the Galaxy, or in close binaries or rapid rotators. While our results do not support the idea of a direct super-Eddington wind driven by continuum photons, the consequences of the Eddington limit in the form of inflation, pulsations

and possibly eruptions may well give rise to a significant enhancement of the time averaged mass-loss rate.

New observational clues to understand macroturbulent broadening in massive O- and B-type stars

S.Simón-Díaz [1,2], M.Godart [1,2], N.Castro [3], A.Herrero [1,2], C.Aerts [4,5], J.Puls [5,6], J. Telting[7], **L. Grassitelli**[3]

[1]Instituto de Astrofísica de Canarias, E-38200 La Laguna, Tenerife, Spain
[2]Departamento de Astrofísica, Universidad de La Laguna, E-38205 La Laguna, Tenerife, Spain
[3]Argelander-Institut für Astronomie, Universität Bonn, auf dem Hügel 71, 53121 Bonn, Germany
[4]Instituut voor Sterrenkunde, KU Leuven, Celestijnenlaan 200D, 3001, Leuven, Belgium
[5]Department of Astrophysics IMAPP, Radboud University Nijmegen, 6500 GL, Nijmegen, The Netherlands
[6]Universitäts-Sternwarte, Scheinerstrasse 1, 81679, München, Germany
[7]Nordic Optical Telescope, Rambla José Ana Fernández Pérez 7, E-38711, Breña Baja, Spain.

Abstract: Context. The term macroturbulent broadening in O- and B-type stars is commonly used to refer to a source of non-rotational broadening affecting their line-profiles. It has been proposed to be a spectroscopic signature of the presence of a certain type of stellar oscillations; however, we still lack from a definitive confirmation of this hypothesis. Aims. We aim to provide new empirical clues about the behaviour of macroturbulent broadening in O- and B-type stars which could eventually used to support/dismiss the pulsational (or any other) scenario to explain its physical origin. Methods.We use high-resolution spectra of 440 stars with spectral types in the range O4 – O9 (all luminosity classes) compiled in the framework of the IACOB project. We characterize the line-broadening of adequate diagnostic metal lines using a combined Fourier transform and goodness-of-fit technique. We perform a quantitative spectroscopic analysis of the whole sample using automatized tools coupled with a vast grid of fastwind models to determine their effective temperatures and gravities. Results. We present a homogeneous and statistically significant overview of the (single snap-shot) line-broadening properties of stars in the whole O and B star domain. We also include and discuss a comparison of the shape and type of line-profile variability found in B main sequence stars with variable line-profiles (due to a well identified type of stellar oscillations or to the presence of spots in the stellar surface) and more massive OB stars showing an important macroturbulent broadening contribution in their line-profiles. We find empirical evidence of the existence of various types of non-rotational broadening agents acting in the realm of massive stars. Even though all of them could be (maybe erroneously in some cases) quoted and quantified as a macroturbulent broadening, their physical origin can be different. Contrarily to the early- to late-B dwarfs and giants, which present a mixture of cases in terms of line-profile shape and variability, the whole O-type and B supergiant domain (or, roughly speaking, stars with $M_{ZAMS} \geq 15 M_{\odot}$) is fully dominated by stars with a remarkable non-rotational broadening component and very similar profiles (including type of variability). We provide some examples illustrating how this observational dataset can be used to evaluate scenarios aimed at explaining the existence of sources on non-rotational broadening in massive stars.

Instabilities in the envelope of Wolf-Rayet stars

L. Grassitelli[1], N. Langer[1], D. Sanyal[1], L.Fossati[1,2], J.M. Bestenlehner[1,3],

[1]Argelander-Institut für Astronomie, Universität Bonn, auf dem Hügel 71, 53121 Bonn, Germany
[2]Space Research Institute, Austrian Academy of Sciences, Graz, Austria
[3]Max-Planck-Institute for Astronomy, Heidelberg, Germany

Proceeding of the International Workshop on Wolf-Rayet stars

Abstract: Wolf-Rayet stars are very hot stars close to the Eddington limit. In the conditions encountered in their radiation pressure dominated outer layers several instabilities are expected to arise. These instabilities could influence both the dynamic of their optically thick winds and the observed spectral lines introducing small and large scale variability. We investigate the conditions in the convective envelopes of our helium star models and relate them to the appearance of a high number of stochastic density inhomogeneities, i.e. clumping in the optically thick wind. We also investigate the pulsational stability of these envelope, considering the effect of the high stellar wind mass loss rates.

New grid of models for extremely low-mass helium white dwarfs including element diffusion and rotational mixing

A. G. Istrate [1], P. Marchant[1], T. M. Tauris [2,3], N. Langer [1], R. Stancliffe [1], **L. Grassitelli**[3],

[1]Argelander-Institut für Astronomie, Universität Bonn, auf dem Hügel 71, 53121 Bonn, Germany
[2]Max-Planck-Institut für Radioastronomie, Auf dem Hügel 69, 53121 Bonn, Germany

Monthly Notices of the Royal Astronomical Society, 459, 1201M

Abstract: A large number of extremely low-mass helium white dwarfs (ELM WDs) have been discovered in recent years. The majority of them are found in close binary systems suggesting they are formed either through a common-envelope phase or via stable mass transfer in a low-mass X-ray binary (LMXB) or a cataclysmic variable (CV) system. Here, we investigate the formation of these objects through the LMXB scenario with emphasis on the proto-WD evolution in environments with different metallicities. We study the effects of rotational mixing (for the first time) and element diffusion in the evolution of proto-WDs and investigate ELM WD cooling track properties. We present state-of-the-art binary stellar evolution models computed with MESA for metallicities of Z = 0.02, 0.01, 0.001 and 0.0002, producing WD masses between 0.16–0.45 $M_{\odot}$. Our results confirm that element diffusion plays a significant role in the evolution of proto-WDs which experience hydrogen shell flashes and that the occurrence of these flashes produces a clear dichotomy in the cooling timescales of ELM WDs, which has important consequences e.g. for the age determination of binary millisecond pulsars. In addition, we demonstrate how the threshold mass at which this dichotomy occurs is dependent on metallicity. Rotational mixing is found to counteract the effect of gravitational settling in the surface layers of young, bloated ELM proto-WDs and therefore plays a key role for their observed chemical abundances. Otherwise, we find that the general properties of ELM proto-WDs, e.g. including the number of flashes, are not influenced significantly by the presence of rotational mixing. Besides from being dependent on WD mass and metallicity, the hydrogen envelope mass of ELM WDs is shown to depend on whether the progenitor star evolves through the red bump on the RGB close to the end of the LMXB phase.

Uniform rotation on the main sequence: a case study of KIC 7661054

S. J. Murphy [1,2], L. Fossati [3], T. R. Bedding [1,2], H. Saio [4], D. W. Kurtz[5], **L. Grassitelli**[6], E. Wang[1]

[1]Sydney Institute for Astronomy (SIfA), School of Physics, University of Sydney, NSW 2006, Australia
[2]Stellar Astrophysics Centre, Department of Physics and Astronomy, Aarhus University, 8000 Aarhus C, Denmark
[3]Space Research Institute, Austrian Academy of Sciences, Schmiedlstrasse 6, 8042 Graz, Austria
[4]Astronomical Institute, Graduate School of Science, Tohoku University, Sendai, Miyagi 980-8578, Japan
[5]Jeremiah Horrocks Institute, University of Central Lancashire, Preston PR1 2HE, UK
[6]Argelander-Institut für Astronomie, Universität Bonn, auf dem Hügel 71, 53121 Bonn, Germany

Abstract: We present the rotation profile of KIC 7661054, a chemically normal γ-Dor star on the main sequence at spectral type F2.5 V. The core rotation period of 26.997 ±0.044 d is obtained from the rotational splittings of a series of dipole g modes. The surface rotation period is calculated from a spectroscopic projected rotation velocity and a stellar radius computed from models. Literature data, obtained without inclusion of macroturbulence as a line-broadening mechanism, imply a reversed rotation profile with the surface rotating more quickly than the core, while our detailed analysis shows the rotation profile to be uniform. We discuss the pitfalls associated with the determination of surface rotation rates of slow rotators from spectroscopy in the absence asteroseismic constraints

Bibliography

Abbett, W. P., Beaver, M., Davids, B., et al. 1997, ApJ, 480, 395

Aerts, C., Puls, J., Godart, M., & Dupret, M.-A. 2009, A&A, 508, 409

Aerts, C. & Rogers, T. M. 2015, ApJ, 806, L33

Antoci, V., Cunha, M., Houdek, G., et al. 2014, ApJ, 796, 118

Appenzeller, I. 1970, A&A, 5, 355

Arnett, W. D., Meakin, C., Viallet, M., et al. 2015, ApJ, 809, 30

Balona, L. A. 2010, Challenges In Stellar Pulsation

Bedding, T. R., Mosser, B., Huber, D., et al. 2011, Nature, 471, 608

Belkacem, K., Dupret, M. A., & Noels, A. 2010, A&A, 510, A6

Belkacem, K. & Samadi, R. 2013, in Lecture Notes in Physics, Berlin Springer Verlag, Vol. 865, Lecture Notes in Physics, Berlin Springer Verlag, ed. M. Goupil, K. Belkacem, C. Neiner, F. Lignières, & J. J. Green, 179

Berghoefer, T. W., Schmitt, J. H. M. M., Danner, R., & Cassinelli, J. P. 1997, A&A, 322, 167

Bestenlehner, J. M., Gräfener, G., Vink, J. S., et al. 2014, A&A, 570, A38

Blaes, O. & Socrates, A. 2003, ApJ, 596, 509

Blecha, A., Schaller, G., & Maeder, A. 1992, Nature, 360, 320

Blomme, R., Vanbeveren, D., & van Rensbergen, W. 1991, A&A, 241, 479

Böhm-Vitense, E. 1958, ZAp, 46, 108

Bouabid, M.-P., Montalbán, J., Miglio, A., et al. 2011, A&A, 531, A145

Bradley, P. A., Guzik, J. A., Miles, L. F., et al. 2015, AJ, 149, 68

Brott, I., de Mink, S. E., Cantiello, M., et al. 2011, A&A, 530, A115

Bruntt, H., De Cat, P., & Aerts, C. 2008, A&A, 478, 487

Burbidge, E. M., Burbidge, G. R., Fowler, W. A., & Hoyle, F. 1957, Reviews of Modern Physics, 29, 547

Cantiello, M. & Braithwaite, J. 2011, A&A, 534, A140

Cantiello, M., Braithwaite, J., Brandenburg, A., et al. 2011, in IAU Symposium, Vol. 273, IAU Symposium, ed. D. Prasad Choudhary & K. G. Strassmeier, 200–203

Cantiello, M., Langer, N., Brott, I., et al. 2009, A&A, 499, 279

Canuto, V. M. & Mazzitelli, I. 1991, ApJ, 370, 295

Carney, B. W., Gray, D. F., Yong, D., et al. 2008, AJ, 135, 892

Castro, N., Fossati, L., Langer, N., et al. 2014, A&A, 570, L13

Catanzaro, G., Ripepi, V., Bernabei, S., et al. 2011, MNRAS, 411, 1167

Chene, A.-N. 2007, PhD thesis, Universite de Montreal, Canada

Chené, A.-N., Foellmi, C., Marchenko, S. V., et al. 2011a, A&A, 530, A151

Chené, A.-N. & Moffat, A. F. J. 2011, in IAU Symposium, Vol. 272, IAU Symposium, ed. C. Neiner, G. Wade, G. Meynet, & G. Peters, 445–450

Chené, A.-N., Moffat, A. F. J., Cameron, C., et al. 2011b, ApJ, 735, 34

Chené, A.-N., Moffat, A. F. J., & Crowther, P. A. 2008, in Clumping in Hot-Star Winds, ed. W.-R. Hamann, A. Feldmeier, & L. M. Oskinova, 163

Chené, A.-N. & St-Louis, N. 2011, ApJ, 736, 140

Chené, A.-N., St-Louis, N., & Moffat, A. F. J. 2012, in Astronomical Society of the Pacific Conference Series, Vol. 465, Proceedings of a Scientific Meeting in Honor of Anthony F. J. Moffat, ed. L. Drissen, C. Robert, N. St-Louis, & A. F. J. Moffat, 166

Chiosi, C. & Maeder, A. 1986, ARA&A, 24, 329

Collet, R., Asplund, M., & Trampedach, R. 2007, A&A, 469, 687

Conti, P. S. 1979, in IAU Symposium, Vol. 83, Mass Loss and Evolution of O-Type Stars, ed. P. S. Conti & C. W. H. De Loore, 431–443

Conti, P. S. & Ebbets, D. 1977, ApJ, 213, 438

Cox, J. P. 1968, Principles of stellar structure - Vol.1: Physical principles; Vol.2: Applications to stars

Cox, J. P. 1980, Theory of stellar pulsation

Cranmer, S. R. & Owocki, S. P. 1996, ApJ, 462, 469

David-Uraz, A., Moffat, A. F. J., Chené, A.-N., et al. 2012, MNRAS, 426, 1720

Davies, B., Oudmaijer, R. D., & Vink, J. S. 2005, A&A, 439, 1107

Davies, B., Vink, J. S., & Oudmaijer, R. D. 2007, A&A, 469, 1045

de Jager, C. 1984, A&A, 138, 246

de la Chevrotière, A., St-Louis, N., Moffat, A. F. J., & MiMeS Collaboration. 2013, ApJ, 764, 171

de la Chevrotière, A., St-Louis, N., Moffat, A. F. J., & MiMeS Collaboration. 2014, ApJ, 781, 73

Deharveng, L., Schuller, F., Anderson, L. D., et al. 2010, A&A, 523, A6

Dessart, L. & Chesneau, O. 2002, A&A, 395, 209

Dessart, L. & Owocki, S. P. 2002, A&A, 393, 991

Díaz-Fraile, D., Rodríguez, E., & Amado, P. J. 2014, A&A, 568, A32

Doyle, A. P., Davies, G. R., Smalley, B., Chaplin, W. J., & Elsworth, Y. 2014, MNRAS, 444, 3592

Dufton, P. L., Ryans, R. S. I., Simón-Díaz, S., Trundle, C., & Lennon, D. J. 2006, A&A, 451, 603

Dufton, P. L., Ryans, R. S. I., Trundle, C., et al. 2005, A&A, 434, 1125

Dupret, M.-A., Grigahcène, A., Garrido, R., Gabriel, M., & Scuflaire, R. 2004, A&A, 414, L17

Dupret, M.-A., Grigahcène, A., Garrido, R., Gabriel, M., & Scuflaire, R. 2005, A&A, 435, 927

Eddington, A. S. 1925, MNRAS, 85, 408

Einstein, A. 1906, Annalen der Physik, 324, 371

Einstein, A. 1916, Annalen der Physik, 354, 769

Elmegreen, B. G. 2012, in IAU Symposium, Vol. 284, IAU Symposium, ed. R. J. Tuffs & C. C. Popescu, 317–329

Evans, C., Taylor, W., Sana, H., et al. 2011, The Messenger, 145, 33

Fermi, E. 1956, Thermodynamics

Feynman, R. P. 1963, Feynman lectures on physics - Volume 1

Fossati, L., Ryabchikova, T., Bagnulo, S., et al. 2009a, A&A, 503, 945

Fossati, L., Ryabchikova, T., Bagnulo, S., et al. 2009b, A&A, 503, 945

Fossati, L., Ryabchikova, T., Shulyak, D. V., et al. 2011, MNRAS, 417, 495

Fraser, M., Dufton, P. L., Hunter, I., & Ryans, R. S. I. 2010, MNRAS, 404, 1306

Fullerton, A. W., Gies, D. R., & Bolton, C. T. 1996, ApJS, 103, 475

Gary, G. A. 2001, Sol. Phys., 203, 71

Gayley, K. G. & Owocki, S. P. 1995, ApJ, 446, 801

Glatzel, W. 1994, MNRAS, 271, 66

Glatzel, W. 2005, in Astronomical Society of the Pacific Conference Series, Vol. 332, The Fate of the Most Massive Stars, ed. R. Humphreys & K. Stanek, 22

Glatzel, W. & Kaltschmidt, H. O. 2002, MNRAS, 337, 743

Glatzel, W., Kiriakidis, M., & Fricke, K. J. 1993, MNRAS, 262, L7

Gnedin, N. Y. 2000, ApJ, 535, 530

Goldreich, P. & Kumar, P. 1990, ApJ, 363, 694

Gosling, J. T. & Pizzo, V. J. 1999, Space Sci. Rev., 89, 21

Gosset, E. & Rauw, G. 2009, Communications in Asteroseismology, 158, 138

Gräfener, G., Owocki, S. P., & Vink, J. S. 2012a, A&A, 538, A40

Gräfener, G. & Vink, J. S. 2013, A&A, 560, A6

Gräfener, G., Vink, J. S., Harries, T. J., & Langer, N. 2012b, A&A, 547, A83

Gräfener, G., Vink, J. S., & Owocki, S. P. 2012c, in Astronomical Society of the Pacific Conference Series, Vol. 465, Proceedings of a Scientific Meeting in Honor of Anthony F. J. Moffat, ed. L. Drissen, C. Robert, N. St-Louis, & A. F. J. Moffat, 202

Graham, J. F. & Fruchter, A. S. 2013, ApJ, 774, 119

Grassitelli, L., Chené, A.-N., Sanyal, D., et al. 2016, A&A, 590, A12

Grassitelli, L., Fossati, L., Langer, N., et al. 2015a, A&A, 584, L2

Grassitelli, L., Fossati, L., Simón-Diáz, S., et al. 2015b, ApJ, 808, L31

Gray, D. F. 1984, ApJ, 281, 719

Gray, D. F. 2005, The Observation and Analysis of Stellar Photospheres

Grigahcène, A., Dupret, M.-A., Gabriel, M., Garrido, R., & Scuflaire, R. 2005, A&A, 434, 1055

Groh, J. H., Meynet, G., Georgy, C., & Ekström, S. 2013, A&A, 558, A131

Guzik, J. A., Kaye, A. B., Bradley, P. A., Cox, A. N., & Neuforge, C. 2000, ApJ, 542, L57

Hamann, W.-R., Gräfener, G., & Liermann, A. 2006, A&A, 457, 1015

Hamann, W.-R. & Koesterke, L. 1998, A&A, 335, 1003

Handler, G. & Shobbrook, R. R. 2002, MNRAS, 333, 251

Heger, A., Jeannin, L., Langer, N., & Baraffe, I. 1997, A&A, 327, 224

Heger, A. & Langer, N. 1996, A&A, 315, 421

Heger, A., Langer, N., & Woosley, S. E. 2000, ApJ, 528, 368

Herrero, A., Kudritzki, R. P., Vilchez, J. M., et al. 1992, A&A, 261, 209

Hertzsprung, E. 1915, ApJ, 42

Hillier, D. J. 2008, in Clumping in Hot-Star Winds, ed. W.-R. Hamann, A. Feldmeier, & L. M. Oskinova, 93

Houdek, G. 2000, in Astronomical Society of the Pacific Conference Series, Vol. 210, Delta Scuti and Related Stars, ed. M. Breger & M. Montgomery, 454

Howarth, I. D. 2004, in IAU Symposium, Vol. 215, Stellar Rotation, ed. A. Maeder & P. Eenens, 33

Humphreys, R. M. & Davidson, K. 1979, ApJ, 232, 409

Humphreys, R. M. & Davidson, K. 1984, Science, 223, 243

Hundhausen, A. J. & Gosling, J. T. 1976, J. Geophys. Res., 81, 1436

Iglesias, C. A. & Rogers, F. J. 1996, ApJ, 464, 943

Jiang, S. & Huang, R. 1997, Acta Astrophysica Sinica, 17, 271

Jiang, Y.-F., Cantiello, M., Bildsten, L., Quataert, E., & Blaes, O. 2015, ApJ, 813, 74

Joss, P. C., Salpeter, E. E., & Ostriker, J. P. 1973, ApJ, 181, 429

Keller, S. C. & Wood, P. R. 2006, ApJ, 642, 834

Kippenhahn, R. & Weigert, A. 1990, Stellar Structure and Evolution

Kitiashvili, I. N., Kosovichev, A. G., Mansour, N. N., & Wray, A. A. 2016, ApJ, 821, L17

Kobayashi, C., Umeda, H., Nomoto, K., Tominaga, N., & Ohkubo, T. 2006, ApJ, 653, 1145

Köhler, K., Langer, N., de Koter, A., et al. 2015, A&A, 573, A71

Kozyreva, A., Yoon, S.-C., & Langer, N. 2014, A&A, 566, A146

Kramer, R. H., Cohen, D. H., & Owocki, S. P. 2003, ApJ, 592, 532

Lamers, H. J. G. L. M. & Cassinelli, J. P. 1999, Introduction to Stellar Winds

Landau, L. 1938, Nature, 141, 333

Landau, L. D. & Lifshitz, E. M. 1959, Fluid mechanics

Landau, L. D. & Lifshitz, E. M. 1969, Mechanics

Langer, N. 1989, A&A, 210, 93

Langer, N. 1997, in Astronomical Society of the Pacific Conference Series, Vol. 120, Luminous Blue Variables: Massive Stars in Transition, ed. A. Nota & H. Lamers, 83

Langer, N. 2012, ARA&A, 50, 107

Langer, N., Hamann, W.-R., Lennon, M., et al. 1994, A&A, 290, 819

Langer, N. & Kudritzki, R. P. 2014, A&A, 564, A52

Lecoanet, D. & Quataert, E. 2013, MNRAS, 430, 2363

Lefèvre, L., Marchenko, S. V., Moffat, A. F. J., et al. 2005, ApJ, 634, L109

Lépine, S., Eversberg, T., & Moffat, A. F. J. 1999, AJ, 117, 1441

Lépine, S. & Moffat, A. F. J. 1999, ApJ, 514, 909

Lépine, S. & Moffat, A. F. J. 2008, AJ, 136, 548

Lepine, S., Moffat, A. F. J., & Henriksen, R. N. 1996, ApJ, 466, 392

Lighthill, M. J. 1952, Royal Society of London Proceedings Series A, 211, 564

Lu, L., Sargent, W. L. W., Barlow, T. A., & Rauch, M. 1998, ArXiv Astrophysics e-prints

Lunnan, R., Chornock, R., Berger, E., et al. 2014, ApJ, 787, 138

Mac Low, M.-M. & Klessen, R. S. 2004, Reviews of Modern Physics, 76, 125

MacGregor, K. B. & Cassinelli, J. P. 2003, ApJ, 586, 480

Maeder, A. 2009, Physics, Formation and Evolution of Rotating Stars

Maeder, A. & Meynet, G. 2012, Reviews of Modern Physics, 84, 25

Marchenko, S. V., Moffat, A. F. J., St-Louis, N., & Fullerton, A. W. 2006, ApJ, 639, L75

Markova, N. & Puls, J. 2015, in IAU Symposium, Vol. 307, IAU Symposium, ed. G. Meynet, C. Georgy, J. Groh, & P. Stee, 117–118

Markova, N., Puls, J., Simón-Díaz, S., et al. 2014, A&A, 562, A37

Martinez, P., Kurtz, D., Ashley, R., & Tripe, P. 1994, Nature, 367, 601

Mathis, S., Neiner, C., & Tran Minh, N. 2014, A&A, 565, A47

Meynet, G. & Maeder, A. 2003, A&A, 404, 975

Michaux, Y. J. L., Moffat, A. F. J., Chené, A.-N., & St-Louis, N. 2014, MNRAS, 440, 2

Miglio, A., Montalbán, J., & Dupret, M.-A. 2007, MNRAS, 375, L21

Miglio, A., Montalbán, J., Noels, A., & Eggenberger, P. 2008, MNRAS, 386, 1487

Mitalas, R. & Sills, K. R. 1992, ApJ, 401, 759

Moffat, A. F. J. 2008, in Clumping in Hot-Star Winds, ed. W.-R. Hamann, A. Feldmeier, & L. M. Oskinova, 17

Moffat, A. F. J., Drissen, L., Lamontagne, R., & Robert, C. 1988, ApJ, 334, 1038

Moffat, A. F. J., Marchenko, S. V., Zhilyaev, B. E., et al. 2008, ApJ, 679, L45

Moffat, A. F. J. & Robert, C. 1994, ApJ, 421, 310

Mullan, D. J. 1984, ApJ, 283, 303

Mullan, D. J. 1986, A&A, 165, 157

Nugis, T. & Lamers, H. J. G. L. M. 2000, A&A, 360, 227

Oskinova, L. M., Hamann, W.-R., Feldmeier, A., Ignace, R., & Chu, Y.-H. 2009, ApJ, 693, L44

Owocki, S. P. 2015, in Astrophysics and Space Science Library, Vol. 412, Astrophysics and Space Science Library, ed. J. S. Vink, 113

Owocki, S. P., Castor, J. I., & Rybicki, G. B. 1988, ApJ, 335, 914

Owocki, S. P. & Rybicki, G. B. 1986, ApJ, 309, 127

Pamyatnykh, A. A. 1999, Acta Astron., 49, 119

Parker, E. N. 1958, ApJ, 128, 664

Penny, L. R. & Gies, D. R. 2009, ApJ, 700, 844

Petrovic, J., Langer, N., Yoon, S.-C., & Heger, A. 2005, A&A, 435, 247

Petrovic, J., Pols, O., & Langer, N. 2006, A&A, 450, 219

Prialnik, D. 2000, An Introduction to the Theory of Stellar Structure and Evolution

Prinja, R. K. & Crowther, P. A. 1998, MNRAS, 300, 828

Prinja, R. K., Massa, D., & Fullerton, A. W. 1995, ApJ, 452, L61

Prinja, R. K., Massa, D., & Fullerton, A. W. 2002, A&A, 388, 587

Russell, H. N. 1914, Popular Astronomy, 22, 275

Ryabchikova, T., Piskunov, N., Pakhomov, Y., et al. 2016, MNRAS, 456, 1221

Ryabchikova, T. A., Adelman, S. J., Weiss, W. W., & Kuschnig, R. 1997, A&A, 322, 234

Rybicki, G. B. & Lightman, A. P. 1979, Radiative processes in astrophysics

Saio, H. 1993, Ap&SS, 210, 61

Saio, H. 2009, Communications in Asteroseismology, 158, 245

Saio, H., Baker, N. H., & Gautschy, A. 1998, MNRAS, 294, 622

Salpeter, E. E. 1955, ApJ, 121, 161

Samadi, R., Belkacem, K., Goupil, M. J., et al. 2010, Ap&SS, 328, 253

Sander, A., Hamann, W.-R., & Todt, H. 2012, A&A, 540, A144

Sanyal, D., Grassitelli, L., Langer, N., & Bestenlehner, J. M. 2015, A&A, 580, A20

Sasselov, D. D., Beaulieu, J. P., Renault, C., et al. 1997, A&A, 324, 471

Schneider, F. R. N., Izzard, R. G., de Mink, S. E., et al. 2014, ApJ, 780, 117

Schwarzschild, K. 1992, Gesammelte Werke Vol.1, Vol.2, Vol.3

Shiode, J. H., Quataert, E., Cantiello, M., & Bildsten, L. 2013, MNRAS, 430, 1736

Simón-Díaz, S. 2015, in IAU Symposium, Vol. 307, IAU Symposium, 194–199

Simón-Díaz, S., Caballero, J. A., Lorenzo, J., et al. 2015, ApJ, 799, 169

Simón-Díaz, S., Castro, N., Garcia, M., Herrero, A., & Markova, N. 2011a, Bulletin de la Societe Royale des Sciences de Liege, 80, 514

Simón-Díaz, S., Castro, N., Garcia, M., Herrero, A., & Markova, N. 2011b, Bulletin de la Societe Royale des Sciences de Liege, 80, 514

Simón-Díaz, S., Castro, N., Herrero, A., et al. 2012, in Astronomical Society of the Pacific Conference Series, Vol. 465, Proceedings of a Scientific Meeting in Honor of Anthony F. J. Moffat, ed. L. Drissen, C. Robert, N. St-Louis, & A. F. J. Moffat, 19

Simón-Díaz, S. & Herrero, A. 2014, A&A, 562, A135

Simón-Díaz, S., Herrero, A., Uytterhoeven, K., et al. 2010, ApJ, 720, L174

Slettebak, A. 1956, ApJ, 124, 173

Slettebak, A. 1976, in IAU Symposium, Vol. 70, Be and Shell Stars, ed. A. Slettebak, 123

St-Louis, N. 2013, ApJ, 777, 9

St-Louis, N., Chené, A.-N., Schnurr, O., & Nicol, M.-H. 2009, ApJ, 698, 1951

Stancliffe, R. J., Fossati, L., Passy, J.-C., & Schneider, F. R. N. 2016, ArXiv e-prints

Stein, R. F. & Nordlund, Å. 2001, ApJ, 546, 585

Stix, M. 2003, Sol. Phys., 212, 3

Stothers, R. B. 2003, ApJ, 589, 960

Stothers, R. B. & Chin, C.-W. 1993, ApJ, 408, L85

Sundqvist, J. O., Petit, V., Owocki, S. P., et al. 2013, MNRAS, 433, 2497

Tkachenko, A., Lehmann, H., Smalley, B., Debosscher, J., & Aerts, C. 2012, MNRAS, 422, 2960

Trampedach, R., Stein, R. F., Christensen-Dalsgaard, J., Nordlund, Å., & Asplund, M. 2014, MNRAS, 445, 4366

Valenti, J. A. & Fischer, D. A. 2005, ApJS, 159, 141

Van Reeth, T., Tkachenko, A., Aerts, C., et al. 2015, ApJS, 218, 27

Vink, J. S. 2012, in American Institute of Physics Conference Series, Vol. 1429, American Institute of Physics Conference Series, ed. J. L. Hoffman, J. Bjorkman, & B. Whitney, 147–158

Vink, J. S. 2014, ASTRA Proceedings, 1, 39

Vink, J. S. 2015, in Astrophysics and Space Science Library, Vol. 412, Very Massive Stars in the Local Universe, ed. J. S. Vink, 77

Vink, J. S., Brott, I., Gräfener, G., et al. 2010, A&A, 512, L7

Vink, J. S., de Koter, A., & Lamers, H. J. G. L. M. 2001, A&A, 369, 574

Xiong, D. R. & Deng, L. 2007, MNRAS, 378, 1270

Yoon, S.-C. & Cantiello, M. 2010, ApJ, 717, L62

Yoon, S.-C. & Langer, N. 2005, A&A, 443, 643

Yoon, S.-C., Langer, N., & Norman, C. 2006, A&A, 460, 199

Yusof, N., Hirschi, R., Meynet, G., et al. 2013, MNRAS, 433, 1114

Acknowledgements

L'amor che move il sole e l'altre stelle.
Dante Alighieri
Divina Commedia

It is not easy to collect memories, feelings, and thoughts to thank the people which were part of this path of mine through life. Here are only few honourable mentions.
Neglecting the obvious thanks to my parents, because basically I would not be here if at the time they decided to go out for a pizza, and to my brother because at some point I might need a kidney or something and he will be the first on the list, I have to thank Norbert.
I could thank Norbert for the great amount of knowledge I was and I am still stealing from him, for the advices , and for his patience , etc.. etc.. but these are somehow obvious acknowledgements I am sure he is already aware of. The main thing I would like to thank him for is instead that he thought me how to think, he made my mind grow and improve, and this is probably the thing I feel more in debt for; danke.
Then comes my unofficial advisor, Luca2, to whom I own a lot especially because he gave me passion, strength, he was there when I needed, and he also gave me a very heavy dish from the north of Italy full of garlic that I am still trying to digest.
It is now time to thank the people I shared my time, laughs, and complains (many complains) here in Bonn. Thanks to the bro Jean-Claude, aka JC, aka JJ, aka *he knows what*. Thanks to Alina and her dear crazyness. Thanks to (es-)Ana, PresiBen, Vazzillo, Fabiano, Joachimmo, Alberto^2, Moniccaa, Bia, Aschisch, Richard, JMac, Norberto, all the past and present members of the stellar group.
Thanks al biondo delfino Lovisari e al divino Emiliano.
Thanks to the people I shared the unforgettable years of my master, i.e. Chris, Njanja, Abdiel, Varc-Laura, Smismitar, Giovanna, Rosamaria, Gabriella, and also big and small Boss Luka and Sasá
Then thanks to the friends of a lifetime, all'amico fraterno Pasquale, alle sorelline Maria Teresa e Cristina, alla cara Marilena, al maestro Colucci, e a Miriam, Fabio, Nicola, Valeria, Alessandra, etc..
Thanks to my stellina, my solneska, mia principessa Yulia.
I would like also to thank Kaiser Söze, the stormtrooper with the lightsaber, the left and the right hand of the Devil aka Bambino & Trinita', and India for making of my PhD a funnier time. Thanks for all the fish.
Tante care cose
Luca

Curriculum Vitae

Personal Details

Name	Luca Grassitelli
Date of Birth	15 / 05 / 1987
Email	luca@astro.uni-bonn.de

Education

2006–2010	BSc in Physics, Universitá degli studi di Bari, Bari, Italy.
2010–2012	MSc in Astrophysics, ASTROMUNDUS Erasmus Mundus Master Course, Universities of Innsbruck (Austria), Padova (Italy), Göttingen (Germany), Belgrade (Serbia)
2012–2016	PhD in Stellar Physics, Rheinische Friedrich-Wilhelms-Universität, Bonn, Germany.

Professional Experience

2013–2015	Teaching Assistant at the University of Bonn, Germany. Stellar Structure and Evolution, Nucleosyntesis, Spectroscopy of Stars
2015	Space Weather Summer Camp at University of Alabama, Huntsville, USA and DLR, Neustrelitz, Germany

Languages

Italian	Mother tongue
English	Fluent
German	Basic